

**Studies of cultured neuronal networks using light activated ion channels
and pumps**

PhD Thesis

In partial fulfillment of the requirements

For the degree “Doktor rerum naturalium (Dr. rer. nat.)”

In the Neuroscience Program at

Georg August University Göttingen, Faculty of Biology

Submitted by

Ahmed El Hady

Born in

Cairo, Egypt

Göttingen

September 5, 2012

Supervisor, thesis committee member: Prof. Dr. Fred Wolf
Thesis committee member: Prof. Dr. Walter Stühmer
Thesis committee member: Prof. Dr. Theo Geisel

I hereby declare that I prepared this doctoral thesis, entitled “Studies of cultured neuronal networks using light activated ion channels and pumps”, on my own and with no other sources and aids than those cited.

Ahmed El Hady

September 5th 2012, Göttingen

Dedicated to the revolutionaries in the Middle East and every revolutionary working for a better future of our human species

Table of contents

Preface.....	1
Chapter 1: General introduction.....	2
1. Optical control of neurons.....	2
1.1. Overview.....	2
1.2. Channelrhodopsins.....	4
1.2.1. General Characteristics.....	4
1.2.2. Structure and gating mechanisms.....	4
1.2.3. Photocycle.....	4
1.2.4. Photocurrent characteristics.....	7
1.2.5. Variants and mutants.....	8
1.2.6. Targeting channelrhodopsins.....	10
1.2.7. Delivering channelrhodopsins.....	11
1.2.8. Applications.....	11
2. Network electrophysiology.....	13
3. References.....	16
Chapter 2: Optogenetic induction of network level plasticity.....	21
1. Introduction.....	21
1.1. Bursting in neuronal networks.....	21

1.2.	Synchronization in neuronal networks.....	22
1.3.	Synaptic plasticity.....	24
1.4.	Network level plasticity.....	27
1.5.	Aim of the study.....	31
2.	Results.....	32
2.1.	Experimental system design.....	32
2.2.	Network firing rate increases after stimulation.....	35
2.3.	Network bursting dynamics change after stimulation.....	35
2.4.	Network synchronization increases after stimulation.....	39
2.5.	Genes responsible for early phase long term potentiation mainly involved in the network changes as revealed by microarray analysis of synaptic plasticity genes.....	44
2.6.	Network dynamics changes are NMDA dependent.....	48
3.	Discussion.....	51
4.	References.....	56
Chapter 3: Continuous Dynamic Photostimulation.....		65
1.	Introduction.....	65
1.1.	Aim of the study.....	71
2.	Results.....	72
2.1.	Characteristics of channelrhodopsin 2 and ChIEF photocurrents.....	72
2.2.	Highly reproducible fluctuating light activated currents.....	75
2.3.	Channelrhodopsin act as low pass filter.....	78

2.4.	Computational reconstruction of conductance fluctuations.....	81
2.5.	Long term CoDyPs of cultured neurons.....	83
3.	Discussion.....	85
4.	References.....	88
Chapter 4: Materials and methods.....		93
1.	Cell culture.....	93
1.1.	Cell preparation.....	93
1.2.	Cleaning procedure of the multielectrode arrays.....	94
1.3.	Coating procedure of the multielectrode arrays.....	95
1.4.	Neuronal cultures quality control.....	95
2.	Electrophysiology.....	97
2.1.	Multielectrode array measurements.....	97
2.2.	Perfusion system.....	97
2.3.	Synaptic blockade experiments.....	98
3.	Whole field illumination.....	99
3.1.	Illumination setup.....	99
3.1.1.	Light source used for illumination.....	99
3.1.2.	Irradiance measurement.....	100
3.2.	Photostimulation paradigms.....	102
4.	Molecular biology.....	104
4.1.	Cloning.....	104
4.1.1.	Cloning Channelrhodopsin 2 construct under an α MHC	

	promoter for cardiac specific expression.....	104
4.1.1.1.	Transformation procedure of pcDNA 3.1-CHOP2-YFP.....	104
4.1.1.2.	Culturing transformed cells.....	104
4.1.1.3.	Maxi-prep of pcDNA3.1-CHOP2-YFP.....	104
4.1.1.4.	Transformation of reverse α MHC plasmids.....	105
4.1.1.5.	PCR cloning.....	106
4.1.1.6.	Gel electrophoresis.....	107
4.1.1.7.	Digestion.....	109
4.1.1.8.	Ligation.....	110
4.1.2.	Cloning tandem construct pcDNA3.1-hChR2-hBR under α MHC promoter for cardiac specific expression.....	112
4.1.3.	Cloning ChIEF into an AAV viral backbone.....	114
4.2.	Site directed mutagenesis.....	114
4.2.1.	The primers design.....	114
4.2.2.	Mutant strand synthesis reaction.....	115
4.2.3.	DpnI digestion of the amplification products.....	115
4.2.4.	Electroporation of XL-1 blue competent cells.....	116
4.2.5.	Transformation of the reaction products.....	116
4.2.6.	Cloning mutated channelrhodopsin 2 (C128S) into the reverse cardiac plasmid.....	117

4.3.	Establishment of HEK-CHOP2 stable cell line.....	119
4.4.	Microarray analysis using RT²PCR array.....	120
4.4.1.	Experimental design.....	120
4.4.2.	RNA isolation.....	122
4.4.3.	cDNA synthesis.....	123
4.4.3.1.	Pre-amplification.....	123
4.4.4.	Quantitative PCR.....	125
4.4.5.	Microarray data analysis.....	125
4.4.6.	Quality control.....	126
4.4.6.1.	Specificity of the PCR products.....	126
4.4.6.2.	PCR array reproducibility.....	126
4.4.6.3.	Reverse transcriptional control.....	126
4.4.6.4.	Genomic DNA contamination.....	127
4.4.6.5.	Stability of the house keeping genes.....	127
4.5.	Western blotting.....	127
4.5.1.	Cells used for western blotting.....	127
4.5.2.	Protein extraction from cells.....	127
4.5.3.	Samples preparation.....	128
4.5.4.	Blotting.....	128
4.5.5.	Blocking.....	129
4.5.6.	Developing the blot.....	129
4.6.	Transfections.....	131

4.6.1. HEK cell transfection with ChIEF.....	131
4.6.2. Viral transfection.....	131
5. Network dynamics data analysis.....	132
5.1. Active electrodes.....	132
5.2. Average firing rate.....	132
5.3. Peri-stimulus time histogram.....	132
5.4. Burst detection.....	133
5.5. Burst structure.....	133
5.6. Cross correlation analysis.....	135
6. Continuous dynamic photostimulation experiments.....	136
6.1. Stimuli generation.....	136
6.2. Data analysis.....	137
References.....	140
Chapter 5: General discussion.....	141
References.....	147
List of figures and tables.....	149
Acknowledgments.....	151
Curriculum Vitae and publications.....	155

Preface

Understanding emergent properties of the brain such as learning and memory is one of the main challenges facing neuroscience. Those properties result from the interactions of many neurons embedded in networks in a self organized manner. It is becoming increasingly clear that current reductionist approaches are not appropriate to fully understand such phenomenon thus novel approaches have to be devised. The power of devising new experimental tools is that it widens the epistemological space of neuroscientific investigation by allowing novel questions to be addressed and by reanswering old questions in innovative ways. Combining novel technical approaches with rigorous theoretical analysis should ultimately help us understand brain functioning. In an ideal situation, novel technical approaches should monitor, read out and control different levels of description of the brain from molecular to cellular to circuit level simulatenously in a parallel and high throughput manner. In such a way, one can reliably and precisely test theoretical predictions. In an iterative process between experiments and theories one can hope that a complete brain theory would likely be a possibility.

For these reasons, I feel privileged to have worked on the interface of experiments and theory. I personally think that the impact of such interdisciplinary research is far reaching and would help us to understand rather than describe the brain.

Ahmed El Hady

September 5th Goettingen

CHAPTER 1

General Introduction

1. Optical control of neurons:

1.1. Overview:

Optical stimulation or photostimulation offers a non invasive method to control neuronal activity. It has the advantage of producing fewer artifacts than electrical stimulation. It also allows stimulating neurons in a high spatial and temporal resolution. Recent advances in genetics, chemistry and optics have provided unprecedented opportunities to use light to stimulate, inhibit or control neuronal activity with molecular specificity and a high temporal & spatial resolution. The optical control strategies can be broadly divided into non genetic and genetic methods for optical control. The non genetic methods comprise: caged neurotransmitters, reversibly caged signaling molecules that can be released by a flash of light allowing the liberated compound to act on endogenous or exogenous neuronal targets before diffusing away (e.g. Bis-Q, GluAzo, XAQs) and photoswitched tethered ligands for native channels (QBr and a Quaternary Ammonium PAL). The genetic methods include genetically engineered light gated channels and receptors (SPARK light gated K⁺ channels and LiGluR: light gated kainate type glutamate receptor) and Opsin based control of neuronal activity. The opsin based tools is a large class of channels that are genetically targeted. It comprises the ChARGe channel, Melanopsin, Channelrhodopsin 1 (ChR1), Channelrhodopsin 2 (ChR2), Volvox Channelrhodopsin 1 (VChR1), Volvox Channelrhodopsin 2 (VChR2) and Halorhodopsin (Szobota, S. and Isacoff, E. Y. 2010). The use of opsin based tools to control neuronal activity has led to the establishment of the field of Optogenetics. It has been chosen as the method of the year 2010 by Nature methods (8, 1(2011)).

The following table summarizing the main tools currently used to control neuronal activity:

Optical Method	Effect on Voltage	Single photon excitation	Temp-oral spike jitter	Precisely timed spike trains	Exogenous chemicals	Spatial resolution
Glutamate Uncaging	Depolarizing	355 nm UV light	1 - 3 ms	not studied	Caged glutamate (e.g. ester)	5 μ m
ChARGe	Depolarizing	400 - 600 nm light	Sec. to Min.	not studied	Retinal	Genetically targeted
ChR2	Depolarizing	480 nm blue light	1 - 3 ms	around 25 Hz maximum	Not needed	Genetically targeted
Modified glutamate receptor	Depolarizing	Activated by 380 nm Inactivated by 580nm	100 ms	not studied	Azobenzene tethered glutamate receptor agonist	Genetically targeted

Table 1.1: Optical methods to control neuronal activity:
comparison between different modalities used to control neuronal activity.

The aforementioned comparison highlights the existence of optical tools that control neuronal activity at various temporal and spatial scales.

On the other hand, progress in optical technologies has a great impact on optical control of neurons. Examples of the state of the art technologies are Digital Light Projection (DLP) and Digital Micromirror Device (DMD) that can target the light to multiple spots simultaneously with high spatial resolution (Wang S et al. 2007). Moreover, holographic methods would offer neuroscientists the ability to stimulate neurons in arbitrary patterns and can be used to mimic complex neuronal inputs (Lutz C et al. 2008, Golan L et al. 2009). On the other hand, genetic targeting and animal transgenic technologies would provide the ability to target optogenetic tools to specific

neuronal structures or sub-structures thus offering the ability to interrogate neuronal networks in a detailed manner (Luo L et al. 2008)

1.2. Channelrhodopsins:

1.2.1. General Characteristics:

One of the first and main tools that have been used to control neuronal activity are channelrhodopsins. Channelrhodopsins are the primary photoreceptors in the eyespot of the *C. Reinhardtii* that are responsible for phototactic and photophobic responses (Berthold P et al. 2008, Sineschekov OA et al. 2009, Sineschekov OA et al. 2002). There are two types of channelrhodopsins in *C. Reinhardtii*, one with fast kinetics and poor light sensitivity, channelrhodopsin-1 (ChR1) (Nagel G et al. 2002), and another with slower kinetics and higher sensitivity, channelrhodopsin-2 (ChR2). The photophobic and phototactic responses are mainly mediated via channelrhodopsin 1.

Channelrhodopsin 2 is an inwardly rectifying non selective cation channels. At neutral pH, permeable to physiologically relevant cations such as H^+ , Na^+ , K^+ , and Ca^{2+} (Nagel G et al. 2003, Wang et al. 2009). The single ion channel conductance of ChR2 has been estimated at 50 fS (Feldbaeuer K. et al. 2009). This is considerably less than a typical voltage dependent sodium channel that may have a conductance on the order of ~10 pS. As the single channel conductance is low, a large number of channels (high expression level) is required to trigger an action potential.

1.2.2. Structure and gating mechanisms:

Channelrhodopsin 2 is a membrane spanning retinylidene protein. It has a 7 transmembrane domain structure. The ion conductance and selectivity are suggested to be defined by TM2. The chromophore is an all *trans* retinal that undergo isomerization to 13-cis-retinal upon

absorption of a blue photon. A protonated Schiff base is linking the retinal moiety and the amino group of the lysine side chain (Lys 296) on TM7. The retinal binding pocket is formed by the Cys 167, Thr 198, Ser 295. Upon illumination, the protonated Schiff base loses a proton which is transferred to the residue Asp 292 which is considered to be the proton acceptor (Kato H.E. et al. 2012).

On the other hand, channelrhodopsin 2 can be regarded as a leaky proton pump as it has been found that it has proton pumping activity. Deprotonation to the extracellular (EC) side at the P390 ~ 400 state and reprotonation from the cytoplasmic (CP) side (P520) lead to the pumping of one proton per photocycle (fig.1.1).

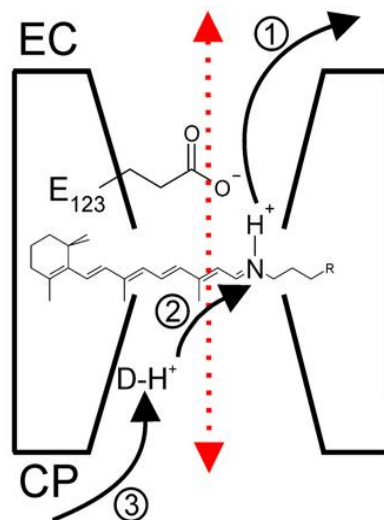


Fig 1.1: Cartoon sketch of the mechanistic model of ChR2 in relation to the photocycle showing the retinylidene chromophore. Deprotonation of Schiff's base (no.1) takes place via the putative proton acceptor (E123). Reprotonation occurs from an intramolecular donor towards (no.2) that is going to be replenished from the cytoplasmic side (no.3) taken with permission from Feldbauer K et al. 2009.

1.2.3. Photocycle:

Upon light absorption, channelrhodopsin 2 undergoes a photocycle that can be summarized as follows: after photon absorption at 480 nm, the retinal moiety undergoes isomerization from all-*trans*-retinal to 13-*cis*-retinal which leads to a fast deprotonation of the schiff's base forming a blue light shifted intermediate (P400) , then this intermediate is converted to a red shifted intermediate upon reprotonation of the

Schiff's base (P520). This intermediate is thought to represent the open state of the channel. The rate of the reprotonation of the Schiff's base determines the lifetime of the open state of the channel. Subsequently the channel goes into a closed desensitized state followed by a slow reisomerization step required for the channel to return to its dark sensitive state (Bamann C et al. 2008).

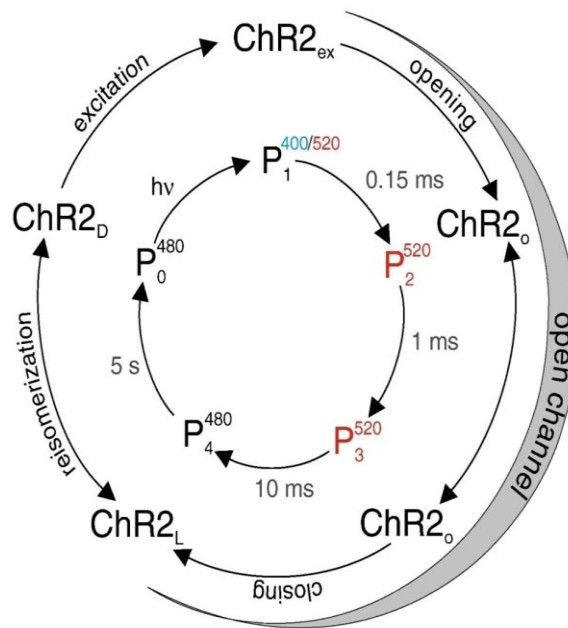


Fig 1.2: Typical photocycle of channelrhodopsin 2 showing the excited, open, closed desensitized and closed sensitive states. Adopted with permission from Bamann C. et al. 2008

As some of the photointermediates are photoreactive, the photocycle can be short-circuited. The conducting P520 state can be converted with green light to the dark state D470. Like P520, the P480b intermediate is photoreactive and can be converted by blue light to the early P500 intermediate which would also result in a shortcut of the photocycle (fig.1.3.) (Ritter E et al. 2008)

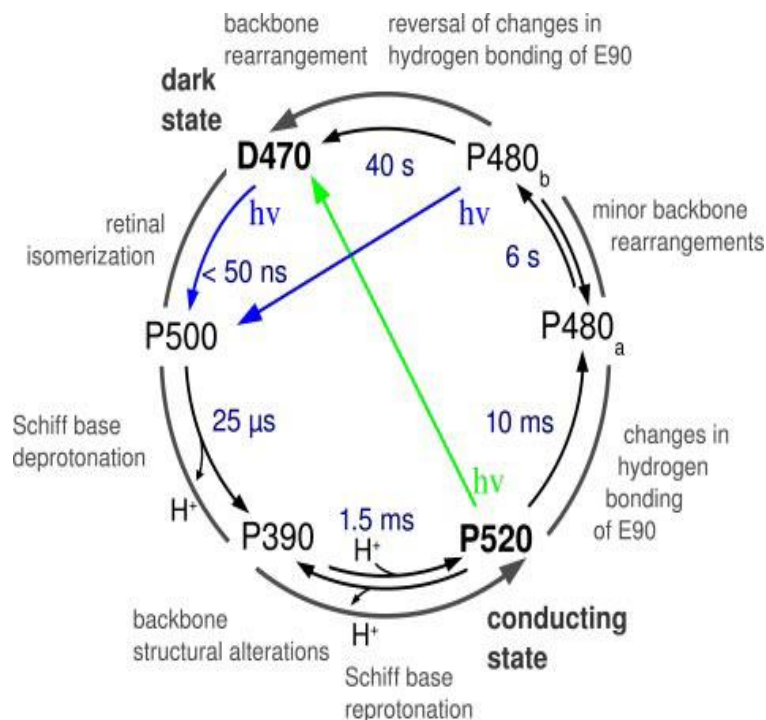


Fig. 1.3: Six state model including the intermediate as identified by UV-visible spectroscopy and infrared difference spectroscopy. To note in this photocycle that the dark state can be recovered by green light absorption of P520 (green arrow). Like P520, P480b intermediate is photoreactive and can be converted by blue light to the P500 intermediate. Adopted with permission from Ritter E. et al. 2008.

1.2.4. Photocurrent Characteristics:

The typical photocurrent of channelrhodopsin 2 consists of a large transient peak that has onset of around 4 – 10 ms (Nagel G et al. 2003, Boyden E et al. 2005, Bamann C et al. 2008); this transient peak quickly decays to a stationary component that is typically <20–50% of the initial peak photocurrent (Nagel G et al. 2003) Upon removing the light, ChR2 closes with a time constant of 10–20 ms (Nagel G et al. 2003). After switching off the light, the photocurrent decays in a biexponential manner (Nikolic K et al. 2009). It is important to note that the transient photocurrent peak is highly dependent on the illumination intensity (Ernest O et al. 2008, Nikolic K et al. 2006) and history . It is mechanistically unclear why the decay of the transient

peak current is happening: it might be attributed to the transition of the channel to a less conducting state (Berndt A et al. 2010) or the rapid desensitization of the channel (Lin JY 2010). The stationary component on the other hand, is less photosensitive and history-independent. The large and fast-onset peak enables ChR2-expressing neurons to spike with a high temporal precision on the millisecond timescale, the timescale of an action potential. However, the large inactivation (or alternatively, the small stationary component) and its slow recovery in the dark, as well as the slow closing rate of ~10–15 ms, limits the ability to drive reliable spike rates above 25 Hz (Lin JY et al. 2009) because (1) the stationary photocurrent may be too small to sufficiently depolarize a neuron to spike threshold, and (2) the channel cannot physically close quickly enough to enable de-inactivation of sodium channels. ChR1-style channelrhodopsins (VChR1, ChR1) (Zhang F et al. 2008, Nagel G et al. 2002) on the other hand demonstrate dramatically faster kinetics than ChR2-style channelrhodopsins (VChR2, ChR2). The stationary photocurrents of ChR1s are >70% of the peak photocurrents, and the channels open and close approximately two- to threefold faster than does ChR2 but it has poor membrane expression that limit the application of natural ChR1.

Based on the available characterization of the channelrhodopsins from *Volvox carteri* (Ernst OP et al. 2008), the general characteristics are similar to those of the analogous molecules in *C. reinhardtii*. VChR2 and ChR2 have nearly identical photocycles and action spectrum. VChR1 and ChR1 exhibit the similar reduced inactivation, and are both red-shifted from their respective VChR2/ChR2 counterparts.

Assuming that ChR1 and ChR2 photocycles are topologically similar, e.g., the ChR2 D470 and P480 photointermediates equate to the ChR1 peaks at 464 and 505 nm, this interpretation of the transient and stationary photocurrents is consistent with the finding that, for ChR1,

the stationary photocurrent is red shifted from the transient photocurrent (Wang H et al. 2009)

1.2.5. Variants and Mutants:

Although wild type channelrhodopsin 2 still the gold standard in optogenetics, it suffers from few shortcomings that prevent it from being used for a wide variety of neuroscience applications. The shortcomings are: non selectivity, fast inactivation, slow recovery, low conductance, variants and mutants are designed to circumvent them.

In the following section, I will enlist some of the variants and mutants of channelrhodopsin 2 that aimed at solving these issues. The E90Q mutation (Ritter E et al. 2008) has increased sodium selectivity and much reduced proton permeability vs. wild-type ChR2. Another channel called CatCh with the mutation L132C had an increased calcium permeability (Kleinlogel S et al. 2011). The variant K132A and Q95A show strong photocurrents and increased potassium selectivity thus enabling suppressing of neuronal activity. On the other hand, the H134R mutant (Nagel G et al. 2005) demonstrates increased conductance by approximately twofold. Step function opsins (SFO) are built using mutations to C128 (Berndt et al. 2009) drastically slowing down the rate of ChR2 closure from the open state, thus effectively creating a bistable open P520 state until illuminated with green light. The SFO mutations are designed to stabilize the active retinal isomer which results in the prolongation of the active state of the channel even after light-off. Another SFO with the mutation D156A have even longer inactivation time constant which can reach eight minute (Bamann C et al. 2010). A new class of channels called Stabilized Step Function Opsins (SSFOs) was constructed by combining both the D156 and C128 mutations that led to spontaneous deactivation times of around 30 minutes (Yizhar O et al. 2011)

In order to allow high frequency stimulation, the E123T mutant, combined with the H134R mutant, speeds channel closure and increases the precision of neural action potential firing at the expense of photocurrent and light sensitivity (Harwood J, Guschine IA 2009) resulting in a mutant called ChETA. The E123T mutation was combined with T159C mutation to produce a channel that can drive neurons at high frequencies and have a high light sensitivity (Berndt A et al. 2011).

Chimeras of ChR1 and ChR2 have been constructed by several researchers (Wang H et al. 2009, Lin Y et al. 2009, Tsunoda SP, Hegemann P 2009) one of which was that composed of ChR1 helices A–E and ChR2 helices F–G (called ChEF). These chimeras displayed the small inactivation of ChR1, but the large photocurrents of ChR2 on account of improved membrane localization and light sensitivity. An I190 V substitution to ChEF led to the molecule, “ChIEF,” capable of driving more reliable fast spiking due to the much larger stationary current and faster channel closing kinetics after light offset (Lin Y et al. 2009). Another chimera called C1V1 was constructed. C1V1 is composed of the first two and one half helices of ChR1 and the last four and one half helices of VChR1 which led to a red shifted activation spectrum for the chimeric channel and nanoampere currents.

1.2.6. Targeting Channelrhodopsins:

In order to stimulate specific neuronal structure and structures, channelrhodopsins can be molecularly targeted using specific promoters and targeting sequences. CamKII α promoter is used to target channelrhodopsin 2 to pyramidal neurons, GFAP promoter can be used to target it to astrocytes (Figueriredo M. et al. 2012), Myosin VI was used to target channelrhodopsins to both dendrites and axons (Lewis TL et al. 2011). On the other hand, channelrhodopsins were specifically

expressed in interneurons using parvalbumin promoter (Atallah BV et al. 2012).

Moreover, channelrhodopsin 2 has also been expressed in cardiac cells using the cardiac specific promoter (Arrenberg H et al. 2010).

1.2.7. Delivering Channelrhodopsins:

Channelrhodopsin 2 is increasingly being delivered to cells using Adeno-Associated virus (AAV) mediated viral transfection as it is a relatively safe method and certain AAV serotypes can be used with human subjects. Generally, a viral expression system offers a fast robust way to express constructs at high levels in neuronal systems. It has the disadvantage of the maximum genetic payload length which is circumvented by the development of Cre-dependent viruses (Warnock JN et al. 2011, Ortolano S et al. 2012).

1.2.8. Applications:

Optogenetic tools have been proposed and implemented for advancing the analysis of neuronal systems on all levels from single cells through circuits' structure and function up to the level of behaviour.

Optogenetics have been used in many animal models. It was used to control the c.elegans muscle wall motor neuron and mechanosensory neuron activity (Nagel et al. 2005). It was also used in flies to investigate the neuronal basis of the nociceptive response (Hwang et al. 2007) and appetitive/aversive odorant learning at the receptor (Bellmann et al. 2010). On the other hand, it was also used in Zebrafish to examine cardiac function & development (Arrenberg et al. 2010), transduction of sensory neuron mechanoreception (Low et al.

2010) command of swim behaviour (Arrenberg et al. 2009) and saccade generation (Schoonheim et al. 2010).

In the mouse, ChR2 was used to investigate the contribution of the hypothalamic hypocretin neurons to sleep and wakefulness (Adamantidis et al. 2007). Optogenetic stimulation was also used to stimulate axonal terminals in the nucleus accumbens which lead to the discovery that dopamine neurons co-release glutamate (Stuber et al. 2010, Tecuapetla et al. 2010). Reports on the functions of parvalbumin expressing fast spiking interneurons demonstrated directly their involvement in gamma oscillations and information processing in mouse prefrontal (Sohal et al. 2009) and somatosensory cortex (Cardin et al. 2009, 2010). Focal stimulation of pyramidal neurons in Thy1::ChR2 mice had enabled rapid functional mapping of motor control across the motor cortex (Ayling et al. 2009).

Optogenetics is also being used to discern the possible therapeutic mechanism of cortical intervention in mouse models of depression (Covington et al. 2010) and to develop novel strategies for control of peripheral neurons (Llewellyn et al. 2010). It will increase our understanding for disease states and the development of novel therapeutics as it has been used for example by Gradinaru et al. 2009 to optically control symptoms of Parkinson's disease and also by Tonnesen et. 2009 for control of epileptiform activity.

Interestingly in rats, virally delivered optogenetic tools were used to examine the blood oxygen level dependent (BOLD) responses in functional magnetic resonance imaging. Driving ChR2 in excitatory neuronal populations was sufficient to elicit a BOLD response not only in local cortical targets but also in downstream thalamic regions allowing global maps of activity causally driven by defined cell populations to be obtained within intact living mammals.

There has also been some work on optogenetic modulation of primate neurons (Han et al. 2009, Diester et al. 2011) by ChR2 delivery to cortical neurons of macaques via lentiviral transduction but behavioural responses have not yet been observed. Optogenetics will have great impact on the development of neuroprosthetics specially retinal prosthetics that are now reaching a mature and advanced stage that might allow it to be translated for use in human beings.(Busskamp V, Roska B 2011)

2. Network electrophysiology:

There is a growing consensus that individual elements of information are encoded by populations or clusters of cells not by single cells. This encoding strategy is named “Population coding”. Visual features for example such as orientation, colour, direction of motion and depth are encoded with population codes in visual cortical areas (Ursey et al. 1999, Zemel R et al. 2000) Motor commands in the motor cortex rely also on population codes (Tolhurst et al. 1983). Thus, it became more clear that sensory processing in our brain and memory & learning processes are coordinated by the activity of many neurons in a network. Another crucial aspect that is crucial for neuronal information processing is the topology and connectivity of the networks. Over the past decades experimental and theoretical studies have revealed candidate connectivity architectures that are expected to enable networks of neurons to operate as memory storage devices, as sensory modules that can track rapidly changing sensory inputs or as discrimination devices that can support e.g. categorical perception. It further highlights the crucial role of networks to perform computations that are relevant to the brain cognitive functions.

In order to study the problem of distributed network processing and the network structure function relationship, it is important to develop experimental tools that address neurons on the network level. Moreover this will help us to understand the relationship between single neuron properties and population activity.

Neurons spontaneously form functional synapses when cultured in vitro and develop complex patterns of activity that closely resemble those recorded from developing brains of animals (Ben-Ari, 2001). Neurons retain their morphological and

pharmacological identities in culture but there are likely to be numerous subtle changes in their properties due to the unnatural environment in which they have been placed. Many techniques have been developed recently in order to track the activity of neurons grown in vitro and to tackle these network level activities. These techniques can be divided into electrophysiological or optical methods. Optical methods either use fast population calcium imaging or voltage sensitive imaging in order to track the activity of multiple neurons simultaneously. Electrical methods include planar titanium nitride based multielectrode arrays, CMOS based microelectrode arrays (Hafrizovic S et al. 2007), field effect transistor arrays (Fromherz P 2006), vertical nanowire arrays (Robinson JT et al. 2012) and gold mushroom shaped microelectrodes (Spira M et al. 2010) . Of particular interest are the nanoelectrode arrays that are still in the initial development phase and that promise to provide intracellular recordings & stimulation of many individual neurons while the electrodes maintain an extracellular position. Micha Spira coined the term “In cell recording” (Hai A et al. 2010) reflecting the fact that interfacing neurons with these arrays of nanoelectrodes will allow recordings of individual action potentials and sub-threshold potentials with matching quality and signal to noise ratio of conventional intracellular sharp glass microelectrodes or patch electrodes. Moreover, it will ultimately offer a high spatial resolution and might achieve the single synapses resolution so that one can monitor several synapses simultaneously.

Titanium nitride based multielectrode arrays (MEA) are produced with variable layouts, number of electrodes, electrode materials, electrode size and interelectrode distances specially for slice recording where a specific geometry is required to monitor activity of different brain regions: retina (Grumet et al. 2000, Meister et al. 1991), spinal cord (Borkholder et al. 1997) and Hippocampus (Boppart et al. 1992, Egert et al. 1998)

Multielectrode arrays have the advantages of being able to gather data from multiple sites in parallel, and to avoid the need to place all electrodes individually by hand.

On the other hand, they have the following limitations: Smaller amplitude recordings as compared to traditional instrumentation such as intracellular recordings because

the electrodes are not inserted inside the cells or the tissue and the electrodes cannot be moved independently because they are arranged in fixed patterns.

On the application side, MEAs have been used in neuronal and cardiac electrophysiological applications. They were used for multisite slice recordings on hypothalamic slices to investigate the effect of Ghrelin on hypothalamic network activity, on the activity of dissociated root ganglia cell cultures and on acute hippocampal slices investigating oscillations and rhythmic activity (Shimono et al. 2000) and to monitor synchronized cardiac muscle and stem cell culture activity. It can also be used for studying learning and memory on the network level (Eytan and Marom 2001, Jimbo et al. 1999) and to study of development of network electrical activity and population bursting dynamics (Wagenaar, D. et al. 2006). MEAs were also used to study retinal information processing and the role of correlations in the retinal circuitry (Ganmor E et al. 2011, Shneidmann E et al. 2006)

MEAs might also be used to establish highthroughput systems to perform drug screenings and toxicology studies (Gross and Pancrazio, 2006)

In the following chapters, I will present applications for a system “*Optical Network Electrophysiology*” we established that combines optical neurostimulation using optogenetics tools and multielectrode array recording of channelrhodopsin 2 transfected hippocampal neuronal culture. The first chapter will focus on the use of optical neurostimulation to induce network level plasticity and to modify the intrinsic network bursting dynamics. The second chapter will focus on a novel application of optical neurostimulation to establish a high throughout put technique that mimics in vivo like naturalistic activity.

3. References:

- Adamantidis AR, Zhang F, Aravanis AM, Deisseroth K, de Lecea L. (2007) Neural substrates of awakening probed with optogenetic control of hypocretin neurons. *Nature* 450:420–24
- Arrenberg AB, Del Bene F, Baier H. (2009). Optical control of zebrafish behavior with halorhodopsin. *Proc. Natl. Acad. Sci. USA* 106:17968–73
- Arrenberg AB, Stainier DY, Baier H, Huisken J. (2010) Optogenetic control of cardiac function. *Science*. Nov 12;330(6006):971-4.
- Atallah BV, Bruns W, Carandini M, Scanziani M. (2012) Parvalbumin-expressing interneurons linearly transform cortical responses to visual stimuli. *Neuron*. Jan 12;73(1):159-70.
- Ayling OG, Harrison TC, Boyd JD, Goroshkov A, Murphy TH. (2009). Automated light-based mapping of motor cortex by photoactivation of channelrhodopsin-2 transgenic mice. *Nat. Methods* 6:219–24
- Bamann C, Kirsch T, Nagel G, Bamberg E (2008) Spectral characteristics of the photocycle of channelrhodopsin-2 and its implication for channel function. *J Mol Biol* 375:686–694
- Bamann C, Gueta R, Kleinlogel S, Nagel G, Bamberg E.(2010) Structural guidance of the photocycle of channelrhodopsin-2 by an interhelical hydrogen bond. *Biochemistry*. 49(2):267-78.
- BellmannD, Richardt A, Freyberger R, NuwalN, Schwarzel M, et al. (2010). Optogenetically induced olfactory stimulation in *Drosophila* larvae reveals the neuronal basis of odor-aversion behavior. *Front. Behav. Neurosci.* 4:27
- Ben-Ari Y. (2001) Developing networks play a similar melody. *Trends Neurosci.* Jun;24(6):353-60.
- Berndt A, Yizhar O, Gunaydin LA, Hegemann P, Deisseroth K (2009) Bi-stable neural state switches. *Nat Neurosci* 12:229–234
- Berndt A, Schoenenberger P, Mattis J, Tye KM, Deisseroth K, Hegemann P, Oertner TG. (2011) High-efficiency channelrhodopsins for fast neuronal stimulation at low light levels. *Proc Natl Acad Sci U S A*. May 3;108(18):7595-600.
- Berndt A, Prigge M, Gradmann D, Hegemann P. (2010) Two open states with progressive proton selectivities in the branched channelrhodopsin-2 photocycle. *Biophys J*. Mar 3;98(5):753-61
- Berthold P et al (2008) Channelrhodopsin-1 initiates phototaxis and photophobic responses in *Chlamydomonas* by immediate light-induced depolarization. *Plant Cell* 20:1665– 1677.
- Boppart SA, Wheeler BC, Wallace CS. (1992) A flexible perforated microelectrode array for extended neural recordings. *IEEE Trans Biomed Eng.* Jan;39(1):37-42.

- Borkholder DA, Bao J, Maluf NI, Perl ER, Kovacs GT. (1997) Microelectrode arrays for stimulation of neural slice preparations. *J Neurosci Methods*. Nov 7;77(1):61-6.
- Busskamp V, Roska B. (2011) Optogenetic approaches to restoring visual function in retinitis pigmentosa. *Curr Opin Neurobiol*. Dec;21(6):942-6. Epub 2011 Jun 25.
- Cardin JA, Carlén M, Meletis K, Knoblich U, Zhang F, et al. (2010). Targeted optogenetic stimulation and recording of neurons in vivo using cell-type-specific expression of channelrhodopsin-2. *Nat. Protoc*. 5:247–54
- Cardin JA, Carlen M, Meletis K, Knoblich U, Zhang F, et al.(2009). Driving fast-spiking cells induces gamma rhythm and controls sensory responses. *Nature* 459:663–67
- Covington HE 3rd, Lobo MK, Maze I, Vialou V, Hyman JM, et al. (2010). Antidepressant effect of optogenetic stimulation of the medial prefrontal cortex. *J. Neurosci*. 30:16082–90
- Diester I, Kaufman MT, Mogri M, Pashaie R, Goo W, et al. (2011). An optogenetic toolbox designed for primates. *Nat. Neurosci*. 14:387–97
- Ernst OP et al (2008) Photoactivation of channelrhodopsin. *J Biol Chem* 283:1637–1643
- Egert U, Schlosshauer B, Fennrich S, Nisch W, Fejtl M, Knott T, Müller T, Hämmerle H. (1998) A novel organotypic long-term culture of the rat hippocampus on substrate-integrated multielectrode arrays. *Brain Res Brain Res Protoc*. Jun;2(4):229-42.
- Feldbauer K, Zimmermann D, Pintschovius V, Spitz J, Bamann C, Bamberg E.(2009) Channelrhodopsin-2 is a leaky proton pump. *Proc Natl Acad Sci U S A*. Jul 28;106(30):12317-22.
- Figueiredo M, Lane S, et al. (2011) Optogenetic experimentation on astrocytes. *Exp Physiol*. Jan;96(1):40-50.
- Fromherz P. (2006) Three levels of neuroelectronic interfacing: silicon chips with ion channels, nerve cells, and brain tissue. *Ann N Y Acad Sci*. Dec;1093:143-60.
- Golan L, Reutsky I, Farah N and Shoham S, (2009) Design and Characteristics of Holographic Photo-stimulation Systems, *Journal of Neural Engineering* 6(6), 66004.
- Gradinaru V, Mogri M, Thompson KR, Henderson JM, Deisseroth K. (2009). Optical deconstruction of parkinsonian neural circuitry. *Science* 324:354–59
- Ganmor E, Segev R, Schneidman E. (2011) The architecture of functional interaction networks in the retina. *J Neurosci*. Feb 23;31(8):3044-54.
- Grumet AE, Wyatt JL Jr, Rizzo JF 3rd. (2000) Multi-electrode stimulation and recording in the isolated retina. *J Neurosci Methods*. Aug 15;101(1):31-42.

- Hafizovic S., Heer F., Ugniwenko T. , Frey U., Blau A. , Ziegler C., Hierlemann A. (2007) "A CMOS-based microelectrode array for interaction with neuronal cultures" *Journal of Neuroscience Methods*, Vol. 164 p. 93-106.
- Hai A, Shappir J, Spira ME. (2010) In-cell recordings by extracellular microelectrodes. *Nat Methods*. Mar;7(3):200-2.
- Hai A, Shappir J, Spira ME. (2010) Long-term, multisite, parallel, in-cell recording and stimulation by an array of extracellular microelectrodes. *J Neurophysiol*. Jul;104(1):559-68.
- Han X, Qian X, Bernstein JG, Zhou HH, Franzesi GT, et al. (2009). Millisecond-timescale optical control of neural dynamics in the nonhuman primate brain. *Neuron* 62:191–98
- Harwood JL, Guschina IA (2009) The versatility of algae and their lipid metabolism. *Biochimie* 91:679–684
- Hwang RY, Zhong L, Xu Y, Johnson T, Zhang F, Deisseroth K, Tracey WD. (2007) Nociceptive neurons protect *Drosophila* larvae from parasitoid wasps. *Curr Biol*. 2007 Dec 18;17(24):2105-16
- Jimbo Y, Tateno T, Robinson HP. (1999) Simultaneous induction of pathway-specific potentiation and depression in networks of cortical neurons. *Biophys J*. Feb;76(2):670-8.
- Kato HE, Zhang F, Yizhar O, et al. (2012). Crystal structure of the channelrhodopsin light-gated cation channel. *Nature*. Jan 22;482(7385):369-74.
- Kleinlogel S, Feldbauer K, Dempski RE, Fotis H, Wood PG, Bamann C, Bamberg E. (2011) Ultra light-sensitive and fast neuronal activation with the Ca²⁺-permeable channelrhodopsin CatCh. *Nat Neurosci*. Apr;14(4):513-8.
- Lewis TL Jr, Mao T, Arnold DB. (2011) A role for myosin VI in the localization of axonal proteins. *PLoS Biol*. Mar;9(3):e1001021.
- Lin JY, Lin MZ, Steinbach P, Tsien RY (2009) Characterization of engineered channelrhodopsin variants with improved properties and kinetics. *Biophys J* 96:1803–1814
- Lin JY. (2011) A user's guide to channelrhodopsin variants: features, limitations and future developments. *Exp Physiol*. Jan;96(1):19-25.
- Llewellyn ME, Thompson KR, Deisseroth K, Delp SL. (2010). Orderly recruitment of motor units under optical control in vivo. *Nat. Med*. 16:1161–65
- Low SE, Ryan J, Sprague SM, Hirata H, Cui WW, et al. (2010). touche is required for touch-evoked generator potentials within vertebrate sensory neurons. *J. Neurosci*. 30:9359–67
- Luo L, Callaway EM, Svoboda K. (2008) Genetic dissection of neural circuits. *Neuron*. Mar 13;57(5):634-60.

- Lutz C., T. Otis, V. de Sars, S. Charpak, D. DiGregorio, V. Emiliani, (2008). Holographic photolysis of caged neurotransmitters. *Nature Methods*. vol.5. 9. September. 821-827
- Marom S, Shahaf G. (2002) Development, learning and memory in large random networks of cortical neurons: lessons beyond anatomy. *Q Rev Biophys*Feb;35(1):63-87
- Meister M, Wong RO, Baylor DA, Shatz CJ. (1991) Synchronous bursts of action potentials in ganglion cells of the developing mammalian retina. *Science*. May 17;252(5008):939-43.
- Nagel G et al (2002) Channelrhodopsin-1: a light-gated proton channel in green algae. *Science* 296:2395–2398
- Nagel G et al (2003) Channelrhodopsin-2, a directly light-gated cation-selective membrane channel. *Proc Natl Acad Sci U S A* 100:13940–13945
- Nagel G, Brauner M, Liewald JF, Adeishvili N, Bamberg E, Gottschalk A. (2005) Light activation of channelrhodopsin-2 in excitable cells of *Caenorhabditis elegans* triggers rapid behavioral responses. *Curr Biol*. Dec 20;15(24):2279-84.
- Nikolic K, Grossman N, Grubb MS, Burrone J, Toumazou C, Degenaar P. (2009) Photocycles of channelrhodopsin-2. *Photochem Photobiol*. Jan-Feb;85(1):400-11.
- Pouget A, Dayan P, Zemel R.(2000) Information processing with population codes. *Nat Rev Neurosci*. Nov;1(2):125-32.
- Ritter E, Stehfest K, Berndt A, Hegemann P, Bartl FJ (2008) Monitoring light-induced structural changes of channelrhodopsin-2 by UV-visible and Fourier transform infrared spectroscopy. *J Biol Chem* 283:35033– 35041.
- Robinson JT, Jorgolli M, Shalek AK, Yoon MH, Gertner RS, Park H. (2012) Vertical nanowire electrode arrays as a scalable platform for intracellular interfacing to neuronal circuits. *Nat Nanotechnol*. Jan 10;7(3):180-4.
- Schneidman E, Berry MJ 2nd, Segev R, Bialek W. (2006) Weak pairwise correlations imply strongly correlated network states in a neural population. *Nature*. Apr 20;440(7087):1007-12.
- Schoonheim PJ, Arrenberg AB, Del Bene F, Baier H. (2010) Optogenetic localization and genetic perturbation of saccade-generating neurons in zebrafish. *J. Neurosci*. 30:7111–20
- Shimono K, Brucher F, Granger R, Lynch G, Taketani M.(2000) The origin and distribution of cholinergically induced beta rhythm in hippocampal slices. *J Neurosci*. 2000 Nov 15;20(22):8462-73.
- Sineshchekov OA, Govorunova EG, Spudich JL (2009) Photosensory functions of channelrhodopsins in native algal cells. *Photochem Photobiol* 85:556–563

- Sineshchekov OA, Jung KH, Spudich JL (2002) Two rhodopsins mediate phototaxis to low- and high-intensity light in *Chlamydomonas reinhardtii*. *Proc Natl Acad Sci U S A* 99:8689–8694
- Sohal VS, Zhang F, Yizhar O, Deisseroth K. (2009). Parvalbumin neurons and gamma rhythms enhance cortical circuit performance. *Nature* 459:698–702
- Stenger DA, Gross GW, Keefer EW, Shaffer KM, Andreadis JD, Ma W, Pancrazio JJ. (2001) Detection of physiologically active compounds using cell-based biosensors. *Trends Biotechnol.* Aug;19(8):304-9
- Stuber GD, Hnasko TS, Britt JP, Edwards RH, Bonci A. (2010). Dopaminergic terminals in the nucleus accumbens but not the dorsal striatum corelease glutamate. *J. Neurosci.* 30:8229–33
- Szobota, S. and Isacoff, E. Y. (2010). Optical control of neuronal activity. *Annu Rev Biophys*, 39, 329-348.
- Tecuapetla F, Patel JC, Xenias H, English D, Tadros I, et al. (2010). Glutamatergic signaling by mesolimbic dopamine neurons in the nucleus accumbens. *J. Neurosci.* 30:7105–10
- Tolhurst DJ, Movshon JA, Dean AF (1983) The statistical reliability of signals in single neurons in cat and monkey visual cortex. *Vision Res* 23:775–785.
- Tønnesen J, Sørensen AT, Deisseroth K, Lundberg C, Kokaia M. (2009) Optogenetic control of epileptiform activity. *Proc Natl Acad Sci U S A.* Jul 21;106(29):12162-7. Epub 2009 Jul 6.
- Tsunoda SP, Hegemann P (2009) Glu 87 of channelrhodopsin-1 causes pH-dependent color tuning and fast photocurrent inactivation. *Photochem Photobiol* 85:564–569
- Usrey WM, Reid RC. (1999) Synchronous activity in the visual system. *Annu Rev Physiol.* 61:435-56.
- Wagenaar DA, Pine J, Potter SM. (2006) An extremely rich repertoire of bursting patterns during the development of cortical cultures. *BMC Neurosci.* Feb 7;7:11.
- Wang H et al (2009) Molecular determinants differentiating photocurrent properties of two channelrhodopsins from *Chlamydomonas*. *J Biol Chem* 284:5685–5696
- Wang, S., Szobota, S., Wang, Y., Volgraf, M., Liu, Z., Sun, C., Trauner, D., Isacoff, E.Y., and Zhang, X (2007). All optical interface for parallel, remote, and spatiotemporal control of neuronal activity. *Nano Lett.* 7, 3859-63.
- Warnock JN, Daigre C, Al-Rubeai M. (2011) Introduction to viral vectors. *Methods Mol Biol.* 737:1-25.
- Yizhar O, Fenno LE, Prigge M, Schneider F, et al. (2011) Neocortical excitation/inhibition balance in information processing and social dysfunction. *Nature.* Jul 27;477(7363):171-8.

CHAPTER 2

Optogenetic Induction of Network Level Plasticity

1. Introduction:

1.1. Bursting in neuronal networks:

Regular synchronized bursting of population of neurons has been observed in hippocampus (Kandel and Spencer 1961), visual cortex (Cattaneo et al. 1981a), in the lateral geniculate nucleus (Reinagel P et al 1999) and in Striate cortex (Martinez – Conde S et al. 2000). Bursting has been implicated in the development of neural circuits in visual system (Hanganu IL et al. 2006, Rochefort et al. 2009), in barrel cortex (Minlebaev et al. 2009) and in hippocampus (Leinekugel X. et al. 2002).

Bursting has also been proposed as a coding scheme (Kepecs A. et al. 2003) for neuronal communication in primary sensory neurons (Krahe R. et al. 2004), in insect auditory system (Eyherabide HG et al. 2008) and lateral geniculate nucleus (Lesica NA. et al. 2004). In vitro pyramidal neurons bursting underlie population synchrony in hippocampal and cortical slices (Silva LR. et al. 1991, Miles R. et al. 1988). Moreover, bursting also has been implicated in synaptic plasticity (Huerta PT. 1995, Thomas MJ. et al. 1998). In addition, neuronal network bursting and synchronization have clinical implications. Increased neuronal bursting and synchronization are hallmarks for many neurological diseases specially epilepsy (Holtkamp M. et al. 2011) and Parkinson's disease (Heimer G. et al. 2006). On the other hand, there are diseases where lack of neural synchrony might lead to cognitive dysfunction as has been argued for the case of schizophrenia (Uhlhass PJ. et al. 2010).

Cultured networks of hippocampal neurons exhibit spontaneous synchronized network bursts that can serve as a simplified model system for studying the origins and determinants of bursting dynamics. Bursts in cultured hippocampal networks critically depend on excitatory glutamatergic neurotransmission. In addition, GABAergic interneurons control the exact degree of synchronization in the network's activity by restricting the temporal spread of individual network bursts. Thus the temporal structure of these bursts underlies network synchronization (Cohen E. et al. 2008). Cultured hippocampal neurons plated on substrate integrated multielectrode arrays can be used reliably to measure the synchronized bursting behavior with high coverage and temporal precision (Wagenaar D.A. et al. 2006)

1.2. Synchronization in neuronal networks:

Synchrony is an important temporal relationship between neurons which can be broadly defined as a temporally correlated activity between neurons (Salinas E. et al. 2001) Dual intracellular recording during visual stimulation demonstrated that correlations of membrane potential fluctuations which reflect the cells' input can be stimulus dependent too (Lamp I et al. 1999, Yu I et al. 2010). Decoding strategies that exploit the inter-neuron spike dependencies in the primate retina are capable of extracting 20% more information about the visual scene than decoding under the assumption of independence and also preserve 40% more visual information than optimal linear decoding (Pillow J. et al. 2008) Pairwise correlations have been shown to predict multineuronal firing patterns in the vertebrate retina (Schneidman E. et al. , 2006) and across larger distances in the cortex (Ohiorhenuan I. et al. 2010).

Correlation has been seen as an additional coding dimension which by its turn seems to be important in gating the flow of information across neural network, without effects on the meaning of the conveyed information (deCharms R.C. et al. 1996, Moreno-Bote R. et al., 2008). The emergence of synchronous events can result from a variety of mechanisms (Pikovsky A. et al. , 2002). In neuronal networks, stimulus induced and intrinsic noise spike

correlations both originate to a great degree from the connectivity of a neuronal network. Each cortical neuron receives inputs from approximately 10^4 other neurons and sends out signals via its synapses to about 10^4 others (Abeles M. , 1991; Braitenberg V. 1998). Because neurons are highly interconnected, it is highly probable that two neurons in a network share some of their inputs. It is important to mention here that synchronized oscillations have been shown to establish the precision in spike timing that is crucial for use dependent synaptic plasticity (Wespatat, V et al. 2004) A subtle change in the amount of synchrony can make a large difference for many cellular processes such as synaptic plasticity or synaptogenesis. It can also strongly affect the information content conveyed by the spike trains. Moreover, synchronization is greatly influenced by the network connectivity.

Synchronous oscillatory activity encodes information about stimuli and influence transmission of activity from one a neuronal population to another (Tiesinga PH et al. 2004, Reyes, AD 2003). Synchronous activity allows groups of neurons with common postsynaptic targets to depolarize these targets more effectively leading to better propagation of spiking to downstream targets (Burkitt A.N., Clark G.M. 1999) Such short range and long range synchronization might be generated by several distinct mechanisms. Local oscillations are often considered to arise owing to features of local circuit connectivity. For example, Gamma oscillations (which typically range from 40 to 80 Hz) can be generated from the interplay of pyramidal cells and local circuit interneurons. On the other hand, Spike time dependent plasticity (STDP) plays a crucial role in neuronal networks development. The interplay between between STDP and neuronal synchronization has profound functional consequences (Peter J. Uhlhaas et al. 2009). STDP requires that pre and postsynaptic spiking to happen within a critical window (Markram, H. et al. 1997). Stimulation at the depolarizing peak of the theta cycle in the hippocampus favors long term potentiation whereas stimulation in the trough causes depression (Huerta, P.T. & Lisman, J.E. 1993). In general terms, significant cross-correlations are due to the presence of direct synaptic connections and/or from common or correlated inputs between two neurons

(Turker KS. et al. , 2002, Fujisawa S. et al. 2008, Ostojic S. et al., 2009, Tchumatchenko T. et al . 2010). The amplitude of the cross correlations, hence, depends on the properties of the synapses involved but it is also modulated by the general activity of the network (Constantinidis et al. 2001, Ostojic et al. 2009, Battaglia et al. 2012)

1.3. Synaptic plasticity:

Electrical activity plays crucial roles in the structural and functional refinement of neuronal circuits throughout an organisms lifetime (Katz LC and Shatz CJ 1996) Learning and memory are likely to be mediated by activity dependent circuit modifications. Modification of neuronal network dynamics is due to its ability to undergo synaptic plasticity. Plasticity is the term referred to the ability of neurons to change its synaptic efficacy in response to experience and it is thought to be the principle underlying learning and memory (Milner B. et al., 1998). Long-term potentiation (LTP) in the hippocampus is the most characterized model of synaptic plasticity. Two features of LTP, the associativity and input specificity, match the properties of some forms of learning and memory, suggesting that LTP may underlie such cognitive functions. It can be induced in hippocampal slices by a high-frequency train of stimulation of the Schaffer collaterals that make synaptic contacts with the dendrites of CA1 neurons and is characterized by an increase in the amplitude of the excitatory postsynaptic potentials (Bliss TV & Lomo T, 1973). The canonical pathway involved in LTP includes depolarization of the postsynaptic neuron and the activation of its NMDA receptors by glutamate, which leads to an increase in intracellular Ca^{+2} concentrations that activates Ca^{2+} -calmodulin dependent protein kinase 2 (CamKII), that in turn phosphorylates the subunit 1 of the AMPA receptors, increasing thus the amount of functional AMPA receptors in the membrane. Additionally, Ca^{+2} can activate other kinases as PKC and together with CamKII phosphorylate other signaling proteins involved in gene transcription (*e.g.* CREB) (Lee YS & Silva AJ, 2009).

LTP has been reported for a large number of neural circuits including various neocortical areas (Artola & Singer 1987, Iriki et al. 1989, Hirsch et al. 1992), the amygdala (Chapman et al. 1990) and the midbrain reward circuit (Liu et al. 2005).

It is widely agreed that LTP has two phases: the first one, called early-LTP, with a duration of minutes to less than 2 hours, and independent of protein synthesis; the second is called late-LTP, lasts more than 2 hours and depends on protein synthesis and gene transcription (Gkogkas *et al.*, 2010). In spite of the fact that not ongoing transcription is necessary to induce early-LTP, it has been reported (as early as 20 minutes after LTP induction) an up-regulation in the transcription of many immediate early genes considered to have a crucial role in stabilize and maintain the LTP response (Ryan *et al.*, 2011).

LTP requires newly synthesized mRNA and proteins, while the short-term forms of synaptic plasticity do not (Kandel, 2001). However, there is a time period that is critical for both synaptic plasticity and memory formation. This is evident from the fact that LTP can be prevented only when mRNA or protein synthesis is blocked immediately post the LTP-inducing stimulation. Hence, the gene expression occurring immediately after induction is critical of establishing and maintaining long-term neuronal changes (Nguyen, et al., 1994). The genes that fall in this category are classified as immediate early genes.

Immediate early genes (IEGs) are the subset of genes which show rapid but transient increase in expression in response to extracellular signals such as growth factors and neurotransmitters. This increase in expression is protein synthesis independent, which explains its fast kinetics as protein synthesis is a slower process (Wickliffe, et al., 1992). IEGs are expressed in adult neurons both as constitutive genes and in response to afferent activity. Neuronal IEGs encompass a large repertoire; they may encode transcription factors (*c-fos*, *fos B*, *c-jun*, *zif268*), cytoskeletal proteins (*Arc*), growth factors (*Activin β A*), metabolic enzymes (*Cox-2*) and proteins involved in signal transduction

(RSG-2, SNK/Plk-2), that may result in expression of genes critical for consolidation of long-term memory (Lanahan et al., 1998, Okuno, 2011).

As mentioned earlier IEGs can either be transcription factors or directly modify cellular function. For example *Zif268* is transcribed in the dentate gyrus of the hippocampus upon LTP induction. *Zif268* encodes a zinc finger transcription factor and is needed for maintenance of LTP and for the expression of long term memories (Jones, et al., 2001). IEGs are induced following LTP and IEG response is linked to the course of LTP via the IEG transcription factors that regulate the expression of other genes, referred to as the effector genes. These effector genes may directly support LTP expression or may only play a role in the stabilization of LTP (Wickliffe, et al., 1992).

Some IEGs that are implicated in directly modifying cellular function e.g. *Arc*, a cytosolic protein which is a regulator of AMPAR trafficking, interacts with cytoskeletal proteins and may also be involved in modifying structural proteins and kinases (Shepherd et al., 2011). IEGs generally form a part of a well structured programme that regulates long-term cellular responses.

An important immediate early gene that is upregulated upon LTP induction is the IEG *Arc*. *Arc* accumulates at sites of synaptic activity (Lyford et al. 1995). It has been suggested that it couple synaptic activity to protein synthesis dependent synaptic plasticity. The induction *Arc* mRNA and protein in the hippocampus, during exploration of new environments is so robust and reproducible that mapping *Arc* induction is a powerful method to pin-point neuronal networks responsible (Shepherd et al. , 2011). It is stipulated that sustained *Arc* synthesis is necessary to maintain LTP, for protein synthesis-dependent consolidation of synaptic modifications and *Arc* also maintains normalized neuronal output without changing the relative strength of individual synapses by scaling of AMPAR (Shepherd et al. , 2011). Activation of NMDA type glutamate receptors and extracellular regulated kinase (ERK) are necessary for *Arc* transcription following LTP induction

(Steward et al. 1998, Steward et al. 2001) and in response to neuronal activity in primary hippocampal or cortical neuronal cultures (Rao et al. 2006).

There is yet another form of plasticity that is relevant to neuronal network dynamics referred to as Spike timing-dependent plasticity (STDP). If pre-synaptic activity occurs before the post-synaptic action potential, then LTP occurs. However, if the pre-synaptic activity follows post-synaptic action potential, long term depression (LTD) occurs. This precise timing between pre- and post-synaptic activities for the induction of different forms of synaptic plasticity has led to this phenomenon being called Spike timing-dependent plasticity. STDP mainly arises from timing-dependent differences in post-synaptic Ca^{2+} signals (Dan et al., 2006). Spike timing dependent plasticity (STDP) (Abbott et al. 2000) has been observed at excitatory synapses in a wide variety of neural circuits (Boettinger et al. 2001, Cassenaer et al. 2007, Egger et al. 1999) Compared with the correlational forms of synaptic plasticity, STDP captures the importance of causality in determining the direction of synaptic modifications. STDP in vivo has important implications in the developmental refinement of the retinotectal projection: a strong input that can elicit spiking by itself should have a competitive advantage among converging inputs. The functional consequence of STDP has also been examined in the mammalian visual system. STDP has also been found in many other circuits in vivo such as rat barrel cortex (Allen et al. 2003), in the hippocampus (Mehta et al. 2000) and in the human motor cortex (Stefan et al. 2002).

1.4. Network level plasticity:

As previously mentioned that bursting dynamics is a hallmark of in vitro cultured neuronal networks and considering the importance of bursting phenomenon, it is crucial to understand how network burst can be modified experimentally or therapeutically. Acknowledging its importance, it is important to develop experimental paradigms to control bursting dynamics on one hand or to change the ability of the network to synchronize on the other hand.

A number of studies have tackled the properties of network level plasticity. Eytan et al. 2003 have used electrical stimulation to look at the response of two stimulus of different frequencies and the network was more sensitive to the less frequent stimulus provided the network is primed by a high ,not tetanizing stimulus ,from another site. This means that the network can selectively adapt for the detection of a particular stimulus. It highlights that the network can undergo what can be called “selective learning”. In another study, Jimbo et al. 1999 has used high frequency tetanic stimulation (20 Hz) at 5 second intervals. The stimulus was applied to multiple stimulation sites which trigger either potentiation or depression depending on the pathway that a specific site activates. It indicates that are distinct pathways either potentiating or depressing within the network. Bakkum et al. 2008 used patterned electrical stimulation with a 0.5 Hz stimulation rate for 40 minutes to induce activity dependent long term plasticity of action potential propagation which is considered to be a new substrate for network level plasticity. In another study, Madhavan et al. 2007 have used strong local tetanic stimulation which resulted in significant changes in the occurrences of spontaneous bursts belonging to different clusters indicating that the dynamic flow of information in the neuronal network had been altered. They observed changes in burst size and the burst duration along with the burst initiation zone. Maeda et al. 1998 have used tetanic stimulation to elicit changes in the bursting dynamics. The aforementioned paradigm has led to an increase of the burst rate and the intraburst firing rate

Modification of bursting dynamics in neuronal networks is crucial for the design of stimulation paradigms to modify disease states such as epilepsy, parkinson’s and schizophrenia. It will also have implications on the design og novel neuro-electronic interfaces and the establishment of neurocomputing systems that harness the distributed information processing capabilities of neuronal networks (Wagenaar et al. 2005, Feinermann et al. 2008) .

Studies focusing on neuronal plasticity have primarily used electrical stimulation. Electrical stimulation has the disadvantage of producing huge artifacts (Wageenar D, Potter S 2002) microelectrodes are fixed in position “substrate embedded” so the stimulation sites are fixed. Thus, it is only possible to stimulate a small subset of neurons. Previous studies aiming to activate neuronal networks globally used chemical induction methods. Chemical induction offers the advantage of activating several synapses simultaneously but pose problems as the added chemicals might interfere with the physiological state of the network and its development (Molnar 2011). Moreover, it lacks the temporal control. Ivenshitz et al. 2006 used chemical LTP to induce persistent changes in excitatory and inhibitory neurons that remained persistent for one hour after potentiation.. Moreover, the network synchronization increased after chemically induced plasticity in this case. On the other hand, Cohen et al. 2009 have used chronic exposure to low concentration of NMDA for 2 to 7 days to destroy network bursts and it recovered within two days of removing the drug. The previous two studies highlight the fact that global chemical plasticity induction can be used to dramatically modify network bursts either abolishing or increasing it.

Another form of network level plasticity is homeostatic plasticity which can be induced by chronic treatment with pharmacological blockers. Chronic depolarization using GABAergic transmission blockers or activity deprivation using tetrodotoxin leads to homeostatic plasticity. Homeostatic plasticity is mechanistically mediated via synaptic scaling or intrinsic homeostatic mechanisms (Turrigiano G.2011, 2012).

Alternative to the aforementioned chemical induction method for global network activation, optogenetic tools offer a non invasive method to globally activate neuronal networks by whole field optical stimulation. Optogenetic tools such as channelrhodopsin 2 has proven efficient to stimulate neurons with a high temporal and spatial resolution (refer to the general introduction 1.1.) .Optogenetics can help the network to change its intrinsic dynamics and can also be used to manipulate the network synchronization. Some studies

have used optogenetics to mimic natural neuronal synchronization in the olfactory system (Blumhagen F. et al. 2011) or to manipulate neural synchrony by affecting the neuronal spike timing to study its role in neural computation (Han X et al. 2009). On the other hand, few studies have used optogenetics to increase or decrease network level synchronization. A study by Tonnesen et al. 2009 has established optogenetic hyperpolarization of neurons in the hippocampal neurons using halorhodopsin to suppress synchronized epileptiform activity. An interesting question is whether one can enhance network synchronization using optogenetic stimulation or these network states are stable and cannot be pushed further.

On the other hand, Channelrhodopsin 2 has also been used to induce plasticity at single synapses using 0.5 Hz stimulation frequency that lead to an increase in the spine volume accompanied by an increase in the (Zhang Y et al. 2008). Grubb M et al. 2010 have used a photostimulation paradigm (steady photostimulation of 1Hz light pulses grouped in bursts) for two days to induce significant distal changes in AIS location which leads to changes in neuronal excitability.

1.5. Aim of the Study:

Acknowledging the importance of modifying intrinsically generated collective network dynamics, the study in this chapter aims at investigating the use of mild photostimulation paradigm to modify neuronal networks' collective dynamics. The study focuses on the modification of the firing rate dynamics, bursting dynamics and synchronization. Moreover, it aims at investigating the cellular and molecular mechanisms underlying the modification of network collective dynamics.

Contributions:

In the following study, I have done all experimental procedures including preparing primary hippocampal cultures on multielectrode arrays, transfecting cultures with AAV-ChR2, performing & establishing the photostimulation and recording routines. I also performed all the experimental procedures related to the gene microarray analysis. On the side of data analysis, the firing rate dynamics (including the firing rate and the peri stimulus time histogram), burst detection and burst analysis was performed by Ghazaleh Afshar (Max Planck Institute for Dynamics and Self Organization, Goettingen). On the other hand, I performed the cross correlation analysis, the conditional firing rate analysis and the microarray data analysis.

2. Results

2.1. Experimental system design

Our experimental setup as shown in Fig 2.1 combines multichannel recording using microelectrode arrays and whole field photo-stimulation using blue light emitting diode (LED). Whole field illumination is performed using a high power blue LED that allows homogeneous illumination. Fig.2.1 shows 21DIV embryonic hippocampal neurons plated on 60 channels multi-electrode array (MEA) transfected with AAV1/2-CHOP2-YFP virus. The transfection efficiency was consistently high which allowed us to drive the whole network with our optical stimulation paradigm. As has been previously reported that 21DIV neuronal cultures show spontaneous activity characterized by burst separated by periods of silence (Wageenar D et al. 2006), our cultures show bursting interrupted by periods of silence (fig.2.1). It is important to note that in our experiments electrode spikes (waveforms) were used without any attempt for spike sorting.

The typical 20 minutes recording obtained from one culture and photo-stimulation paradigms are shown in Fig 2.1. For each experiment, we have four phases of activity: (1) spontaneous activity of unperturbed culture; (2) stimulation; (3) silent period and (4) spontaneous activity after stimulation. For each experiment, the spontaneous activity of the culture was recorded for 5 min before the onset of the stimulation. Using whole field blue light stimulation, the neuronal cultures on MEA were stimulated with either constant or ramp 40x1 second pulses of frequency 0.5Hz. Then the stimulation was switched off and the spontaneous activity was recorded for 15minutes. During the stimulation, the network responds as expected to the blue light stimulation by an increase in the firing rate. We found that the average firing rate dynamics during constant stimulation is different from ramp stimulation. This difference can be seen in the peri-stimulus time histogram (PSTH) plot in Fig. 2.1. With constant photostimulation, the firing rate during each pulse of stimulation raises to maximum faster than the

stimulation with ramp. With the ramp photo-stimulation, channelrhodospin 2 inactivates much slower and thus firing rate rises more slowly to the maximum and the maximum firing rate is lower than in the case of the constant stimulation. The aforementioned differences in the firing rate dynamics in the case of constant and ramp photostimulation indicate that in the case of ramp stimulation there are less spikes driving the neuronal networks. After stimulation, there is a silent period that varies in length from a couple of seconds to tens of seconds where no synchronized activity is detected. Then the network resumes the state of ongoing bursting activity.

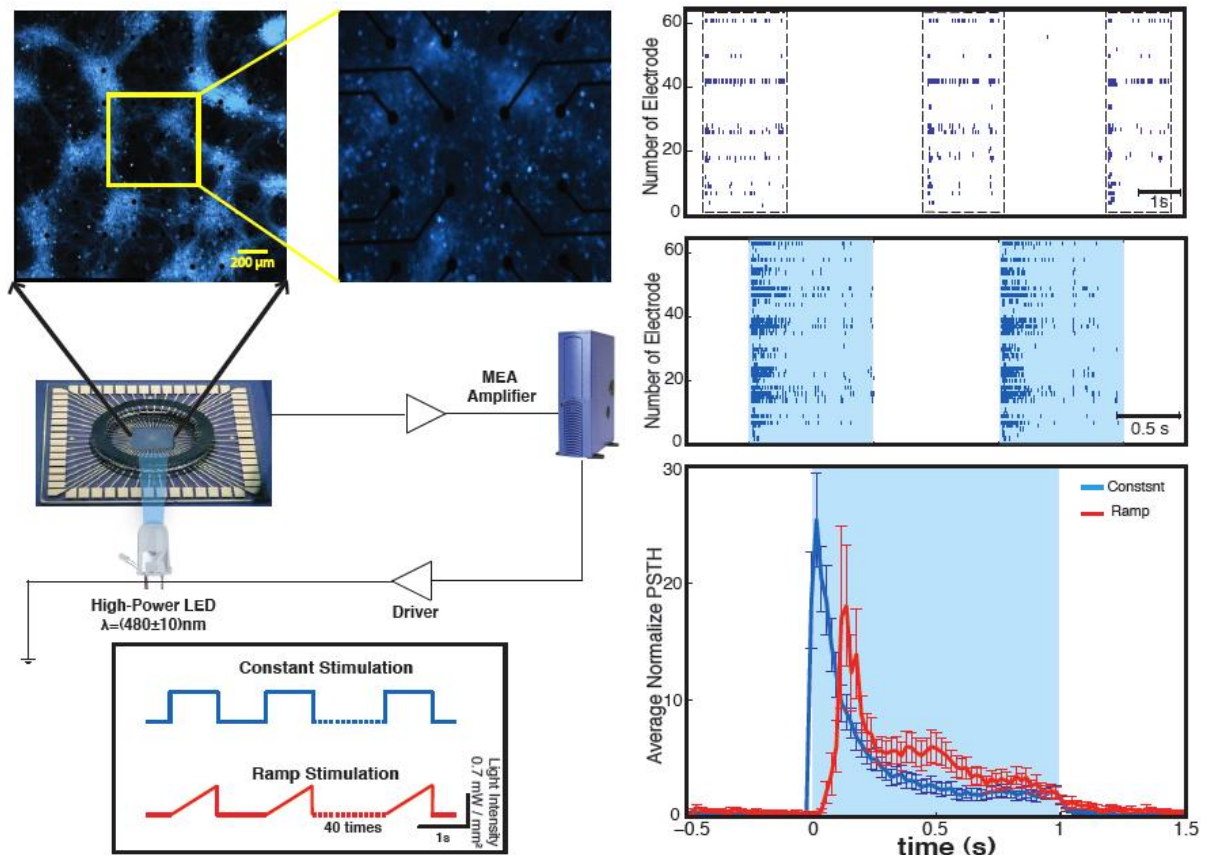


Fig 2.1.: Optical Network Electrophysiology: In the upper left side is the experimental setup depicting channelrhodopsin 2 transfected neurons plated on multi-electrode arrays stimulated with the whole field blue light illumination using high power LED (middle left). The cultures are stimulated with either constant or ramp stimuli (inset in the lower left). The data is acquired by the MEA amplifier and fed into a recording computer.. The upper right panel is a representative raster plot of the spontaneous activity of the network before stimulation across the 60 electrodes. The middle right figure is the spontaneous activity of the network during blue light stimulation. The light blue color indicates the blue light stimulation. The lower right figure is the peri-stimulus time histogram (PSTH) for both constant (dark blue) and ramp stimulation (red). The PSTH and spiking activity plots were provided by Ghazaleh Afshar (Max Planck Institute for Dynamics and Self Organization, Goettingen)

2.2. Network firing rate increases after stimulation

We investigated the change in firing rate dynamics of the recovered network activity after switching off the stimulation (Fig 2.2.). With both ramp and constant stimulation, we found that the normalized average firing rate increased significantly after stimulation compared to the unperturbed spontaneous activity before stimulation. In case of constant illumination, the normalized average firing rate (average over 22 experiments from a total of 19 cultures) significantly increases 26% after stimulation ($p < 10^{-7}$, significant, Wilcoxon's rank sum test).. As for the ramp illumination, the normalized average firing rate (averaged over 19 experiments from 16 cultures) significantly increases 35% after stimulation ($p < 10^{-5}$, significant, Wilcoxon's rank sum test).

The increase in the normalized average firing rate after stimulation is higher in case of ramp illumination compared to constant illumination. It is important to note that with the control untransfected cultures stimulated with blue light and the control transfected unstimulated culture, there was no change observed in the average normalized firing rate (Fig 2.3).

2.3. Network bursting dynamics change after stimulation

As previously mentioned, bursts are a hallmark of matured hippocampal cultures and its modification is one of the mechanisms by which information is encoded in the network. The network bursting dynamics were assessed using burst rate and intraburst firing rate that reflect the underlying network burst structure. With constant and ramp illumination, the normalized average burst rate and normalized average intra-burst firing rate significantly increase after stimulation.

In case of constant illumination, the normalized average intraburst firing rate (averaged over 22 experiments from a total of 19 cultures) significantly increases 25% after stimulation compared to before stimulation ($p < 10^{-6}$, significant, Wilcoxon rank sum test). The normalized average burst rate

(averaged over 22 experiments from a total of 19 cultures) significantly increases 20% after stimulation compared to before stimulation ($p < 10^{-6}$, significant, Wilcoxon's rank sum test).

In case of ramp illumination, the normalized average intraburst firing rate (averaged over 22 experiments from a total of 19 cultures) after stimulation has 35% significant increase compared to before stimulation with ($p < 10^{-5}$, significant, Wilcoxon rank sum test). On the other hand, the normalized average burst rate significantly increases 24% after stimulation compared to before stimulation ($p < 10^{-5}$, significant, Wilcoxon rank sum test).

Concerning the burst duration distribution, the burst duration slightly changes after stimulation in case of ramp and constant illumination (Fig. 2.4.). In case of constant illumination, the mean burst duration before stimulation is $0.82\text{s} \pm 0.07\text{ s}$ (average over 1276 bursts), the mean burst duration after stimulation is $0.83\text{ s} \pm 0.10\text{ s}$ (average over 1434 bursts). In case of ramp illumination, the mean burst duration before stimulation is $0.94\text{ s} \pm 0.14\text{ s}$ (average over 1060 bursts) and the mean burst duration after stimulation is mean is $0.88\text{ s} \pm 0.13\text{ s}$ (average over 1202 bursts).

At this point, it is becoming apparent that mild whole field blue light stimulation can modify network bursting dynamics and that stimulation with ramps of light have more pronounced effect on bursting dynamics than constant stimulation.

It is important to note that with the control untransfected cultures stimulated with blue light and control transfected non stimulated cultures, there was no change observed in the average normalized intraburst firing rate and the average normalized burst rate (Fig. 2.3.)

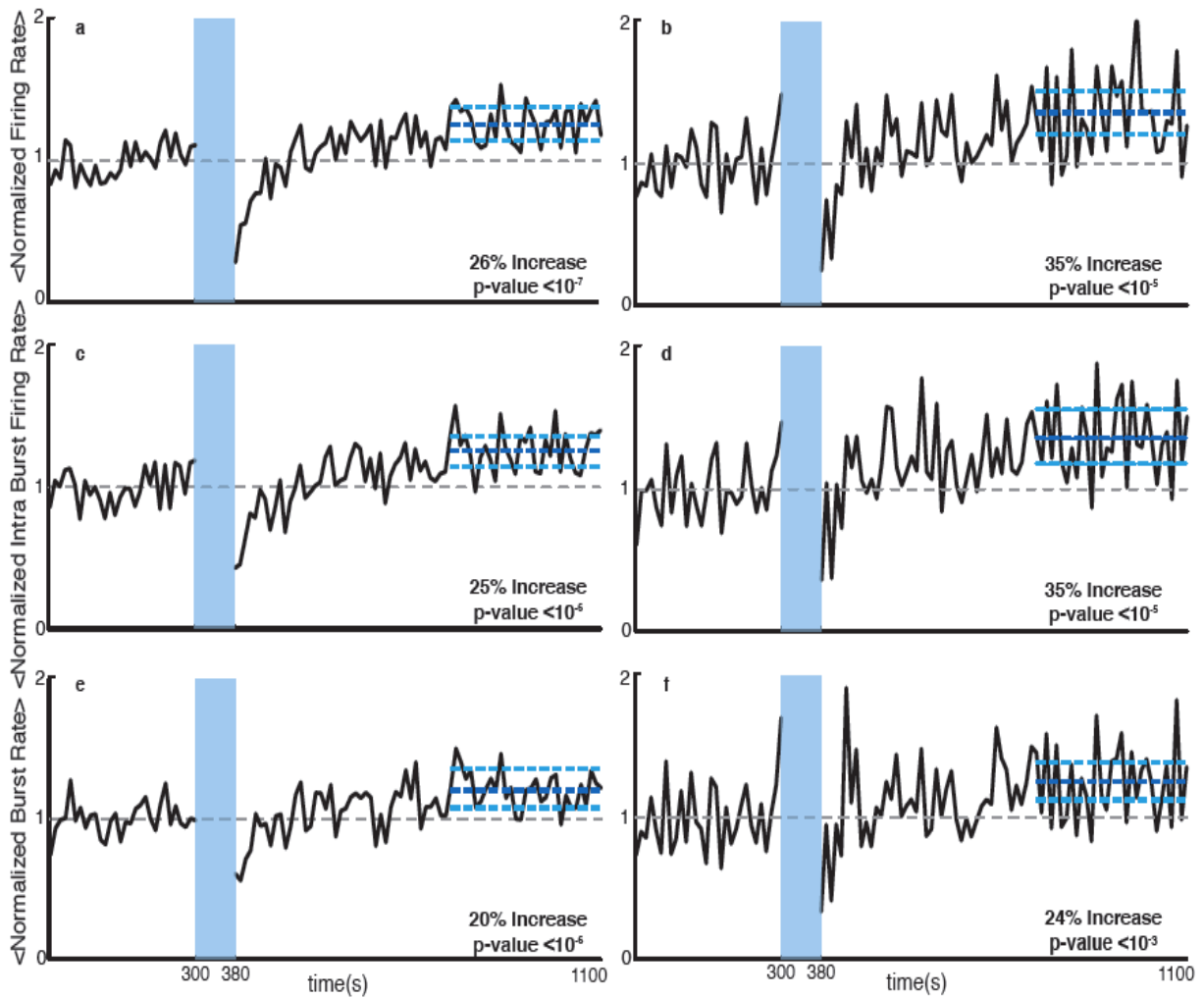


Fig 2.2: The network collective dynamic changes: Plots on the left side are for constant stimulation and the plots on the right side are for the ramp stimulation. **(a,b)** The normalized average firing rate before and after stimulation. The dotted grey line is the mean firing rate before stimulation and the dark blue line is the mean firing rate after stimulation. **(c,d)** The average normalized intraburst firing rate. The dotted grey line is the mean intraburst firing rate and the dark blue line is the mean intraburst firing rate after stimulation. **(e,f)** The normalized average burst rate. The dotted grey line is the mean burst rate before the stimulation and the dark blue line is the average burst rate after stimulation. In all plots, the light blue lines are the 95% bootstrap confidence interval. The light blue column in all figures between 300 s and 380 s is the blue light stimulus. The p values are indicated on each plot indicating the significance level computed for the increase of either firing rate, burst rate or intraburst firing rate in the last 5 minutes of recording. The results with the constant stimulation are averages over 22 experiments from 19 cultures and the results with the ramp stimulation are averages over 19 experiments from 16 cultures. The figure and the data analysis included in the figure were provided by Ghazaleh Afshar (Max Planck Institute for Dynamics and Self Organization, Goettingen).

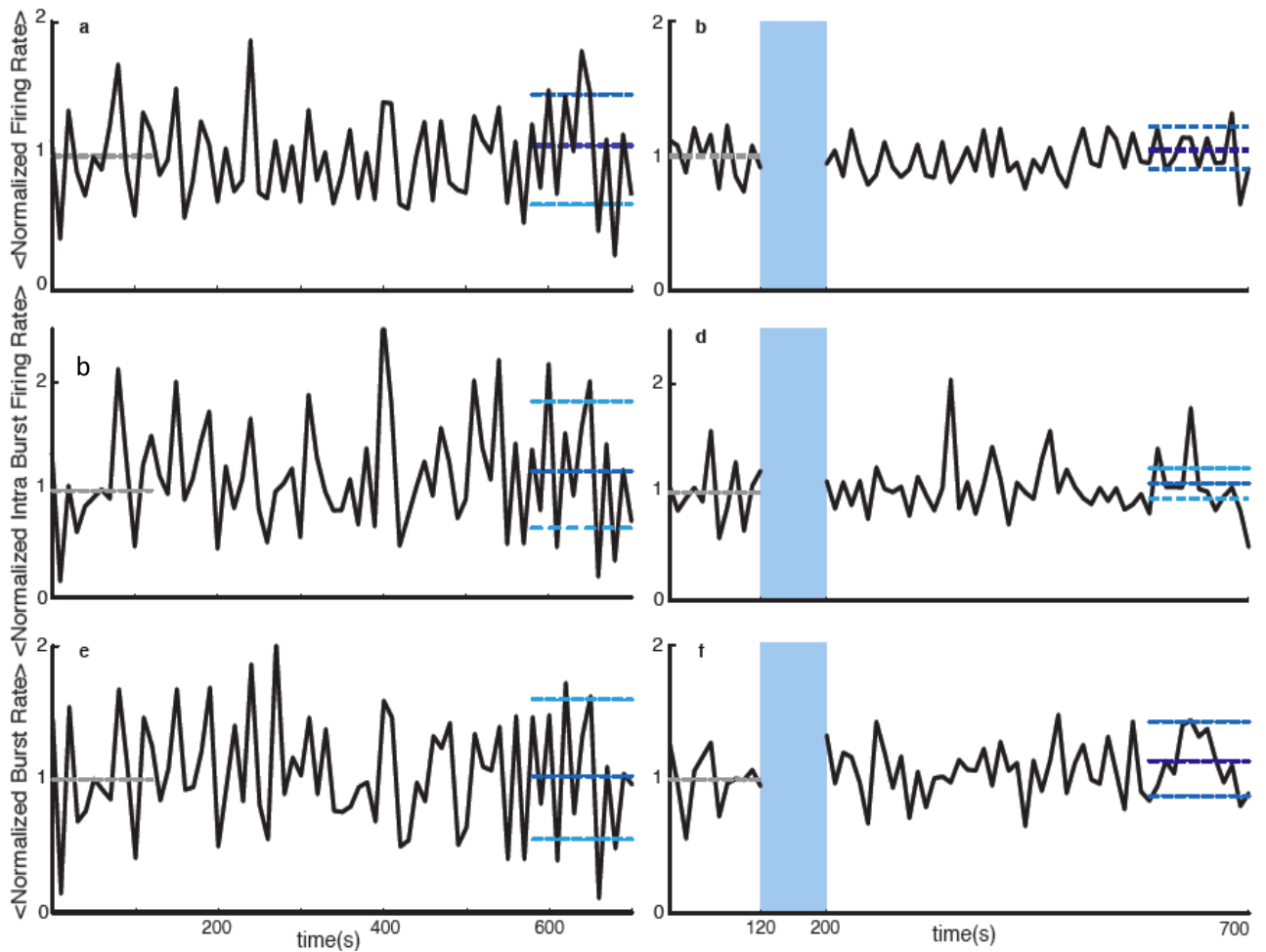


Fig 2.3: Control cultures collective network dynamics Plots on the left side are for control transfected non stimulated cultures and the plots on the right side are for untransfected and blue light stimulated culture (**a,b**) The normalized average firing rate before and after stimulation. The dotted grey line is the mean firing rate before stimulation and the dark blue line is the mean firing rate after stimulation. (**c,d**) The average normalized intraburst firing rate. The dotted grey line is the mean intraburst firing rate and the dark blue line is the mean intraburst firing rate after stimulation. (**e,f**) The normalized average burst rate. The dotted grey line is the mean burst rate before the stimulation and the dark blue line is the average burst rate after stimulation. In all plots, the light blue lines are the 95% bootstrap confidence interval. The light blue column in figures (b,d,f) between 120 s and 200 s is the blue light stimulus. The results with both conditions are averages over 5 experiments. The figure and the data analysis included in the figure were provided by Ghazaleh Afshar (Max Planck Institute for Dynamics and Self Organization, Goettingen)

2.4. Network synchronization increases after stimulation

To complement the analysis of the changes in bursting dynamics, it is crucial to assess whether stimulation with constant or ramp pulses of blue light modify network synchronization. We used cross correlation analysis in order to characterize changes in network synchronization after stimulation by computing the fold change of conditional firing rate and the cross correlation coefficients before and after stimulation. It is important to note that the cross correlation functions goes to zero at large times (Fig 2.4) and the conditional firing rate fold change goes to one at large times (Fig 2.5. and Fig 2.6). In case of constant and ramp illumination, there was a significant increase in the average cross correlation coefficients and the average conditional firing rate fold change decreases after stimulation.

We compared the averaged cross correlation functions before and after stimulation. We found that after stimulation, the averaged cross correlation functions increases significantly in case of constant (average over 4451 pairs from 22 experiments performed a total number of 19 cultures) and ramp illumination (average over 2710 pairs from 19 experiments performed on a total number of 16 cultures). The increase in the cross correlation coefficients in case of ramp photostimulation is larger than in the case of constant illumination (Fig 2.4).

The half width at half maximum of the cross correlation function is as follow: for constant stimulation, before the stimulus it is 52 ms and after the stimulus it is 52 ms, as for the ramp stimulation, before the stimulus it is 36 ms and after the stimulus it is 40 ms. It is important to note that the half width at half maximum of basically all cross correlation functions is around 50 ms which is the NMDA synaptic decay time constant.

We also compared the averaged conditional firing rate fold change before and after stimulation. In case of constant illumination, there was a significant decrease in the average fold change of the conditional firing rate (average over 4451 pairs from 22 experiments performed a total number of 19 cultures) compared to before stimulation (Fig 2.5). In case of ramp

illumination, there was a significant decrease in the average fold change of conditional firing rate (average over 2710 pairs from 19 experiments performed on a total number of 16 cultures) compared to before stimulation (Fig 2.6).

It is important to note again that the changes in the average cross correlation functions and the average conditional firing rate fold change are much more pronounced in the case of ramp illumination than in the case of constant illumination further highlighting the effectiveness of mild photostimulation to induce more pronounced effects on the network level. It is important to note that the conditional firing rate fold change goes to one asymptotically.

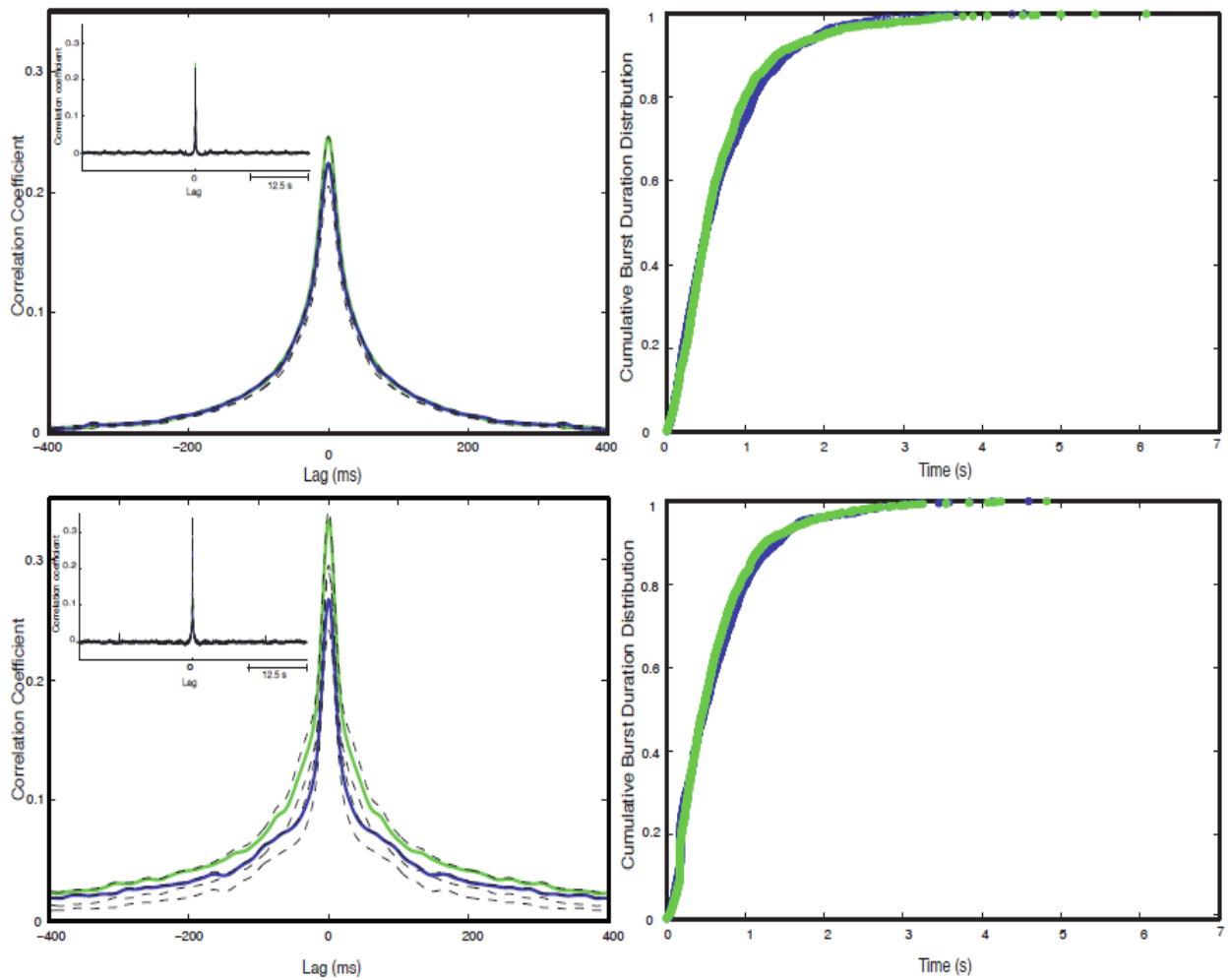


Fig 2.4.: Network synchronization changes: the upper row of the figures represents the changes in response to constant light stimulation. The upper left figure is the average cross correlation function. The blue line represents the average cross correlation function before stimulation and the green line represents the average cross correlation function after stimulation. The dotted lines represent the Jackknife confidence intervals. The inset represents the long term dynamics of the average cross correlation function. The upper right is the cumulative distribution of the burst duration before stimulation (blue line) and after stimulation (green line). The lower row of the figures represents the changes in response to ramp light stimulation. The upper left figure is the average cross correlation function. The blue line represents the average cross correlation function before stimulation and the green line represents the average cross correlation function after stimulation. The dotted lines represent the Jackknife confidence intervals. The inset represents the long term dynamics of the average cross correlation function. The upper right is the cumulative distribution of the burst duration before stimulation (blue line) and after stimulation (green line).

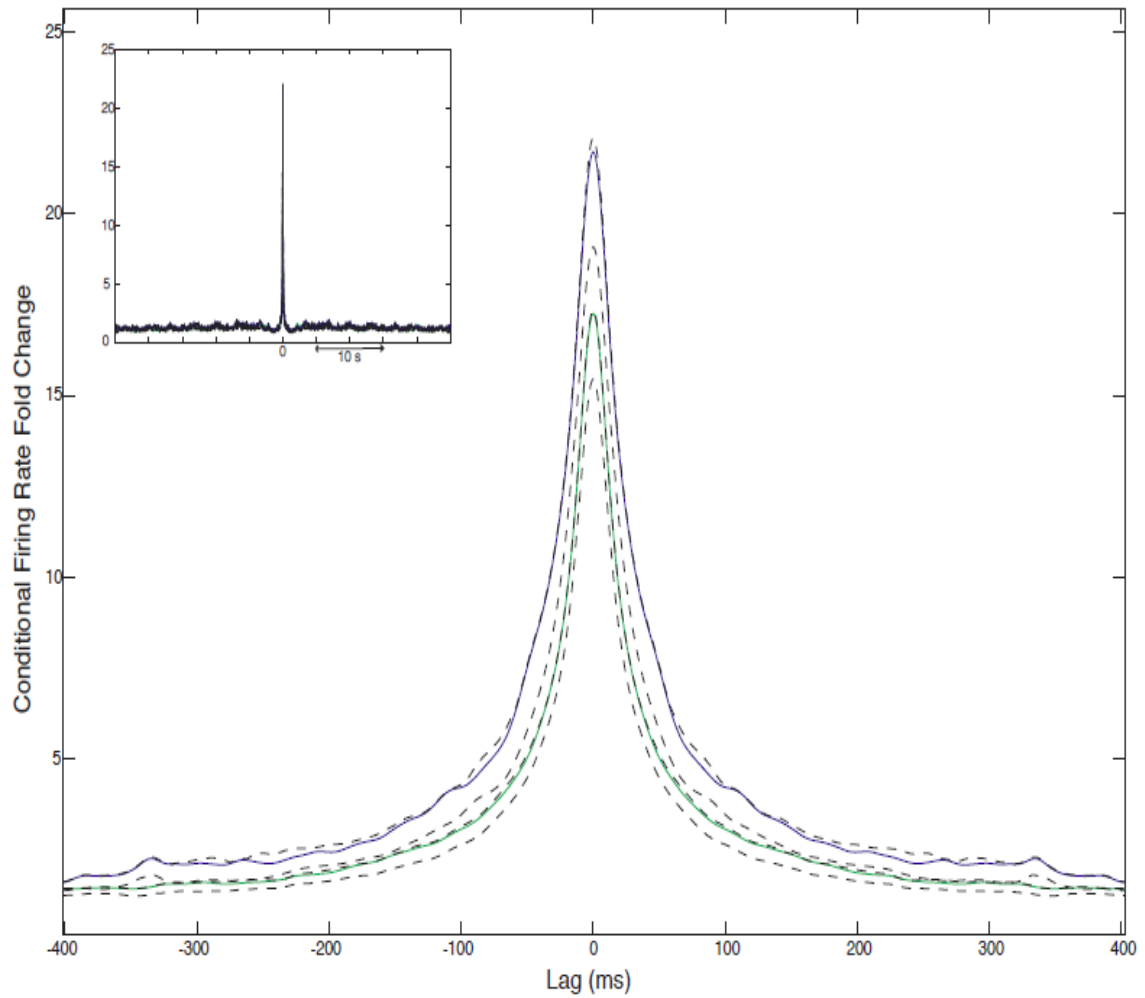


Fig 2.5.: Conditional firing rate fold change after constant photostimulation. The blue line represents the conditional firing rate fold change before stimulation and the green line is the conditional firing rate fold change after stimulation. The dotted lines are the jackknife 99% confidence intervals. The inset is the long term dynamics of the conditional firing rate fold change.

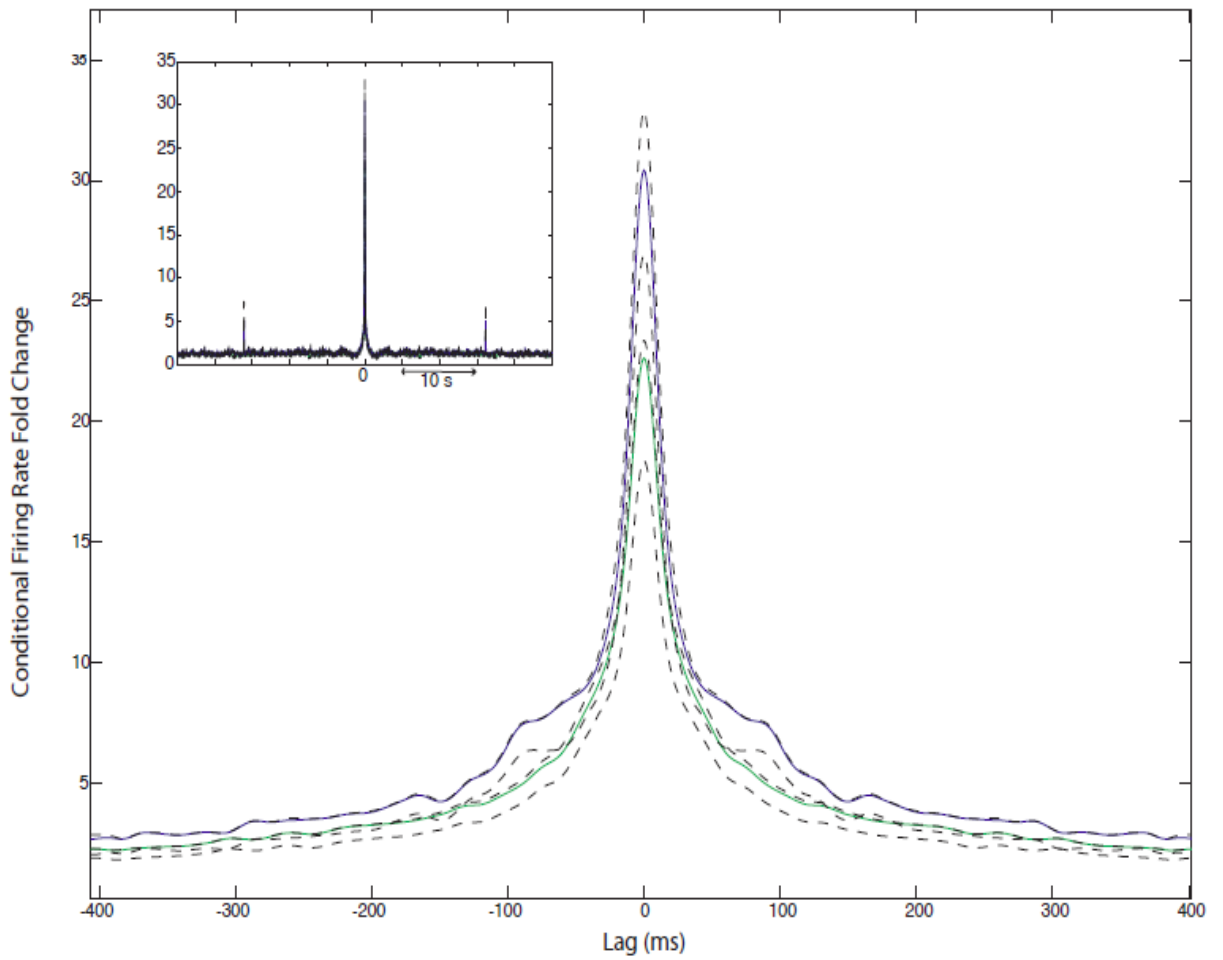


Fig 2.6. :Conditional firing rate fold change after ramp photostimulation.
 The blue line represents the conditional firing rate fold change before stimulation and the green line is the conditional firing rate fold change after stimulation. The dotted lines are the jackknife 99% confidence intervals. The inset is the long term dynamics of the conditional firing rate fold change.

2.5. Genes responsible for early phase long term potentiation are mainly involved in the network level changes as revealed by microarray analysis of synaptic proteins

In order to get insight into the molecular mechanisms underlying the collective changes on the network level, we performed microarray analysis of synaptic plasticity proteins in order to give us an idea which signaling pathways might be regulated that will guide further experiments to tackle the detailed molecular mechanisms. The RNA was immediately extracted from the channelrhodopsin 2 transfected neurons after the end of the experimental session then cDNA was synthesized and quantitative PCR is performed.

In each set of experiment, the fold change in synaptic plasticity proteins according to the procedure mentioned in the methods section (chapter 4 section 4.1.2) was calculated by comparing a test culture with its corresponding control culture (our fold change cutoff was ± 2). In order to determine the genes that are consistently regulated across our experiments, all set of experiments (a total of 3 experiments with their controls) were averaged to obtain an averaged fold change to determine which synaptic plasticity genes are upregulated or downregulated.

The genes having an averaged fold change bigger than 2 are summarized in the following table (Table 2.1):

Gene Symbol	Averaged Fold Change
Adam10	2,1006
Adcy1	4,7184
Adcy8	2,9724
Arc	6,2801
Bdnf	6,7582
Cebpd	7,239
Cnr1	3,7342
Dlg4	2,1311
Egr1	4,2845
Egr2	2,7367
Egr4	7,9399
Gabra5	4,6696
Gria3	2,1238
Grin2a	3,0933
Grin2b	2,448
Grin2c	3,9108
Grm1	4,3872
Grm2	4,0581
Grm3	2,7053
Grm4	3,9517
Grm5	4,4228
Grm7	2,2255
Grm8	3,63
Igf1	3,2962
Jun	2,1772
Junb	4,521
Mapk1	2,5009
Nfkb1	2,181
Ngf	2,3742
Nptx2	3,9631
Nr4a1	2,4495
Ntf3	4,0698
Ntrk2	2,3147
Pcdh8	2,6253
Plcg1	2,0633
Ppp2ca	3,6363
Prkg1	2,8928
Sirt1	3,079
Gapdh	2,2987

Table 2.1 Synaptic plasticity genes and their averaged fold change.

In order to determine the statistical significance of our regulated genes, we applied Student T-test to compare between the different replicas of our experiment. We used the standard criteria is that a gene is considered significantly upregulated if it has a fold change higher than 2 and p value of < 0.05 .

Applying the aforementioned criteria, we found that the significantly upregulated genes belong to the family of immediate early genes and specifically Arc, Egr4, Junb as shown in the volcano plot (Fig.2.7). The upregulation of activity regulated genes indicated that changes observed on the network levels are presumably mediated via genes responsible for early phase long term potentiation.

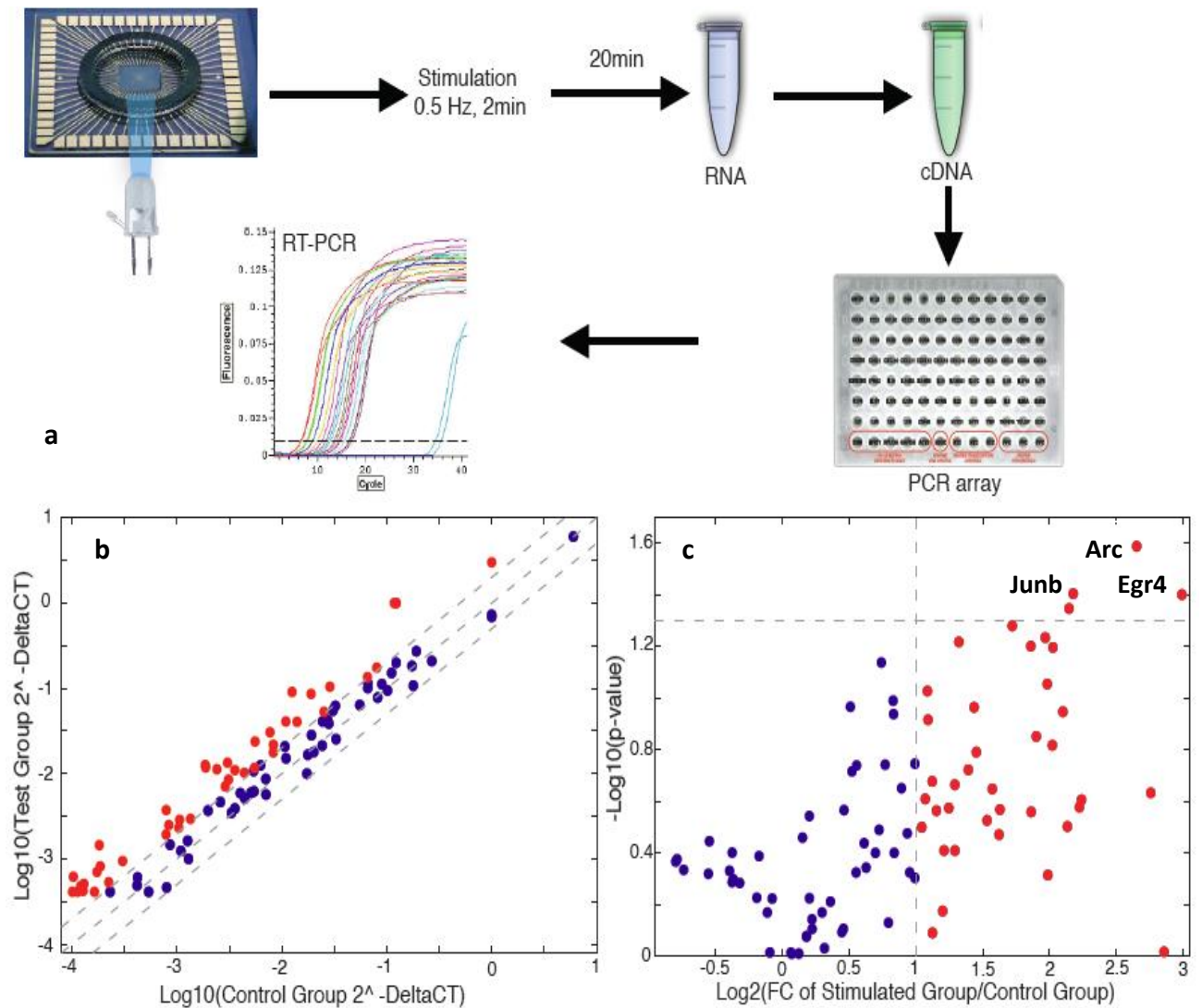


Fig 2.7.: Microarray analysis of synaptic plasticity proteins. The experimental procedure is shown in (a) where RNA is extracted immediately after recording and photostimulation, then cDNA is prepared and a quantitative real time PCR is performed. The average fold change (average over 3 experiments with their controls) is shown in (b) where the red dots represent the genes that have an averaged fold change > 2 . The blue dots are the genes that have an averaged fold change lower than 2. The statistical significance of regulated genes can be seen in the volcano plot in c where the red dots represents the genes that have an average fold change > 2 . The significantly up-regulated genes (having a p value lower than 0.05 computed using a Student t-test) are tagged by their names in the volcano plot. Arc has a p value of 0.025, Egr4 has a p value of 0.03 and Junb has a p value of 0.03.

2.6. Network dynamics changes are NMDA dependent

As hippocampal neuronal cultures are primarily consisting of pyramidal excitatory neurons (~80%) and to a lesser extent inhibitory interneurons (~20%), we therefore test the involvement of excitatory and inhibitory sub-networks in the observed network level changes. To study the effect of NMDA excitatory receptors, we add NBQX which blocks the activity of AMPA type excitatory receptors and Picrotoxin which blocks GABA_A inhibitory receptors to the hippocampal neuronal cultures on multielectrode arrays throughout the recording session. We found that the normalized average firing rate, the normalized average burst rate and the normalized average intraburst firing rate increases significantly after stimulation. We found that the normalized average firing rate (13 experiments from 7 cultures) increase significantly 30% after stimulation ($p < 10^{-7}$, significant, Wilcoxon's rank sum test). The normalized average intraburst firing rate increases 13 experiments from 7 cultures) significantly by 17% ($p < 10^{-6}$, significant, Wilcoxon's rank sum test). The normalized average burst rate (13 experiments from 7 cultures) increases significantly by 29% ($p < 10^{-4}$, significant, Wilcoxon's rank sum test). This indicates the sufficiency of NMDA dependent mechanisms to induce the optogenetically induced network level changes (Fig 2.9).

On the other hand, in order to study the effect of AMPA receptor type (fig 2.8), we add APV which blocks the NMDA receptors and Picrotoxin. We found that the normalized average firing rate (average over 15 experiments from 9 cultures) does not increase significantly after stimulation ($p = 0.06$, not significant, Wilcoxon rank sum test). On the other hand, the bursting dynamics changes after stimulation. The normalized average burst rate (average over 15 experiments from 9 cultures) significantly increases 30% after stimulation ($p < 10^{-3}$, significant, Wilcoxon rank sum test). The normalized average intraburst firing rate (average over 15 experiments from 9 cultures) significantly increase 14% after stimulation ($p < 10^{-7}$, significant,

Wilcoxon rank sum test). The previous results strongly indicate that the observed changes on the network level are NMDA dependent and to a less extent AMPA receptors.

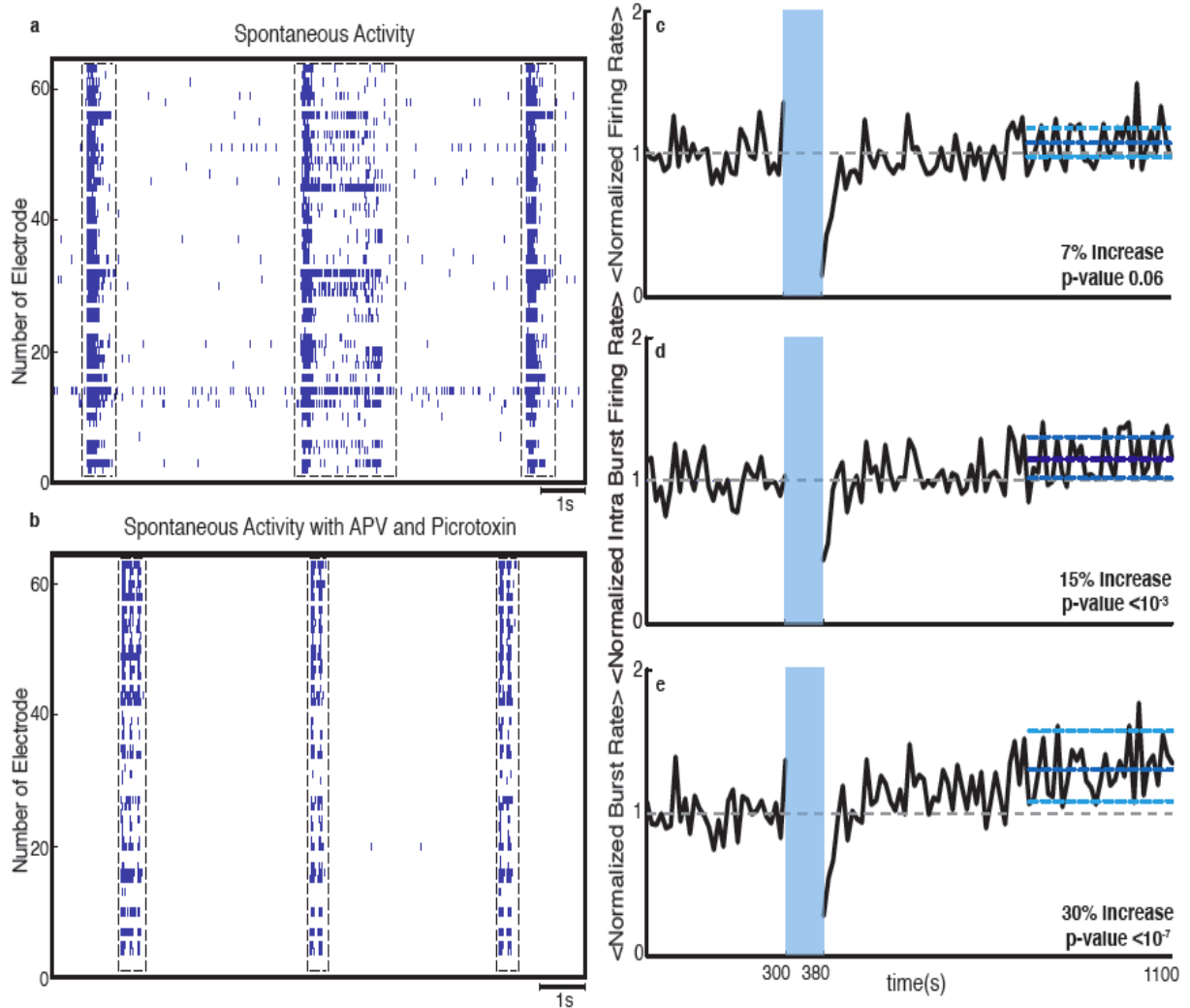


Fig 2.8.: Collective network dynamics in the presence of APV/Picrotoxin. (a) The spontaneous activity (before stimulation) of the neuronal culture before adding APV/Picrotoxin. (b) The spontaneous activity (before stimulation) after adding APV/Picrotoxin. (c) The average normalized firing rate. The dotted grey line is the mean normalized firing rate before stimulation and the dotted dark line is the mean normalized firing rate after stimulation. (d) The normalized average intraburst firing rate. The dotted grey line is the mean normalized intraburst firing rate before stimulation and the dotted dark blue line is the mean normalized intraburst firing rate after stimulation. (e) The normalized average burst rate. The dotted grey line is the mean burst rate before stimulation and the dotted dark blue line is the mean burst rate after stimulation. The dotted light blue line is the 95% bootstrap confidence interval. In all plots, the light blue lines are the 95% bootstrap confidence interval. The light blue column in all figures between 300 s and 380 s is the blue light stimulus. The p values are indicated on each plot indicating the significance level computed for the increase of either firing rate, burst rate or intraburst firing rate in the last 5 minutes of recording. The results are averages over 13 experiments from 7 cultures. The figure and the data analysis included in the figure were provided by Ghazaleh Afshar (Max Planck Institute for Dynamics and Self Organization, Goettingen)

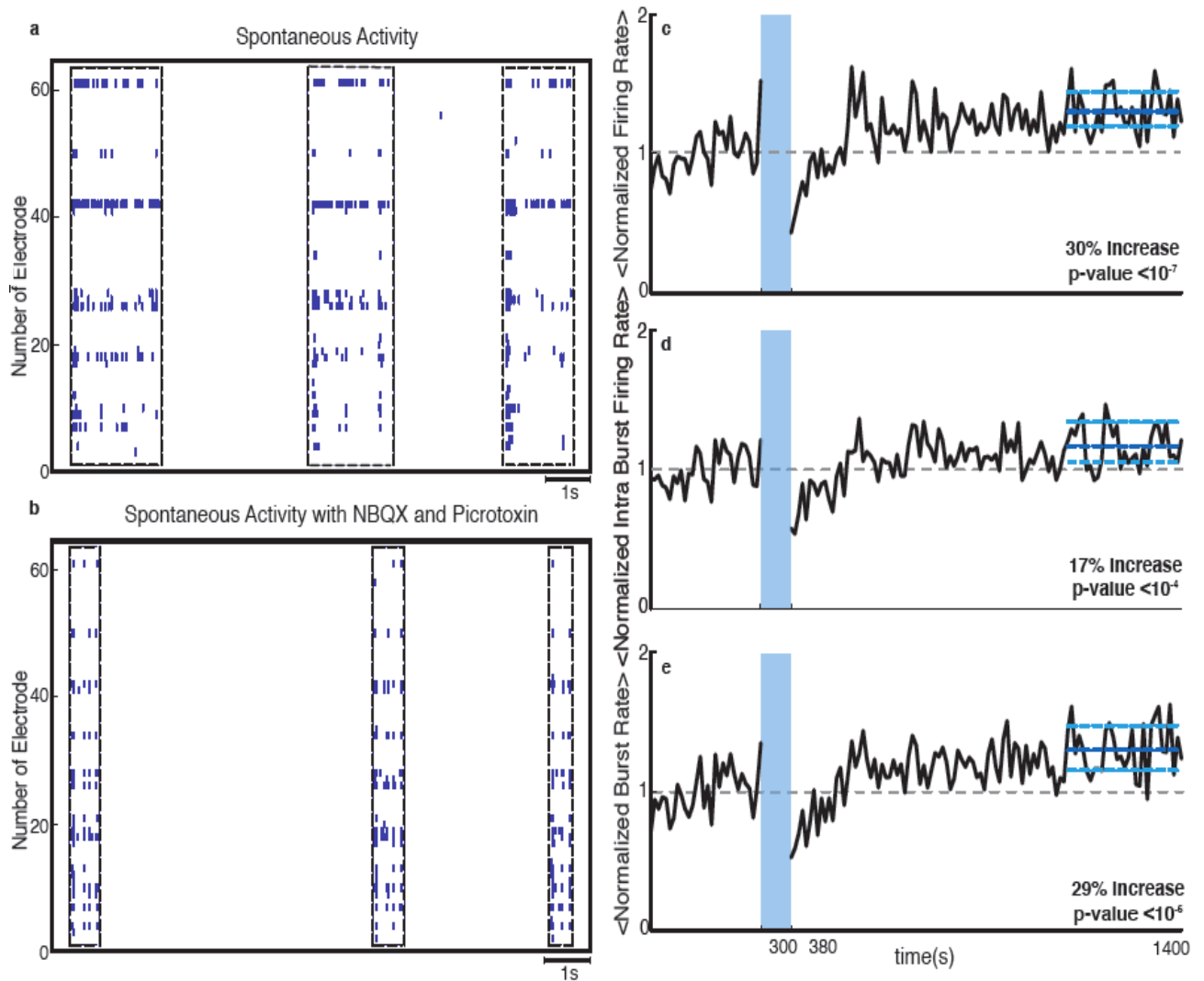


Fig 2.9.: Collective network dynamics in the presence of NBQX/Picrotoxin. (a) The spontaneous activity (before stimulation) of the neuronal culture before adding NBQX/Picrotoxin. (b) The spontaneous activity (before stimulation) after adding NBQX/Picrotoxin. (c) The average normalized firing rate. The dotted grey line is the mean normalized firing rate before stimulation and the dotted dark line is the mean normalized firing rate after stimulation. (d) The normalized average intraburst firing rate. The dotted grey line is the mean normalized intraburst firing rate before stimulation and the dotted dark blue line is the mean normalized intraburst firing rate after stimulation. (e) The normalized average burst rate. The dotted grey line is the mean burst rate before stimulation and the dotted dark blue line is the mean burst rate after stimulation. The dotted light blue line is the 95% bootstrap confidence interval. In all plots, the light blue lines are the 95% bootstrap confidence interval. The light blue column in all figures between 300 s and 380 s is the blue light stimulus. The p values are indicated on each plot indicating the significance level computed for the increase of either firing rate, burst rate or intraburst firing rate in the last 5 minutes of recording. The results are averages over 13 experiments from 7 cultures. The figure and the data analysis included in the figure were provided by Ghazaleh Afshar (Max Planck Institute for Dynamics and Self Organization, Goettingen)

3. Discussion

In our study we found that mild types of photostimulation paradigm, i.e. using low blue light power density and low frequency at which light pulses are delivered, are sufficient to induce global changes in neuronal network dynamics. Whole field photostimulation of channelrhodopsin 2 transfected hippocampal neuronal cultures increased firing rate, intraburst firing rate, burst rate and spike synchronization after the stimulation. These changes in network dynamics were found to be mediated predominantly via NMDA dependent mechanism of synaptic plasticity and calcium dependent signaling pathways. Studying the duration and internal structure of 4972 synchronized network bursts in 35 cultures we observed that the process terminating network bursts is virtually unaffected by photostimulation while the coordination among distant neurons is selectively strengthened. Perhaps the most surprising result of our experiments was that slowly increasing light stimulation, in which the number of optically elicited spikes is much smaller than for pulsed light stimulation was in every respect as effective in reorganizing network dynamics as the stronger stimulation paradigm. Presumably this reflects that with this milder form of stimulation light-induced activity patterns more closely reflect the detailed synaptic organization of a particular culture. We thus conclude that a small number of events that are matched to the synaptic organization of a culture can more effectively induce a change of the collective dynamics than massive externally imposed activity.

Overall our results indicate that optical stimulation is a viable and powerful tool to examine –network plasticity in cultures. Previously, studies of neuronal plasticity in neuronal cultures have primarily used electrical stimulation. Electrical stimulation has the disadvantage of producing substantial artifacts for MEA recordings (Wagenaar D. 2001) and microelectrodes are fixed in position “substrate embedded” so the stimulation sites are fixed. Thus, it is only possible to stimulate a small subset of neurons. In order to activate neuronal networks globally, alternative methods previously used are the chemical induction methods that offer the advantage of activating many synapses simultaneously. Chemical induction, however, requires chronic treatment with pharmacological agents which might interfere with the physiological state of the neurons and offers no temporal control (Molnar 2011). Alternative to chemical induction, Channelrhodopsin 2 has been used to induce

plasticity at single synapses using a frequency of 0.5 Hz blue light stimulation. As a result of stimulation, a lasting increase in spine volume accompanied by increase in α CamKII concentration (Zhang P 2008). The aforementioned study has looked at the changes in the single neuron dynamics induced by an optogenetic plasticity induction protocol. Our study examines the network level changes to a paradigm of 0.5 Hz frequency which has been previously shown to avoid network fatigue (Darbon P. et al. 2002).

The set of firing statistics examined was sufficient to reveal the overall character of network reorganization. The network collective dynamics consistently changed after stimulation with respect to all three firing statistics: firing rate, intraburst firing rate, and burst rate. The firing rate after offset of the stimulation increased compared to the spontaneous activity of the culture as a result of network level potentiation. Concerning bursting dynamics, the intraburst firing rate increased after offset of the stimulation. The increased intraburst firing rate was largely due to the increased firing rate after stimulation and to a minimal extent due to decrease in burst duration. Furthermore, the interburst interval decreased after stimulation which is mainly responsible for the increase in burst rate. Our results are consistent with findings from previous studies that used electrical stimulation. Maeda et al. 1998 were able to induce an increase of the burst rate and the intraburst firing rate using high frequency tetanic stimulation. Some of the changes reported previously in bursting dynamics using electrical stimulation in relatively small data sets appeared more pronounced than our findings. The large size of the data set collected by us nevertheless which makes it quite easy to identify and characterize the change in network dynamics with good precision and significance.

Our pharmacological and microarray analyzes consistently indicate that the network level potentiation we found is mediated largely via typical NMDA dependent synaptic plasticity mechanisms. Many features of the collective network dynamics changes in firing rate were also observed when both AMPA type and GABA_A receptors were blocked and the effect was largely abolished when NMDA receptor was blocked with APV. Ivenshitz et al. 2006 observed an enhancement of spontaneous activity using a chemical plasticity induction method involving exposure of the culture to conditioning medium following the growth of the culture

for 2 days in APV. These changes also appeared to be NMDA receptor dependent. Our microarray analysis indicated that the activity regulated gene *Arc* was consistently activated across all experiments. The immediate early gene *Arc* is activated downstream of NMDA receptors and is found to be upregulated following LTP induction (Steward et al. 2008, Rao et al. 2006). In addition, activity regulated transcription factors e.g. *Egr4* were upregulated in photostimulated cultures which are also known to be involved in synaptic plasticity (Alberini 2009).

In our experiments, we also examined changes in correlation structure of the network after offset of the stimulation. We found an increase in the amplitude of cross correlation functions after stimulation reflecting an increase in spike synchronization. Synchrony is a form of temporal relationship between neurons which can be broadly defined as a temporally correlated activity between neurons (Salinas and Sejnowski 2001, Abeles M 1991, Tchumatchenko T et al. 2010 Fries et al. 2007 Uhlhaas et al. 2009 Lampl et al. 1999). Correlation has been seen as an additional coding dimension independent of neuronal firing rate and might be important in gating the flow of information across neural network, without effects on the meaning of the conveyed information (deCharms and Merzenich, 1996, Moreno-Bote et al., 2008, Battaglia D. et al. 2012, Pillow, J. W. et al. 2008, Schneidmann E. et al. 2006). Significant cross-correlations can arise in the presence of direct synaptic connections and/or from common or correlated inputs between pairs of neurons (Turker and Powers, 2002, Fujisawa et al. 2008, Ostojic et al., 2009). The amplitude of the cross correlations, depends on the properties of the synapses involved but it is also modulated by the general activity of the neurons (Constantinidis et al. 2001, Ostojic et al. 2009, Battaglia et al. 2012, Tchumatchenko et al. 2010). It is important to note also that precise spike time that is crucial for many forms of synaptic plasticity (Frégnac, Y. et al. 2010 , Morrison, A. et al., 2008, Dan, Y. 2008). The increase in spike synchronization that we observed is likely to reflect tighter coupling between neurons rather than a change in the overall organization of the bursts. The width of the cross correlation functions was generally much smaller than the mean burst duration either before or after stimulation for both ramp and constant photostimulation demonstrating that the change in correlation structure results from modifications in the fine structure within the burst. The half width at half maximum

of the cross correlation function is on the order of 50 ms. This time is close to the decay time constant of NMDA receptor mediated synaptic currents constant is indicating that the strong enhancement of correlations under all conditions can be explained by an enhancement of common input that has substantial NMDA synaptic inputs. Our results are consistent with the increased spike correlations that have been observed in the case of hippocampal neurons where chemical plasticity induction method was used (Ivenshitz M. et al 2006). Though the observed changes appeared somewhat more pronounced in this study but it was based on a relatively small number of cross correlations pairs (23 pairs) compared to our data set (2710 pairs for ramp photostimulation and 4451 pairs for constant photostimulation). Our correlation results that again highlight the sensitivity gained by harnessing the potential of high yield network electrophysiology combining optogenetic stimulation and multielectrode recordings that allow efficient gathering of large data sets for a precise and reliable characterization of network dynamics.

On the other hand, we observed a decrease in the conditional firing rate fold change after stimulation reflecting the fact that there is a very strong firing rate modulation.

In conclusion, we presented a simple photostimulation paradigm able to modify the intrinsic collective dynamics of a cultured neuronal network, potentially maximizing spike synchronization. It offers an attractive alternative to stimulation paradigms that externally control neuronal networks. As important target applications of optogenetics include optical deep brain stimulation (Gradinaru et al. 2009) and the optical control of epileptic activity (Tønnesen et al. 2009), the need for mild effective stimulation paradigms that minimize side effects and tissue damage is of great importance. Modifying neuronal network synchronization may have profound therapeutic implications for Schizophrenia, Parkinson's disease and Epilepsy in which aberrant synchronization is a hallmark symptom and causal element. Modifying network synchronization can also be expected to be relevant in studying activity dependent developmental processes where the correlation structure of neural activity as in the visual pathway (e.g. Weliky, M. 1999) or in the hippocampus (Quilichini et al. 2012) . For all such applications modifying the intrinsic ability of a network to generated correlated activity patterns might often be preferable to

permanently impose desired activity patterns from the outside. We are confident that the approach presented here will substantially aid in the search for a photostimulation paradigms that strengthen, reduce or abolish network synchronization building a toolbox for modifying collective neuronal network dynamics.

4. References:

- Abbott LF, Nelson SB (2000). Synaptic plasticity: taming the beast. *Nat Neurosci.* Nov;3 Suppl:1178-83.
- Abeles, M. (1991). *Corticonics: Neural Circuits of the Cerebral Cortex*. Cambridge: Cambridge University Press.
- Allen CB, Celikel T, Feldman DE. (2003) Long-term depression induced by sensory deprivation during cortical map plasticity in vivo. *Nat Neurosci.* Mar;6(3):291-9.
- Arnold FJ, Hofmann F, Bengtson CP, Wittmann M, Vanhoutte P, Bading H. (2005). Microelectrode array recordings of cultured hippocampal networks reveal a simple model for transcription and protein synthesis-dependent plasticity. *J Physiol* 564:3 – 19.
- Artola A, Singer W. (1987) Long-term potentiation and NMDA receptors in rat visual cortex. *Nature.* Dec 17-23;330(6149):649-52.
- Bakkum DJ, Chao ZC, Potter SM. (2008) Long-term activity-dependent plasticity of action potential propagation delay and amplitude in cortical networks. *PLoS One.* May 7;3(5):e2088.
- Battaglia, D., Witt, A., Wolf, F., Geisel, T. (2012) Dynamic Effective Connectivity of Inter-Areal Brain Circuits. *PLoS Comput Biol* 8(3), e1002438.
- Bliss TV, Lomo T. (1973). Long-lasting potentiation of synaptic transmission in the dentate area of the anaesthetized rabbit following stimulation of the perforant path. *J Physiol* 232:331-56.
- Blumhagen F, Zhu P, Shum J, Schärer YP, Yaksi E, Deisseroth K, Friedrich RW (2011). Neuronal filtering of multiplexed odour representations. *Nature.* Nov 13;479(7374):493-8.
- Boettiger CA, Doupe AJ. (2001) Developmentally restricted synaptic plasticity in a songbird nucleus required for song learning. *Neuron.* Sep 13;31(5):809-18.
- Boyden ES, Zhang F, Bamberg E, Nagel G, Deisseroth K. (2005). Millisecond-timescale, genetically targeted optical control of neural activity. *Nat Neurosci* 8:1263-8.
- Brody CD (1999) Correlations without synchrony. *Neural Comput* 11:1537-1551.
- Braitenberg, V., and Schüz, A. (1998). *Cortex: Statistics and Geometry of Neuronal Connectivity*, 2nd Edn. Berlin: Springer-Verlag.
- Burkitt AN, Clark GM.(1999)Analysis of integrate-and-fire neurons: synchronization of synaptic input and spike output. *Neural Comput.* May 15;11(4):871-901.

- Buzsaki G, Geisler C, Henze DA, Wang XJ (2004) Interneuron Diversity series: Circuit complexity and axon wiring economy of cortical interneurons. *Trends Neurosci* 27:186-193.
- Cassenaer S, Laurent G. (2007) Hebbian STDP in mushroom bodies facilitates the synchronous flow of olfactory information in locusts. *Nature*. Aug 9;448(7154):709-13.
- Cattaneo A, Maffei L, Morrone C. (1981) Patterns in the discharge of simple and complex visual cortical cells. *Proc R Soc Lond B Biol Sci*. Jul 14;212(1188):279-97.
- Chapman PF, Kairiss EW, Keenan CL, Brown TH. (1990) Long-term synaptic potentiation in the amygdala. *Synapse*. 6(3):271-8.
- Cohen E, Ivenshitz M, Amor-Baroukh V, Greenberger V, Segal M. (2008) Determinants of spontaneous activity in networks of cultured hippocampus. *Brain Res*. Oct 15;1235:21-30.
- Constantinidis C, Franowicz MN, Goldman-Rakic PS (2001) Coding specificity in cortical microcircuits: a multiple-electrode analysis of primate prefrontal cortex. *J Neurosci* 21:3646-3655.
- Cohen D, Segal M. (2009) Homeostatic presynaptic suppression of neuronal network bursts. *J Neurophysiol*. Apr;101(4):2077-88.
- deCharms RC, Merzenich MM (1996) Primary cortical representation of sounds by the coordination of action-potential timing. *Nature* 381:610-613.
- Darbon P, Scicluna L, Tschertner A, Streit J. (2002) Mechanisms controlling bursting activity induced by disinhibition in spinal cord networks. *Eur J Neurosci*. Feb;15(4):671-83.
- Dan Y, Poo MM. (2006) Spike timing-dependent plasticity: from synapse to perception. *Physiol Rev*. Jul;86(3):1033-48.
- Eytan D, Brenner N, Marom S. (2003) Selective adaptation in networks of cortical neurons. *J Neurosci*. Oct 15;23(28):9349-56.
- Eyherabide HG, Rokem A, Herz AV, Samengo I. (2008) Burst firing is a neural code in an insect auditory system. *Front Comput Neurosci*. 2008;2:3.
- Egger V, Feldmeyer D, Sakmann B. (1999) Coincidence detection and changes of synaptic efficacy in spiny stellate neurons in rat barrel cortex. *Nat Neurosci*. Dec;2(12):1098-105.
- Fenko L, Yizhar O, Deisseroth K. (2011). The development and application of optogenetics. *Annu Rev Neurosci* 34:389-412
- Feinerman O., Rotem A., Moses E. (2008) Reliable neuronal logic devices from patterned hippocampal cultures. *Nature Physics* 4(12) 967-73.

- Fragkouli A, Papatheodoropoulos C, Georgopoulos S, Stamatakis A, Stylianopoulou F, et al. (2012). Enhanced neuronal plasticity and elevated endogenous sAPPalpha levels in mice over-expressing MMP9. *J Neurochem* 121:239-51
- Fries, P., Nikolic D., & Singer, W. (2007). The gamma cycle. *Trends in Neurosciences*, 30(7), 309–316.
- Fujisawa S, Amarasingham A, Harrison MT, Buzsaki G (2008) Behavior-dependent short-term assembly dynamics in the medial prefrontal cortex. *Nature neuroscience* 11:823-833.
- Gkogkas C, Sonenberg N, Costa-Mattioli M. (2010). Translational control mechanisms in long-lasting synaptic plasticity and memory. *J Biol Chem* 285:31913-7
- Glorioso C, Sabatini M, Unger T, Hashimoto T, Monteggia LM, et al. (2006). Specificity and timing of neocortical transcriptome changes in response to BDNF gene ablation during embryogenesis or adulthood. *Mol Psychiatry* 11:633-48.
- Grubb MS, Burrone J. (2010) Activity-dependent relocation of the axon initial segment fine-tunes neuronal excitability. *Nature*. Jun 24;465(7301):1070-4.
- Han X, Qian X, Stern P, Chuong AS, Boyden ES. (2009) Informational lesions: optical perturbation of spike timing and neural synchrony via microbial opsin gene fusions. *Front Mol Neurosci.*;2:12.
- Hanganu IL, Ben-Ari Y, Khazipov R. (2006) Retinal waves trigger spindle bursts in the neonatal rat visual cortex. *J Neurosci*. Jun 21;26(25):6728-36.
- Heimer G, Rivlin M, Israel Z, Bergman H. (2006) Synchronizing activity of basal ganglia and pathophysiology of Parkinson's disease. *J Neural Transm Suppl.* (70):17-20.
- Hetz C, Martinon F, Rodriguez D, Glimcher LH. (2011). The Unfolded Protein Response: Integrating Stress Signals through the Stress Sensor Ire1 Alpha. *Physiological Reviews* 91:1219-43.
- Hirsch JC, Crepel F. (1992) Postsynaptic calcium is necessary for the induction of LTP and LTD of monosynaptic EPSPs in prefrontal neurons: an in vitro study in the rat. *Synapse*. Feb;10(2):173-5.
- Holtkamp M, Buchheim K, Elsner M, Matzen J, Weissinger F, Meierkord H. (2011) Status epilepticus induces increasing neuronal excitability and hypersynchrony as revealed by optical imaging. *Neurobiol Dis*. Jul;43(1):220-7.
- Huerta PT, Lisman JE. (1995) Bidirectional synaptic plasticity induced by a single burst during cholinergic theta oscillation in CA1 in vitro. *Neuron*. Nov;15(5):1053-63.
- Huerta PT, Lisman JE. (1993) Heightened synaptic plasticity of hippocampal CA1 neurons during a cholinergically induced rhythmic state. *Nature*. Aug 19;364(6439):723-5.

- Iriki A, Pavlides C, Keller A, Asanuma H. (1989) Long-term potentiation in the motor cortex. *Science*. Sep 22;245(4924):1385-7.
- Ivenshitz M, Segal M. (2006) Simultaneous NMDA-dependent long-term potentiation of EPSCs and long-term depression of IPSCs in cultured rat hippocampal neurons. *J Neurosci*. Jan 25;26(4):1199-210.
- Jenkins NA, Lanahan AA, Worley PF. (1995) Arc, a growth factor and activity-regulated gene, encodes a novel cytoskeleton-associated protein that is enriched in neuronal dendrites. *Neuron*. Feb;14(2):433-45.
- Jimbo Y, Tateno T, Robinson HP. (1999) Simultaneous induction of pathway specific potentiation and depression in networks of cortical neurons. *Biophys J*. 76(2):670-8.
- Jones MW, Errington ML, French PJ, Fine A, Bliss TV, Garel S, Charnay P, Bozon B, Laroche S, Davis S. (2001) A requirement for the immediate early gene Zif268 in the expression of late LTP and long-term memories. *Nat Neurosci*. Mar;4(3):289-96.
- Kandel ER. (2001) The molecular biology of memory storage: a dialog between genes and synapses. *Biosci Rep*. Oct;21(5):565-611.
- Kandel E, Spencer WA. (1961) Electrophysiology of hippocampal neurons. II. After-potentials and repetitive firing. *J Neurophysiol* 24:243-59.
- Katz LC, Shatz CJ. (1996) Synaptic activity and the construction of cortical circuits. *Science*. Nov 15;274(5290):1133-8.
- Kepecs A, Lisman J. (2003) Information encoding and computation with spikes and bursts. *Network*. Feb;14(1):103-18.
- Kitano K, Fukai T (2007) Variability v.s. synchronicity of neuronal activity in local cortical network models with different wiring topologies. *J Comput Neurosci* 23:237-250.
- Krahe R, Gabbiani F. (2004) Burst firing in sensory systems. *Nat Rev Neurosci*. Jan;5(1):13-23.
- Lanahan A, Worley P. (1998) Immediate-early genes and synaptic function. *Neurobiol Learn Mem*. Jul-Sep;70(1-2):37-43.
- Lampl, I., Reichova, I., and Ferster, D. (1999). Synchronous membrane potential fluctuations in neurons of the cat visual cortex. *Neuron* 22, 361–374.
- Lee YS, Silva AJ. (2009). The molecular and cellular biology of enhanced cognition. *Nat Rev Neurosci* 10:126-40.

- Leinekugel X, Khazipov R, Cannon R, Hirase H, Ben-Ari Y, Buzsáki G. (2002) Correlated bursts of activity in the neonatal hippocampus in vivo. *Science*. Jun 14;296(5575):2049-52.
- Lesica NA, Stanley GB. (2004) Encoding of natural scene movies by tonic and burst spikes in the lateral geniculate nucleus. *J Neurosci*. Nov 24;24(47):10731-40.
- Loeblich S, Nedivi E. (2009). The function of activity-regulated genes in the nervous system. *Physiol Rev* 89:1079-103
- Liu QS, Pu L, Poo MM. (2005) Repeated cocaine exposure in vivo facilitates LTP induction in midbrain dopamine neurons. *Nature*. Oct 13;437(7061):1027-31.
- London M, Häusser M (2005) Dendritic computation. *Annual review of neuroscience* 28:503-535.
- Lyford GL, Yamagata K, Kaufmann WE, Barnes CA, Sanders LK, Copeland NG, Gilbert DJ et al. (1995). Arc, a growth factor and activity-regulated gene, encodes a novel cytoskeleton-associated protein that is enriched in neuronal dendrites. *Neuron* Feb;14(2):433-45.
- Madhavan R, Chao ZC, Potter SM. (2007) Plasticity of recurring spatiotemporal activity patterns in cortical networks. *Phys Biol*. Oct 9;4(3):181-93.
- Maeda E, Kuroda Y, Robinson HP, Kawana A. (1998) Modification of parallel activity elicited by propagating bursts in developing networks of rat cortical neurones. *Eur J Neurosci*. Feb;10(2):488-96.
- Markram H, Lübke J, Frotscher M, Sakmann B. (1997) Regulation of synaptic efficacy by coincidence of postsynaptic APs and EPSPs. *Science*. Jan 10;275(5297):213-5.
- Martinez-Conde S, Macknik SL, Hubel DH. (2000) Microsaccadic eye movements and firing of single cells in the striate cortex of macaque monkeys. *Nat Neurosci*. Mar;3(3):251-8.
- Mehta MR, Quirk MC, Wilson MA. (2000) Experience-dependent asymmetric shape of hippocampal receptive fields. *Neuron*. Mar;25(3):707-15.
- Miles R, Traub RD, Wong RK. (1988) Spread of synchronous firing in longitudinal slices from the CA3 region of the hippocampus. *J Neurophysiol*. Oct;60(4):1481-96.
- Milner B, Squire LR, Kandel ER. (1998). Cognitive neuroscience and the study of memory. *Neuron* 20:445-68
- Minlebaev M, Ben-Ari Y, Khazipov R. (2009) NMDA receptors pattern early activity in the developing barrel cortex in vivo. *Cereb Cortex*. Mar;19(3):688-96.
- Molnár E. (2011) Long-term potentiation in cultured hippocampal neurons. *Semin Cell Dev Biol*. Jul;22(5):506-13.

Moreno-Bote R, Renart A, Parga N (2008) Theory of input spike auto- and cross-correlations and their effect on the response of spiking neurons. *Neural Comput* 20:1651-1705.

Nakamura D, Tsuru A, Ikegami K, Imagawa Y, Fujimoto N, Kohno K. (2011). Mammalian ER stress sensor IRE1 beta specifically down-regulates the synthesis of secretory pathway proteins. *Febs Lett* 585:133-8

Nguyen PV, Abel T, Kandel ER. (1994) Requirement of a critical period of transcription for induction of a late phase of LTP. *Science*. Aug 19;265(5175):1104-7

Ohya T, Hayashi T, Kiyama E, Nishii H, Miki H, et al. (2008). Improved production of recombinant human antithrombin III in Chinese hamster ovary cells by ATF4 overexpression. *Biotechnol Bioeng* 100:317-24

O'Mahony A, Raber J, Montano M, Foehr E, Han V, et al. (2006). NF-kappa B/Rel regulates inhibitory and excitatory neuronal function and synaptic plasticity. *Mol Cell Biol* 26:7283-98

Ostojic S, Brunel N, Hakim V (2009) How connectivity, background activity, and synaptic properties shape the cross-correlation between spike trains. *The Journal of neuroscience : the official journal of the Society for Neuroscience* 29:10234-10253

Oorhenuan, I., Mechler, F., Purpura, K. P., Schmid, A., Hu, Q., and Victor, J. (2010). Sparse coding and high-order correlations in fine-scale cortical networks. *Nature* 466, 617–621.

Pillow, J. W., Shlens, J., Paninski, L., Sher, A., Litke, A. M., Chichilnisky, E. J., and Simoncelli, E. P. (2008). Spatio-temporal correlations and visual signalling in a complete neuronal population. *Nature* 454, 995–999.

Pikovsky, A., Rosenblum, M., and Kurths, J. (2002). *Synchronization: A Universal Concept in Nonlinear Science*. Cambridge: Cambridge University Press.

Quilichini PP, Le Van Quyen M, Ivanov A, Turner DA, Carabalona A, Gozlan H, Esclapez M, Bernard C. (2012) Hub GABA neurons mediate gamma-frequency oscillations at ictal-like event onset in the immature hippocampus. *Neuron*. Apr 12;74(1):57-64.

Rao VR, Pintchovski SA, Chin J, Peebles CL, Mitra S, Finkbeiner S. (2006) AMPA receptors regulate transcription of the plasticity-related immediate-early gene *Arc*. *Nat Neurosci*. Jul;9(7):887-95.

Reinagel P, Godwin D, Sherman SM, Koch C. (1999) Encoding of visual information by LGN bursts. *J Neurophysiol*. May;81(5):2558-69.

Renaudineau S, Poucet B, Laroche S, Davis S, Save E. (2009). Impaired long-term stability of CA1 place cell representation in mice lacking the transcription factor *zif268/egr1*. *Proc Natl Acad Sci U S A* 106:11771-5

Reyes AD. (2003) Synchrony-dependent propagation of firing rate in iteratively constructed networks in vitro. *Nat Neurosci.* Jun;6(6):593-9.

Rochefort NL, Garaschuk O, Milos RI, Narushima M, Marandi N, Pichler B, Kovalchuk Y, Konnerth A. (2009) Sparsification of neuronal activity in the visual cortex at eye-opening. *Proc Natl Acad Sci U S A.* Sep 1;106(35):15049-54.

Ryan MM, Mason-Parker SE, Tate WP, Abraham WC, Williams JM. (2011). Rapidly induced gene networks following induction of long-term potentiation at perforant path synapses in vivo. *Hippocampus* 21:541-53

Salinas E, Sejnowski TJ (2001) Correlated neuronal activity and the flow of neural information. *Nature reviews Neuroscience* 2:539-550.

Schoenenberger P, Gerosa D, Oertner TG. (2009). Temporal control of immediate early gene induction by light. *PLoS One* 4:e8185

Schoenenberger P, Scharer YPZ, Oertner TG. (2011). Channelrhodopsin as a tool to investigate synaptic transmission and plasticity. *Exp Physiol* 96:34-9

Shahaf G, Marom S. (2001). Learning in networks of cortical neurons. *J Neurosci* 21:8782-8

Schneidman, E., Berry, M. J., Segev, R., and Bialek, W. (2006). Weak pairwise correlations imply strongly correlated network states in a neural population. *Nature* 440, 1007–1012.

Stefan K, Kunesch E, Benecke R, Cohen LG, Classen J. Mechanisms of enhancement of human motor cortex excitability induced by interventional paired associative stimulation. (2002) *J Physiol.* 2002 Sep 1;543(Pt 2):699-708.

Shepherd JD, Bear MF. (2011) New views of Arc, a master regulator of synaptic plasticity. *Nat Neurosci.* Mar;14(3):279-84.

Silva LR, Amitai Y, Connors BW. (1991) Intrinsic oscillations of neocortex generated by layer 5 pyramidal neurons. *Science.* Jan 25;251(4992):432-5.

Singer W (1999) Neuronal synchrony: a versatile code for the definition of relations? *Neuron* 24:49-65, 111-125.

Steward O, Wallace CS, Lyford GL, Worley PF. (1998) Synaptic activation causes the mRNA for the IEG Arc to localize selectively near activated postsynaptic sites on dendrites. *Neuron.* Oct;21(4):741-51.

- Steward O, Worley PF. (2001) Selective targeting of newly synthesized Arc mRNA to active synapses requires NMDA receptor activation. *Neuron*. Apr;30(1):227-40.
- Tchumatchenko T, Geisel T, Volgushev M, Wolf F. (2011) Spike correlations - what can they tell about synchrony? *Front Neurosci*. 5:68.
- Thomas MJ, Watabe AM, Moody TD, Makhinson M, O'Dell TJ. (1998) Postsynaptic complex spike bursting enables the induction of LTP by theta frequency synaptic stimulation. *J Neurosci*. Sep 15;18(18):7118-26.
- Tiesinga PH. (2004) Chaos-induced modulation of reliability boosts output firing rate in downstream cortical areas. *Phys Rev E Stat Nonlin Soft Matter Phys*. Mar;69(3 Pt 1):031912.
- Tønnesen J, Sørensen AT, Deisseroth K, Lundberg C, Kokaia M. (2009) Optogenetic control of epileptiform activity. *Proc Natl Acad Sci U S A*. Jul 21;106(29):12162-7.
- Turker KS, Powers RK (2002) The effects of common input characteristics and discharge rate on synchronization in rat hypoglossal motoneurons. *The Journal of physiology* 541:245-260.
- Turker KS, Powers RK (2002) The effects of common input characteristics and discharge rate on synchronization in rat hypoglossal motoneurons. *The Journal of physiology* 541:245-260.
- Turrigiano G. (2012) Homeostatic synaptic plasticity: local and global mechanisms for stabilizing neuronal function. *Cold Spring Harb Perspect Biol*. Jan 1;4(1):a005736.
- Turrigiano G. (2011) Too many cooks? Intrinsic and synaptic homeostatic mechanisms in cortical circuit refinement. *Annu Rev Neurosci*. 34:89-103.
- Uhlhaas PJ, Pipa G, Lima B, Melloni L, Neuenschwander S, Nikolić D, Singer W. (2009) Neural synchrony in cortical networks: history, concept and current status. *Front Integr Neurosci*. 3:17.
- Uhlhaas PJ, Singer W. (2010) Abnormal neural oscillations and synchrony in schizophrenia. *Nat Rev Neurosci*. Feb;11(2):100-13.
- Wagenaar DA, Madhavan R, Pine J, Potter SM. (2005) Controlling bursting in cortical cultures with closed-loop multi-electrode stimulation. *J Neurosci*. Jan 19;25(3):680-8.
- Wagenaar DA, Potter SM. (2002) Real-time multi-channel stimulus artifact suppression by local curve fitting. *J Neurosci Methods*. Oct 30;120(2):113-20.
- Wagenaar DA, Pine J, Potter SM. (2006) An extremely rich repertoire of bursting patterns during the development of cortical cultures. *BMC Neurosci*. Feb 7;7:11.
- Williams J, Dragunow M, Lawlor P, Mason S, Abraham WC, et al. (1995). Krox20 May Play a Key Role in the Stabilization of Long-Term Potentiation. *Mol Brain Res* 28:87-93

Wespapat V, Tennigkeit F, Singer W. (2004) Phase sensitivity of synaptic modifications in oscillating cells of rat visual cortex. *J Neurosci.* Oct 13;24(41):9067-75.

Yu, J., and Ferster, D. (2010). Membrane potential synchrony in primary visual cortex during sensory stimulation. *Neuron* 68, 1187–201.

Zhang YP, Holbro N, Oertner TG. (2008) Optical induction of plasticity at single synapses reveals input-specific accumulation of alphaCaMKII. *Proc Natl Acad Sci U S A.* Aug 19;105(33):12039-44.

CHAPTER 3

Continuous Dynamic Photostimulation

1. Introduction:

In cortical circuits of the intact brain, neurons are subject to an ongoing barrage of synaptic activity. Many types of pyramidal neurons for instance receive on the order of 10,000 synaptic inputs. Assuming that each of these is active with a rate on the order of 1 to 10 Hz one estimates that the postsynaptic cell has to process incoming signals arriving at a rate on the order of 10 kHz. Despite this, neurons fire at relatively low firing rates *in vivo* (Greenberg et al. 2008, Margrie et al. 2002). *In vivo* intracellular recordings from intact cortical circuits established that this synaptic drum-fire results in strong and temporally irregular membrane potential fluctuations, in which only a sparse subset of positive deflections trigger action potentials that are communicated to postsynaptic cells (Chance et al. 2002, Okun et al. 2008, Mokeichev et al. 2007)

The temporally irregular firing pattern reflecting the massive synaptic drum-fire that the neuron is receiving can be understood within the framework of balanced state of cortical networks (Sompolinsky and Van Vreejwick 1996). In a balanced cortical network, the excitatory and inhibitory currents add up such that the net somatic current is nearly zero and very weakly correlated across neurons such that neuronal firing is driven by fluctuations in the input currents. (Okun M, Lampl I 2008, Renart A et al. 2010). A functional advantage offered by the balanced state of cortical networks is that a fraction of the population is always close to threshold enabling a fast population response. The balanced state network and its functional significance has been the focus of many studies (Brunel 2000, Tsodyks et al. 1995, Renart et al. 2010, Weher et al. 2003, Froemke et al. 2007, De la Rocha et al. 2008, Murphy et al. 2009, Shu et al. 2003, Vogels et al. 2009) Despite the accumulating evidence that balanced state is the regime in which cortical networks work, there is

no simple experimental system so far to test single neuron properties in the fluctuation driven regime.

The statistical structure of the background fluctuations depend to a great extent on the synaptic time constants for example synaptic connections mediated by glutamatergic AMPA channels contribute current fluctuations with a short time constant while current fluctuations mediated by the NMDA channels lead to fluctuations with longer time constants (Stern et al. 1992, Hestrin, 1993). In the diffusion limit of synaptic inputs, the synaptic background fluctuations can be modeled using a stochastic Ornstein Uhlenbeck process with a defined mean , variance and correlation time (Gluss 1967, Ditlevsen 2005, Tuckwell 1988, 1989). The correlation time of the OU process reflects the synaptic decay time constants that are thought , as previously mentioned, to contribute to the statistical structure to the synaptic background activity.

There is a great interest in characterizing the single neurons properties under realistic in vivo like conditions. One of the properties: spike triggered average (STA) which is estimation of the mean of the firing rate function within a temporal window preceding each recorded spike (Schwartz et al. 2006). STA has been widely used to characterize sensory systems such auditory neurons (Eggermont et al. 1983) , characterize retinal ganglion cells in the context of the visual system (Meister et al. 1994), Lateral geniculate neurons (Reid et al. 1995) and simple cells in primary visual cortex (DeAngelis et al. 1993). Another neuronal property is the frequency response function which characterizes the response of the neurons of input signals of varying frequencies that will be discussed in more details later. Another important property is the correlation gain meaning how the input correlations are reflected in the output correlations which might contribute to neuronal encoding (also check Chap 2 introduction for an overview of the functional importance of spike correlations). The aforementioned properties were found to be modulated by the background neuronal activity that depends on the noise statistics and by the spike generation mechanism.

Previous modeling studies (Lindner et al. 2001, Brunel et al. 2001, Silberberg et al. 2004, Ostojic et al. 2011, Alijani et al. 2011, Brunel et al. 2003) have shown that the

structure of the noise background can fundamentally change the response properties. The sharpness of the spike onset has little effect on the low and intermediate frequencies but strongly determines the high-frequency cut-off above which the frequency response function decays (Naundorf et al. 2005, Wei et al. 2011).

Intracellular recordings of multiple neurons have shown that dynamical sensory stimuli can modulate input currents to cortical neurons. The incoming external signals can be encoded in the mean or variance of the synaptic current to each neuron in a cortical network (Fig 3.1). In a single neuron the maximal firing rate limits the highest faithfully encoded frequencies. As previously mentioned, the firing rate is remarkably low, often below 1 Hz in cortical neurons (Greenberg et al. 2008, Margrie et al. 2002). Thus, the representation of fast-varying stimuli has to emerge at the population level and not on the single neuron. In neuronal populations the frequency response function quantifies the fidelity of signal representation (Knight 1972, Goldberg et al. 1969, Lindner et al. 2001, Brunel et al. 2001). A key notion that needs to be presented here is the “dynamic gain” of a neuronal population defined as the gain in which a small perturbation of mean input current oscillating at temporal frequency f is represented in the temporally oscillating instantaneous firing rate of the population. Dynamic gain is a function of stimulus frequency f , of intrinsic parameters of neuronal excitability and of the intensity & temporal coherence of the synaptic background activity in which the periodic perturbation is embedded.

Over the past few years a handful of experimental studies have aimed to determine dynamic gain by whole cell recording and dynamic current injection in real neurons (Lundstrom et al. 2008, Koendgen et al 2008, Boucsein et al 2009, Higgs & Spain 2009). The experimental evidence indicates that cortical neurons can indeed encode input frequencies that are tens of times faster than the firing rate of individual neurons, in both mean- and variance-encoding schemes in the presence of *in vivo*-like correlated background noise (Koendgen et al. 2008, Boucsein et al. 2009, Tchumatchenko et al. 2011). Whole cell patch clamp studies have employed two different experimental paradigms for measurement of “dynamic gain”. First, following (Koendgen et al. (2008) and Buchsein et al (2009)) injected superpositions of pseudorandom fluctuating background currents and a deterministic sinusoidal

current component into the cells and obtained dynamic gain from the modulation of the phase dependent mean firing rate in response to stimuli with different frequencies of the sinusoidal component. This approach might be called the “Fourier paradigm”. An alternative “Correlation approach” was used by Carandini et al. 1994, 1996 and recently by Higgs and Spain 2009. In this approach, a stationary pseudorandom current is injected and the dynamic gain calculated from the spike triggered average current and the power spectral density of the current fluctuations. In a Fourier Paradigm measurements of Dynamic Gain would require to reliably generate non-attenuated current components oscillating at frequencies way beyond the gamma range. In a Correlation paradigm, the key requirement would be the reproducibility and detailed knowledge about the time course of the induced fluctuating current and good control of the power spectral composition of the fluctuating current.

While these aforementioned studies have started to reveal important properties of dynamic gain, none of them succeeded in determining dynamic gain in an individual neuron or characterizing its dependence on parameters of background synaptic bombardment. The aforementioned shortcomings of the previous experimental paradigms are due to its reliance on the use of conventional whole cell patch clamp. With whole cell patch clamp, one can record from a one cell at a time and for limited amount of time leads to a gathering of a small number of spikes. In order to reliably characterize neuronal properties, one needs a large number of spikes on the order of 10^4 . Moreover, due to time limitations, experimental conditions cannot be changed during measurements in order to determine the dependence of neuronal properties on different conditions and different stimulus parameters. Non-invasive optogenetic stimulation approaches hold the promise to overcome this limitation by providing remote optical stimulation of neurons without disruption of its physiological state, high spatial & temporal resolution allowing interrogation of individual neurons and the possibility to perform long recordings. While optogenetic tools have been successfully used to manipulate activity patterns in intact neuronal circuits, the strong light flashes typically used completely override intrinsic activity and rigidly imprints artificial spike sequences. Optical neurostimulation combined with multielectrode array recording will help us overcome the shortcomings of whole cell patch clamp. Multielectrode array recordings would allow long term monitoring

electrophysiological activity of several cells simultaneously. Optical neurostimulation would realize long term non invasive stimulation of neurons. We termed the combination of optical neurostimulation and multisite electrical recording: “Continuous Dynamic Photostimulation” (CoDyPs) which offers a high throughput method to reliably characterize single neurons properties non invasively under realistic in vivo like conditions.

Most importantly, the characterization of single neuron computation requires a precise knowledge of the input to compute as mentioned beforehand the spike triggered average or to describe correlation gain and firing rate adaptation in dependence of the stimulus properties. An optical, noninvasive stimulation approach is only possible if the induced conductances:

1. are highly reproducible with correlation times suitable to mimic fluctuating synaptic conductances
2. can be precisely predicted and designed
3. can be stably induced in long-term experiments

Satisfying these requirements would also provide the basis to control the activity of operating circuits *in-vivo*, preserving the natural firing characteristics. It is important to mention that this will contribute tremendously to the optogenetics field as novel photostimulation paradigms, that do not override the naturalistic activity of the neuron but rather mimic it, are highly needed for studies of neuronal networks functioning under naturalistic conditions.

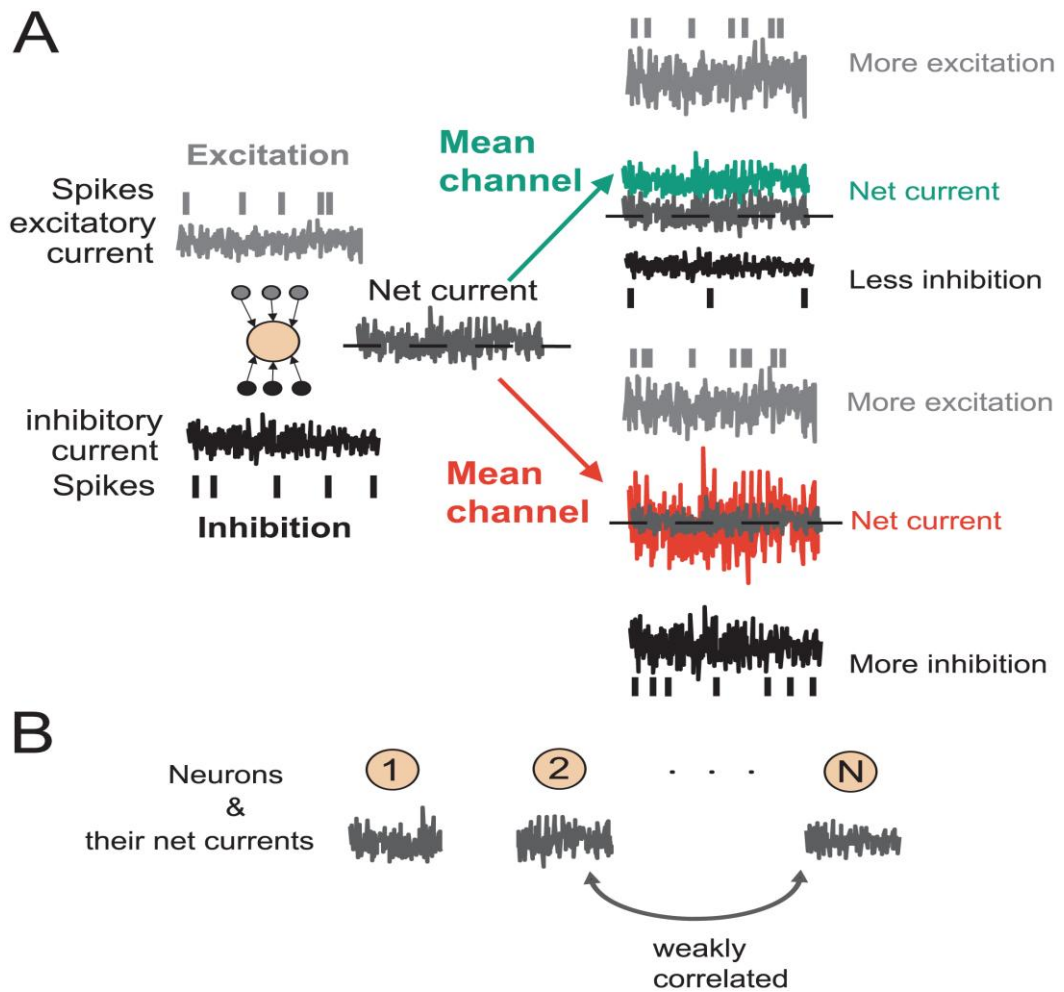


Fig3.1: Encoding in the mean and variance channel (A) Simultaneous increase of excitatory and reduction of inhibitory activity (or vice versa) results in a mean current change (right, green). On the other hand, simultaneous increase (or reduction) in excitatory or inhibitory spiking activity results in modifications in the net current variance (left, red). These modifications constitute two primary channels of communication in a cortical network. (B) In a cortical network the excitatory and inhibitory currents add up such that the net somatic current is only weakly correlated across neurons. The figure has been adopted with permission from Tchumatchenko et al. 2011

1.1. Aim of the study:

In this study, continuous dynamic photostimulation (CoDyPs) is introduced as a novel method to mimic *in-vivo*-like fluctuations using light gated ion channels as a high throughput electrophysiological method which offers advantage over conventional whole cell patch clamp recordings (Fig. 3.2). The study encompasses the validation of the method and its feasibility to replace conventional whole cell patch clamp method to characterize single neuron properties.

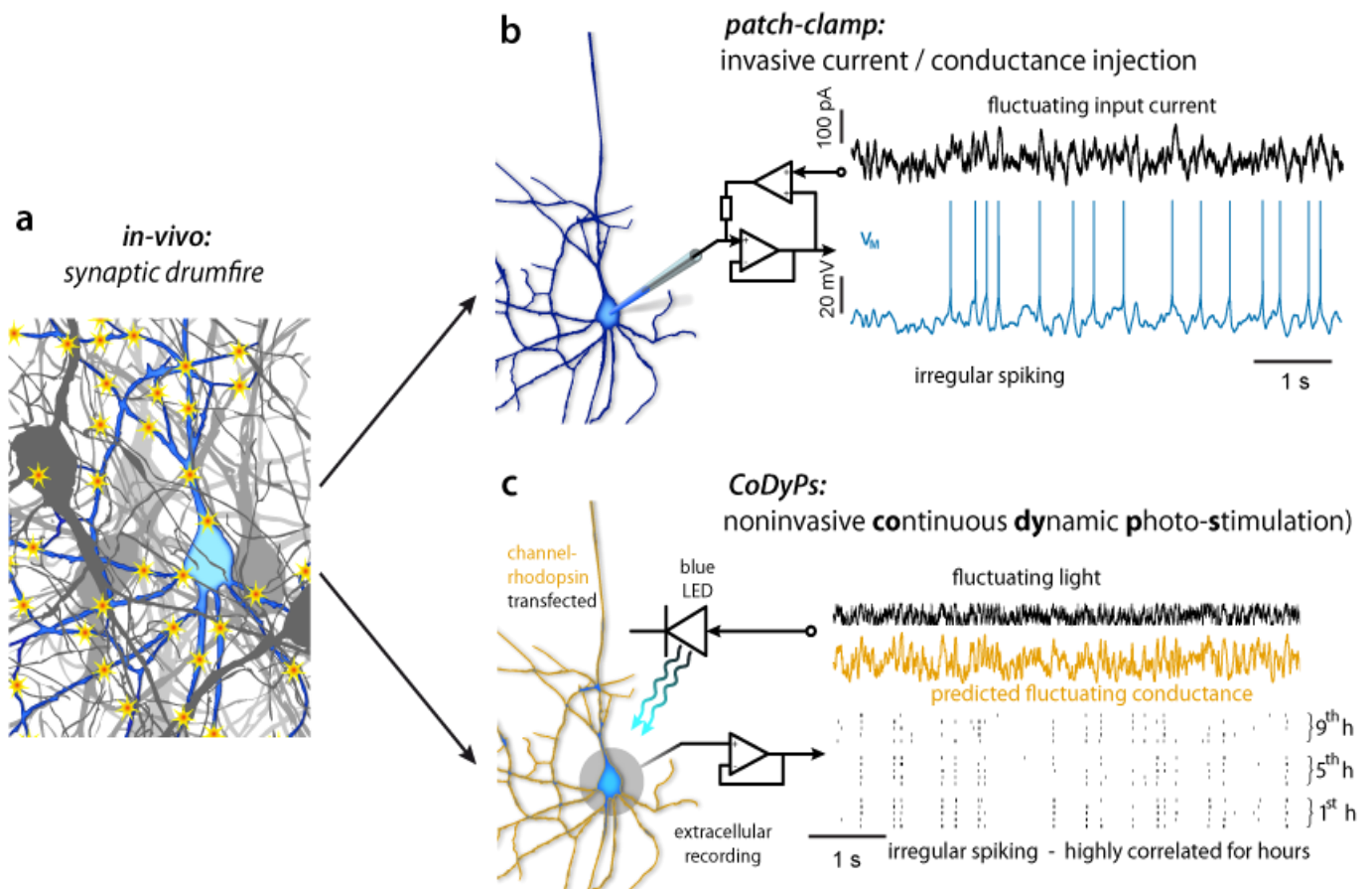


Figure 3.2: Two ways to study *in-vivo*-like fluctuation driven spiking activity under controlled conditions
a, schematic representation of the ongoing synaptic drumfire to which neurons in the CNS are typically exposed. Sparks represent active synapses. Cortical pyramidal neurons will typically receive synaptic inputs at a rate of several kilohertz. **b and c**, two alternative experimental approaches to emulate the resulting input fluctuations and register the fluctuation driven activity *in-vitro*: whole cell current injection (b) and CoDyPs (c), here depicted for a neuron cultured on a circular extracellular electrode. In contrast to the whole cell stimulation/recording, CoDyPs offers extended recording and stimulation/recording of multiple neurons simultaneously.

Contributions:

In the following study, all experimental procedures were done by myself and the data analysis was performed by Andreas Neef (Max Planck Institute for Dynamics and Self Organization, Goettingen).

2. Results:

2.1. Characteristics of Channelrhodopsin 2 and ChIEF photocurrents:

Human embryonic kidney cells 293 (HEK cells) of the stable ChR2-YFP cell-line or HEK cells transiently transfected with ChIEF-tdTomato were selected for patch clamp by their appearance in bright field and their fluorescence intensity. Under whole cell voltage clamp, with the membrane potential fixed at -60 mV, light pulses of different power density were applied. The elicited currents exhibited the typical features of ChR2 and ChIEF currents (Fig. 3a) similar to what has been reported before (Lin et al. 2009): a rapid activation at light onset with activation time constants $\tau_{act} = 4.8 \pm 0.1$ ms for ChR2, $\tau_{act} = 4.8 \pm 0.2$ ms for ChIEF (Fig. 2c and Methods) and a rapid deactivation after cessation of illumination ($\tau_{1deact} = 8.5 \pm 0.9$ ms for ChR2, $\tau_{2deact} = 30 \pm 7$ ms for ChR2, $\tau_{1deact} = 6.9 \pm 0.4$ ms for ChIEF, $\tau_{2deact} = 66 \pm 15$ ms for ChIEF) as well as a much slower inactivation after an initial peak ($\tau_{inact} = 63 \pm 2$ ms for ChR2, $\tau_{inact} = 185 \pm 16$ ms for ChIEF). While the deactivation kinetics and the light dependent activation time constant were similar for ChR2 and ChIEF, the inactivation kinetics and especially the degree of inactivation were substantially different. At the maximum light power density used in this study, 0.27 mW/mm^2 , ChR2 currents showed an inactivation of $58.8 \% \pm 0.8 \%$, resulting in an average current steady state current of only 57 ± 11 pA. The new mutant ChIEF, on the other hand, showed only $13.4 \% \pm 0.9 \%$ inactivation from the peak to steady state level with a steady state level of 280 ± 68 pA. Reported values are mean \pm standard error for 13 cells (ChR2) and 21 cells (ChIEF) respectively.

To mimic naturally occurring input fluctuations, light sensitive channels must provide conductance changes with appropriate magnitude and frequency

bandwidth. Thus, we first analyzed the bandwidth of currents mediated by ChIEF and ChR2. A simple, practical test is the application of chirps: over a 3 s period a pseudo-periodic light stimulus was applied with a frequency modulated continuously from 5 to 100 Hz. While the modulation depth of the stimulus amplitude is constant, the amplitude of the current response decreases as the frequency exceeds the bandwidth of the channel. To avoid a contamination of this amplitude decrease, by the rather slow time and light dependent inactivation of ChIEF, in the case of ChIEF the chirps were preceded by a 3 s constant light stimulus. The photoactivated currents induced by the chirp light stimuli were very similar for ChR2 and ChIEF (Fig. 3d). To compare the effect of the signal transduction with a single pole low-pass filter, the chirp stimuli were digitally filtered and the power spectral density of the results was compared with the power spectral density of the currents. The best match was obtained with a cut-off frequency of 20 Hz (Fig. 3e), corresponding to time constants around 8 ms. This is sufficient to synthesize the fluctuating inputs originating from AMPA, NMDA and GABA mediated synaptic currents, the white noise limit cannot be implemented by these means. ChIEF and ChR2 appear to enable the generation of fluctuating currents with high frequencies to the same degree. The main difference between the two channelrhodopsin variants is the larger amplitude of ChIEF-mediated currents (Fig. 3b), in part due to the strongly reduced inactivation. The larger current amplitude constitutes an advantage per se, enabling adequate depolarization and larger fluctuations with less average light power density. Thereby ChIEF currents promise better reproducibility of fluctuating currents as high frequency stimulus components are not drowning in the noise floor as it is the case for ChR2 currents (Fig. 3e). This difference might be due to the number of channels expressed in HEK cells as in the case of ChR2, a stable cell line is used where the expression is steady but relatively low. On the other hand, in the case of ChIEF, HEK cells were transiently transfected and a higher expression level was observed. Consequently the analysis of fluctuating currents was performed in HEK cells expressing ChIEF.

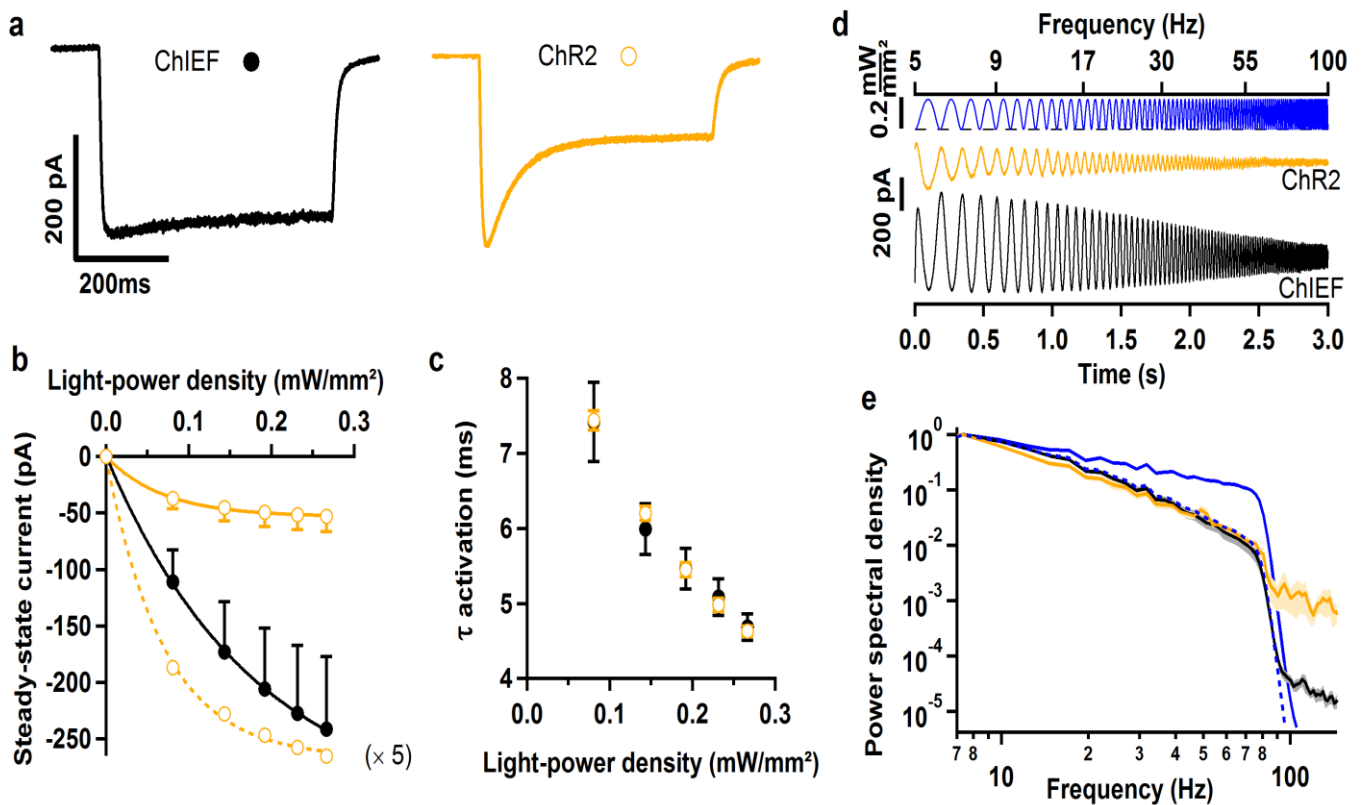


Figure 3.3: ChIEF supports large steady-state currents with a low-pass filter characteristics similar to ChR2

a, Representative current responses to 1 s light stimuli at 0.27 mW/mm² recorded at a membrane potential of -60 mV from HEK 293 cells. Black: stable cell-line expressing ChR2, orange: transiently expressing ChIEF. **b**, Relationship between steady-state current and light-power density for ChR2 (orange, n=8) and ChIEF (black, n=11) (error bars indicate standard error). The straight lines are single exponential fits. A five times scaled up version of the ChR2 data (dashed) is given to highlight the difference between the two Channelrhodopsin variants. **c**, The activation time constants (see Material and Methods) of ChIEF and ChR2 currents are equally dependent on the light-power density. **d**, A chirp stimulus (blue; frequency 5 to 100 Hz, see upper axis) evokes current responses with decreasing modulation depth, indicating the low pass behavior of the light-activated currents. Representative current responses to the chirp stimulus are shown in orange (ChR2) and black (ChIEF). **e**, Average normalized power spectral density of responses from ChR2 (orange) and ChIEF (black) are nearly identical. The power spectral densities of the light stimulus (continuous blue line) and a low-pass filtered version of the light stimulus (dashed blue line, -3 dB cut-off frequency of 20 Hz) are displayed for comparison. Standard errors are shown as brighter bands. Both channelrhodopsin variants transform the power spectrum similar to the single pole low pass filter.

2.2. Highly reproducible fluctuating light-activated currents

Because the drumfire of exponentially decaying postsynaptic currents can be well approximated with Ornstein Uhlenbeck (OU) processes, OU currents have been extensively used to emulate the temporally fluctuating input currents of cortical neurons *in-vivo*. To directly examine whether fluctuating inputs can be reliably imposed by photostimulation, we subjected ChIEF expressing HEK-cells to fluctuating light stimuli synthesized from an OU process.

In total, 12 different stimulus ensembles were used, comprising three different correlation times $\tau_{\text{corr}} = 1, 5$ and 50 ms and four different light power density statistics (conditions c1 to c4, see chapter 4 materials and methods). Assessing the stability and reproducibility of the induced currents, we found the trial to trial variations very small and the photoactivated currents induced by identical, successive stimuli very similar. Correlation coefficients typically ranged from 0.9 to 0.99 for correlation times of 5 and 50 ms (Fig. 4c) and the deviations of individual currents from the average current were generally below 5 pA (orange and black traces in Fig. 4a). We then examined how the amplitude and frequency content of the current signal were influenced by the stimulus parameters. For fluctuations with a correlation time of 50 ms - larger than the activation and deactivation time constants of the channelrhodopsin - the induced current largely mirrors the stimulus (Fig. 4a, left panel), essentially following the steady-state relation between current and light density (Fig. 3b). The probability density function of the current amplitude was very similar to that of the stimulus (Fig. 4b). For faster fluctuating stimuli with correlation times of 5 ms and 1 ms channelrhodopsin's gating kinetics limits the frequency spectrum of the current response such that the amplitude spectrum is of lower bandwidth than the stimulus and the current amplitude distribution becomes narrower (figure 4b middle and right panel).

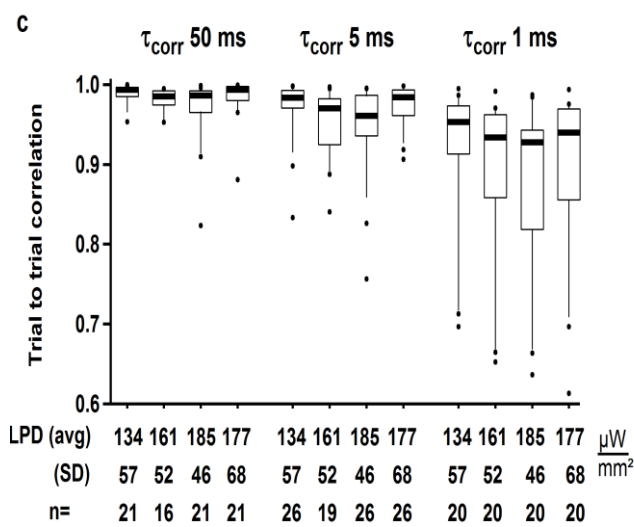
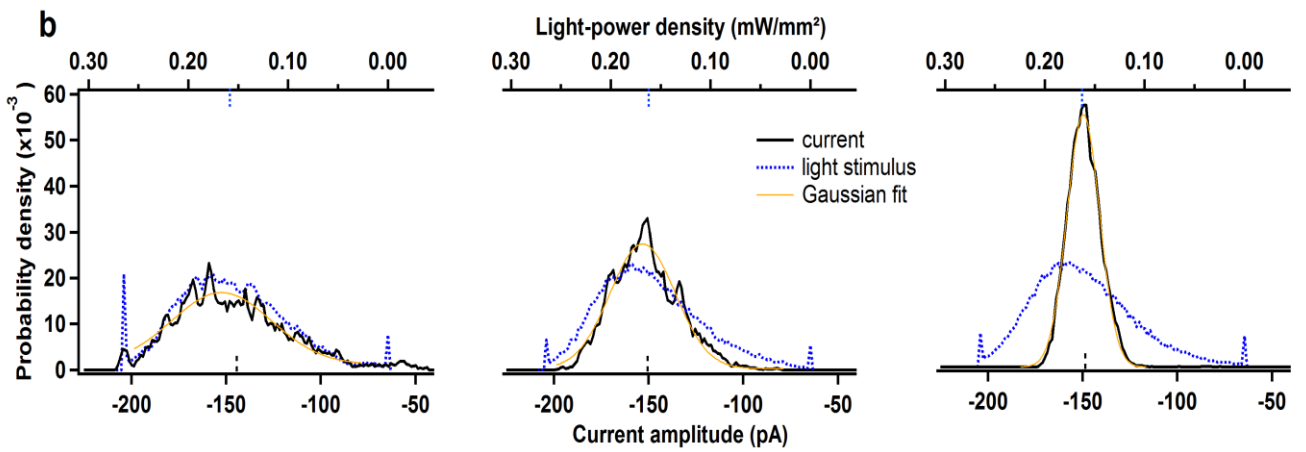
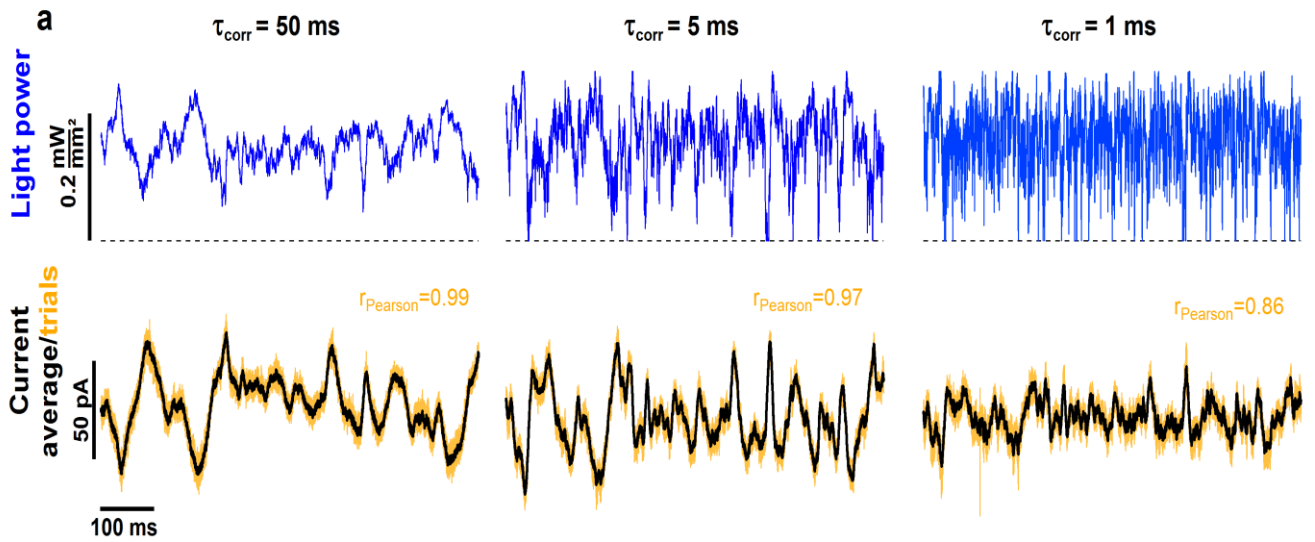


Figure 3.4.: Trial to trial reproducibility of CoDyPs driven currents

a, 700 ms periods from a representative HEK 293 cell expressing ChIEF. All light stimuli (blue) stem from the same realization of a random Ornstein-Uhlenbeck process (condition c2, see Methods). Stimuli only differ in correlation time τ_{corr} , decreasing from 50 ms (left) to 1 ms (right). Ten individual current traces, driven by the light stimuli, are displayed (orange), average currents are superimposed (black). The evoked current is highly reproducible, indicated by the high average correlation coefficients of successive current traces (see also **c**). The dotted line represents zero for both: light stimulus and light activated current response. Note how for $\tau_{\text{corr}}=50$ ms the response essentially mirrors the light stimulus. For shorter correlation times the amplitude of the driven current excursions decreases as the response no longer follows the faster signal amplitude modulation. The residual differences between individual responses and average have a standard deviation of 4 to 5 pA. **b**, Histograms of current amplitude (black) and stimulus amplitude (blue, dotted) are displayed in a tentative alignment. Average values are indicated as short vertical lines at the respective axis. While the stimuli have, by design, nearly identical histograms for all correlation times, the current amplitude histograms narrow as the correlation time decreases. **c**, Box-plot of the trial to trial Pearson correlation coefficients. Data are grouped by illumination condition, the average light-power density and the standard deviation are given in $\mu\text{W}/\text{mm}^2$. Median is indicated by the black bar, the box comprises the central 50 percent of points and the whiskers the central 80 percent. Individual points represent outliers in the lowest and highest 10 percent. The prominent outliers for short correlation time (1 ms) stem from four cells with little light induced current (<100 pA) and a leak current of the same order of magnitude. As the light driven current excursions are larger for longer correlation times the correlation coefficients from the same cells are larger for τ_{corr} of 5 and 10 ms.

2.3. Channelrhodopsin acts as a low pass filter

The characterization of dynamical response properties of neurons under fluctuating current input requires detailed knowledge of the individual applied current waveform. In invasive approaches this waveform is directly available. In a non-invasive photo-stimulation approach the current's statistics and the time course has to be obtained computationally from the light stimulus alone. To further study the relation between stimulus and current change, we calculated the average autocorrelation function and the average impulse response function for each of the three correlation times and the four combinations of mean and standard deviation used (conditions c1 to c4, see chapter 4 materials and methods).

While the autocorrelation functions of the light stimuli decayed exponentially by construction, the autocorrelation functions of the currents fell off slower. They were well described by the autocorrelation function of an Ornstein-Uhlenbeck process with the correlation time τ_{corr} (i.e. 1, 5 or 50 ms) passed through a first order low-pass filter (equation 3 in chapter 4 materials and methods) with time constant $\tau_{\text{cut-off}}$ (Fig. 5a). When the correlation time $\tau_{\text{corr}}=50$ ms is much larger than $\tau_{\text{cut-off}}$, the shape of the autocorrelation function is hardly influenced by the filtering and consequently the estimates of $\tau_{\text{cut-off}}$ do vary between 6.7 ms and 10 ms. For the smaller correlation times however, $\tau_{\text{cut-off}}$ dominates the shape of the autocorrelation function and can be well estimated. It was found to depend only weakly on the stimulus parameters, increasing slightly from 8 ms to 9 ms with decreasing mean light power density. This relation most likely reflects the dependence of the activation kinetics on the light power density (Fig. 3c).

Since those results are consistent with a simple linear filter model of the relation between the light stimulus and the induced currents, we wanted to examine, whether the current waveforms could be predicted by convolution of the impulse response function with the light waveform. To this end impulse response functions were estimated by inverse Fourier-transformation of the ratio between the Fourier-transforms of current response and respective

light stimulus (see chapter 4 materials and methods). As expected, the standard error of the estimated impulse response functions increased with the square root of τ_{corr} (Fig. 5b). In addition, the noise increased slightly with decreasing light amplitude and standard deviation of the light stimulus.

At the membrane potential of -60 mV, at which the fluctuating light stimuli were applied, the photoactivated current is inward and so the main component of the impulse response function is negative too. Initially, however, it starts with a very brief transient of positive amplitude (Fig. 5b, inset in right panel). At the sampling frequency of 10 kHz this transient is represented by a single sample point that appeared consistently in all experiments. This transient decrease in light activated current immediately after an increase in light power density might be reminiscent of the transient response to a 10 ns flash of green light (Bamann et al. 2008) (544 nm) but this needs further investigations. After this brief initial transient, the impulse response function resembles that of a low pass filter: a very rapid onset followed by a single exponential decay (Fig. 5b). Again, as was the case for the autocorrelation, the time constant of this decay was only weakly stimulus dependent and decreased with increasing light power density, from 9 ms at 0.108 mW/mm² to 7.5 ms 0.162 mW/mm². The decay phase of the impulse response function represents an effective rate with which the protein reacts to the light fluctuations around the average light intensity, distinct from activation or inactivation kinetics. This effective rate is a mixture of activation and deactivation rates and therefore increases with light. Different from a simple low-pass filter, the impulse response function of ChIEF has a delay of about 200-300 μ s. It presumably resembles the transition from state P1 to P2 (Bamann et al. 2008), the conformational switch after absorption of a photon.

On the other hand, it turned out also that Channelrhodopsin 2 has a similar impulse response function (similar to ChIEF) but with a smaller amplitude (Fig 6) and the autocorrelation function can be well fitted with the same equation used to fit the autocorrelation function for ChIEF fluctuating currents.

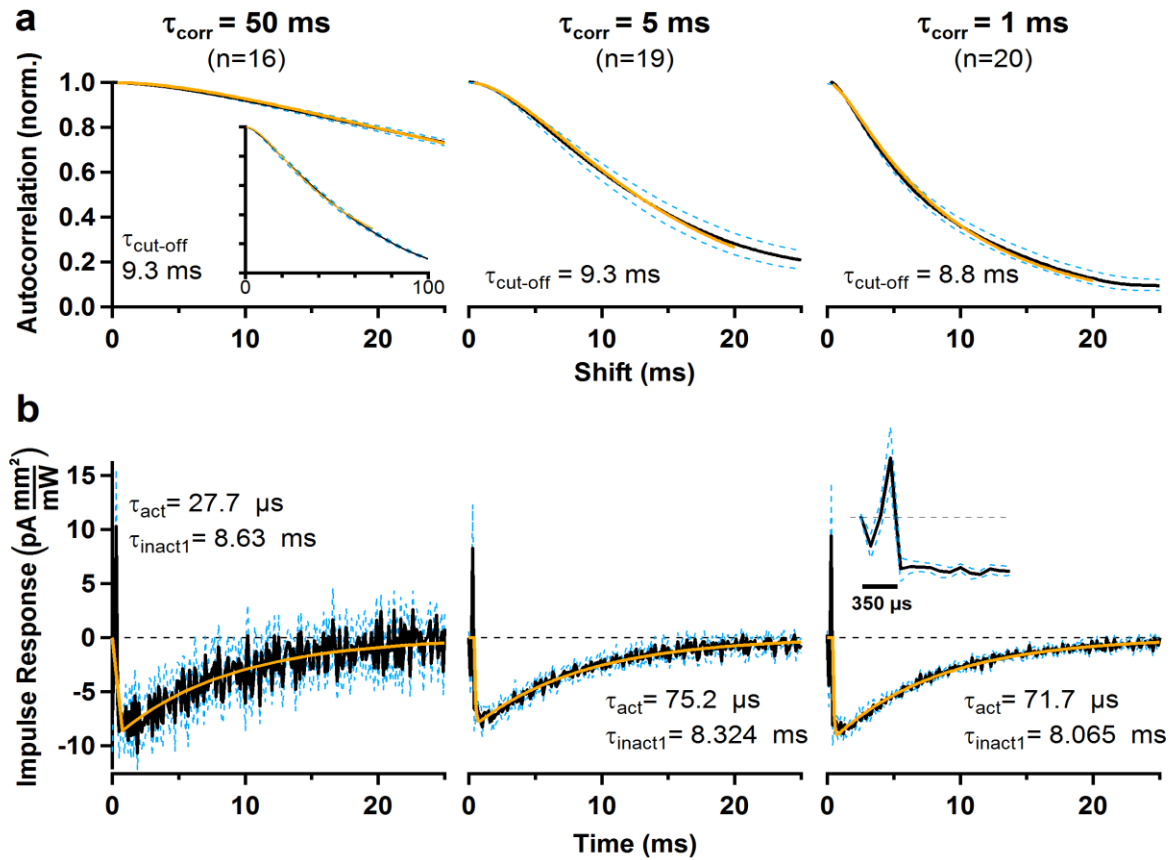


Fig 3.5.: The statistics of CoDyPs driven fluctuating currents obeys linear response theory,

a, The normalized autocorrelation functions (black) conform with the prediction (orange) for an Ornstein-Uhlenbeck process, low-pass with cut-off time constant $\tau_{\text{cut-off}}$ (equation 3). Shown here are results for condition c2 (light-power density $161 \mu\text{W}/\text{mm}^2$ average, $52 \mu\text{W}/\text{mm}^2$ standard deviation).

b, Average impulse response functions (black lines) derived from ChIEF mediated currents activated by fluctuating light stimuli in condition c2. The temporal structure, the τ_{corr} of the stimuli has no influence on the shape of the impulse response function. Following an initial transient (inset for $\tau_{\text{corr}}=1$ ms, see Results) and a rapid onset, the impulse responses are well described by a single exponential function (orange)

The dashed light blue lines in a and b enclose 95 % bootstrap confidence intervals.

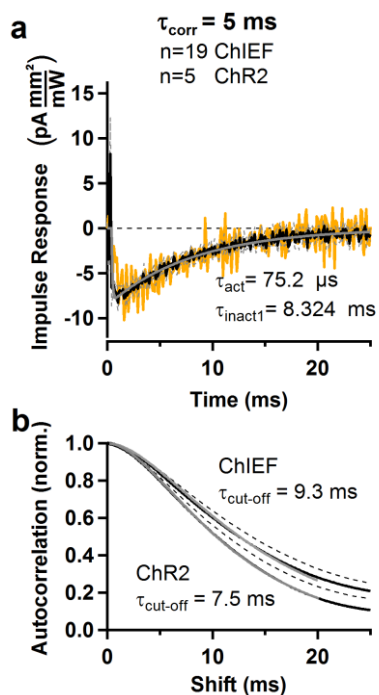


Figure 3. 6: ChR2 and ChIEF have similar response characteristics.

a, The impulse response function of ChR2 has a similar shape but a smaller amplitude. The red trace represents x7 scaled impulse response function of ChR2. The amplitude is much smaller than for ChIEF because the steady state current amplitude is much smaller. The shape of the impulse response function is very similar.

b, The autocorrelation function of ChR2 can be well described by equation 4 (see chapter 4 materials and methods). The cut-off time constant, the only free parameter, was estimated to be slightly smaller than for ChIEF.

2.4. Computational reconstruction of conductance fluctuations

The response of a time-invariant, linear system is fully determined by the stimulus and the impulse response function. We thus tested the predictive power of the impulse response function by convolution with the light stimulus and found that the current waveform predicted in this fashion and the average recorded current were highly congruent (Fig. 7). The mean correlation coefficients between predicted and recorded currents were, across all conditions c1 to c4, 0.976 ± 0.002 for $\tau_{\text{corr}}=1 \text{ ms}$, 0.98 ± 0.0007 for $\tau_{\text{corr}}=5 \text{ ms}$ and 0.973 ± 0.0007 for $\tau_{\text{corr}}=50 \text{ ms}$ (mean \pm standard error, see also Fig. 7 c). Predictability was lowest for cells with a smaller trial-to-trial correlation coefficient of individual current responses, indicating that light-induced currents are indeed predicted very well and that prediction performance was limited by the noise introduced by other conductances such as leak.

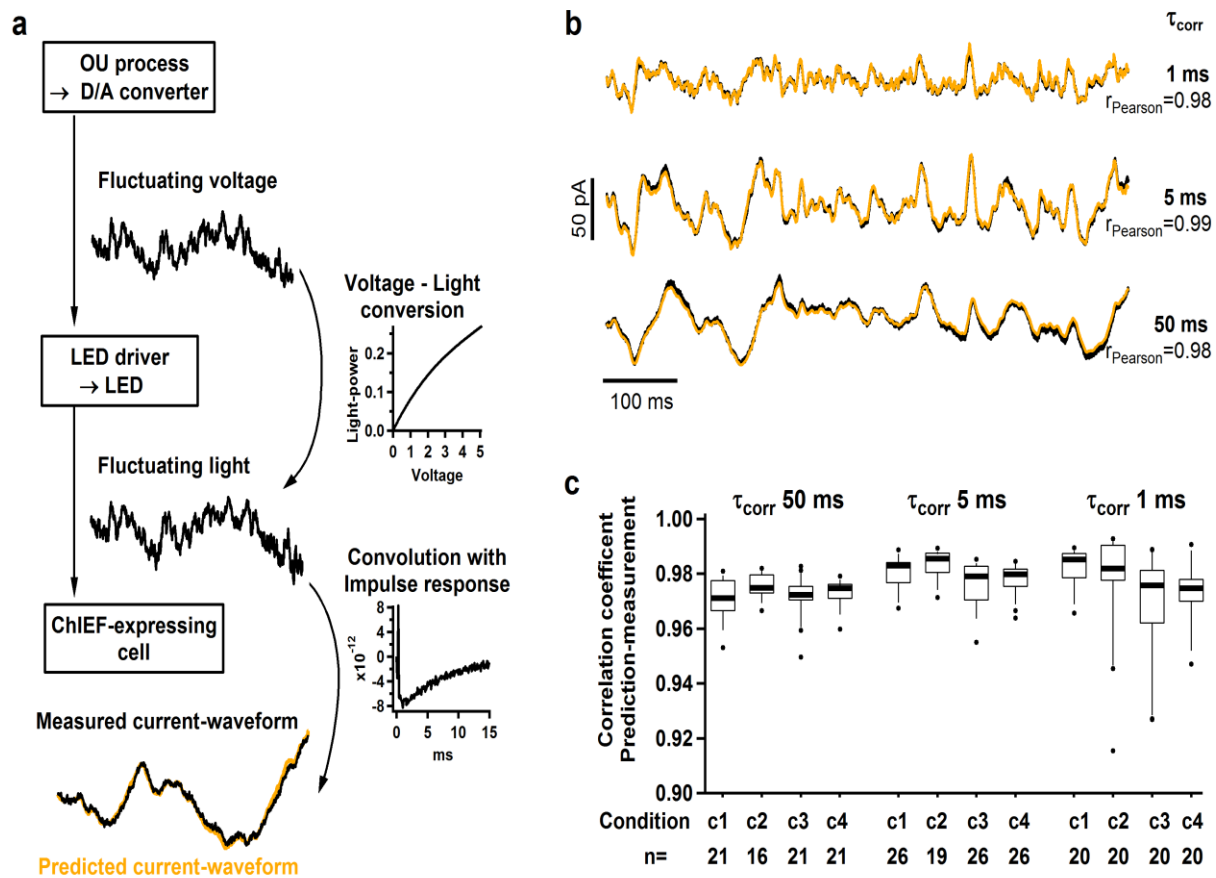


Figure 3.7: Computational prediction of CoDyPs-driven currents

a, flow chart depicting the prediction of CoDyPs induced currents: a fluctuating voltage signal is fed through the digital/analog board to the LED-driver. By means of the transfer function of the LED-driver the light waveform can be calculated. This is folded with the IRF of the employed channelrhodopsin to obtain the predicted conductance change.

b, The average current responses from Fig. 3 are shown in black, vertically displaced for clarity. Response predictions, constructed by convolution of light stimuli (Fig. 3 top panels) and average impulse response functions (a) are overlaid in orange. These predictions closely match the actual currents after they have been scaled and offset according to the mean and standard deviation of the current waveform. For $\tau_{\text{corr}} = 50$ ms the noisy average impulse response function was substituted for by the fit function (grey in a) to reduce the noise level in the prediction. **c**, For each correlation time the coefficient of correlation between the prediction and the average current is very high.

2.5. Long term CoDyPs of cultured neurons

So far our results demonstrate that conceivably CoDyPs satisfies the requirements for a noninvasive stimulation method with respect to reproducibility, bandwidth and predictability. The estimation of the fractional proton flux, however, raises the question whether cells will be able to handle the involved proton influx. We therefore set out to directly test, whether CoDyPs is suitable for noninvasive long-lasting experiments without compromising neuron survival and most importantly neuronal response properties. To this end neurons were cultured on multielectrode arrays to detect the action potentials and transfected with Chop2. Pharmacological block of synaptic transmission abolished all spontaneous action potentials. The cells were repeatedly exposed to 60 minutes continuous stimulation with fluctuating light, interrupted by 60 minutes without light. In experiments lasting up to 9 hours neuronal action potential patterns were remarkably stable and convincingly related to the predicted conductance input (Fig. 8b). The firing rate displayed a systematic relation to stimulus parameter ((Fig. 8a), most notably a transient increase at the begin of each 60 minute stimulation period but also a small increase for when the correlation time was increased from 5 ms to 10 ms. As action potential patterns are very sensitive to changes in the membrane potential we conclude that the neurons' conditions were stable, indicating that CoDyPs is indeed a very valuable tool in studying dynamic properties of neurons, allowing noninvasive stimulation for many hours.

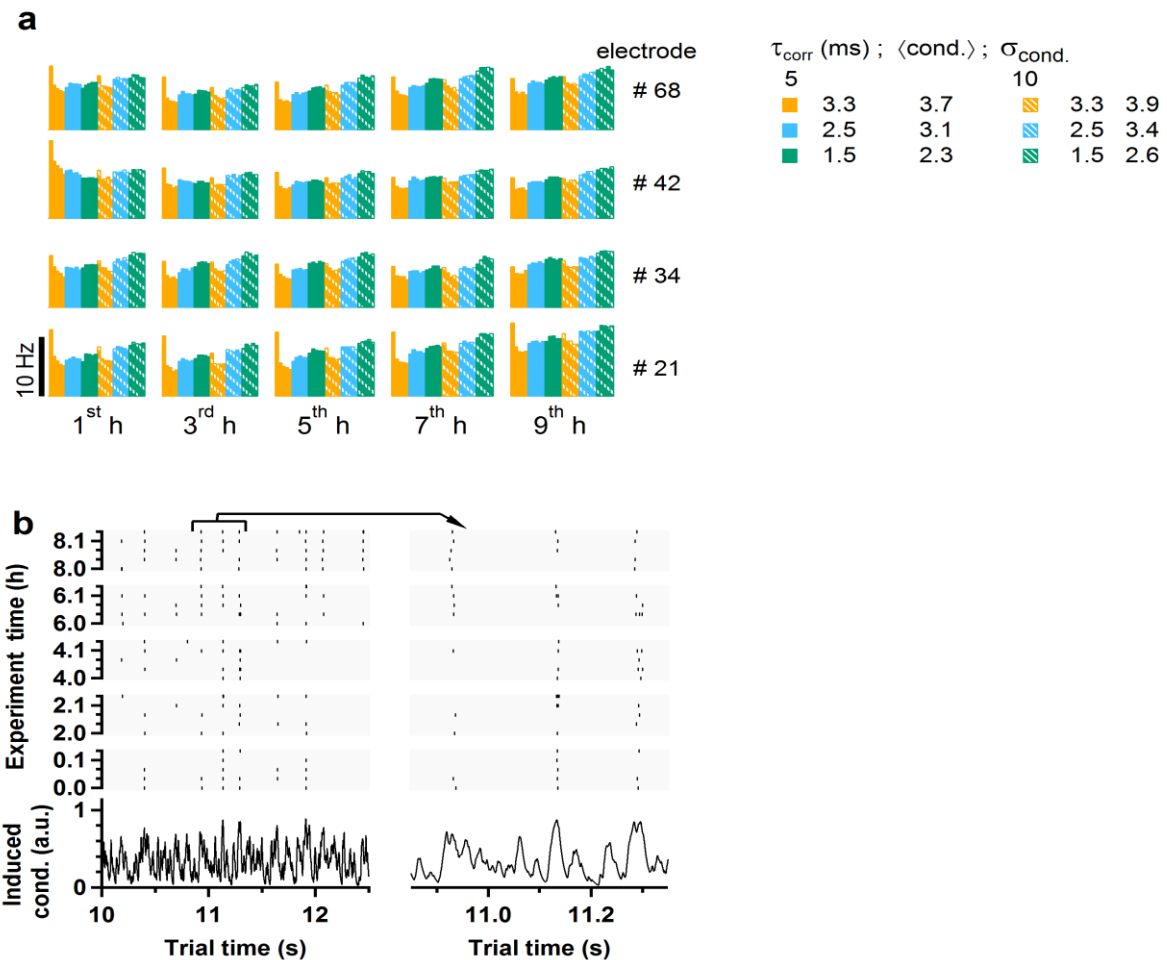


Figure 3.8: CoDyPs elicits stable and highly correlated action potential sequences over many hours

a, Neurons expressing ChR2 were cultured on multi-electrode arrays, permitting non-invasive detection of action potentials. detected by extracellular Each of six different 2 minute light stimuli was presented five times in a row, totalling 60 minutes of stimulation. For the 4 electrodes with the highest firing rates the average rate of action potentials is plotted for each 2 minute stimulation period. The conductance predicted for the stimuli differed by average and standard deviation (3 different levels each) and the correlation time (5 and 10 ms).The 60 minute block was repeated five times interspersed by one hour darkness. Changing the stimulus reproducibly changes the action potential rate. Onset of stimulation after 1 h darkness causes a very strong transient increase in the firing rate **b**, Raster plots of spike times, displayed above the predicted light induced conductance waveform, show that spike patterns were stable and highly correlated over many hours

3. Discussion:

Controlled naturalistic stimulation of neurons and sensory systems is a powerful experimental strategy that has revealed fundamental aspects of neuronal processing including high rates of encoded sensory information (Bialek et al. 1991, Rieke et al. 1995, Borst et al. 1999) and the surprisingly high bandwidth of cortical population dynamics (Boucsein et al. 2009, Kondgen et al. 2008, Higgs et al. 2009, Tchumatchenko et al. 2011). It aims to characterize neuronal dynamics under *in-vivo*-like working conditions. Theoretical neuroscience has developed and validated computational concepts and tools of steadily increasing sophistication to model and analyzes neuronal operations in the fluctuation driven firing regime (Mainen et al. 1995, VanVreeswijk et al. 1996, Brunel et al. 2001, Hansel et al. 2002, Fourcaud-Trocme et al. 2003, Naundorf et al. 2005, de la Rocha et al. 2007, Lundstrom e al. 2008, Tchumatchenko et al. 2010, Monteforte et al. 2010, Wei et al. 2011). In the present study we have developed a non invasive optogenetic approach that meets the key requirements of a stimulation applicable to such studies: the stimuli are reliable, offer the necessary bandwidth and the stimulus waveform can be designed. This non-invasive, yet controlled stimulation method has the potential to revolutionize data collection in this field of neuroscience, enabling large-scale high throughput screening or targeted studies of cellular mechanisms. CoDyPs is distinct from most previous applications of excitatory optogenetic tools. Both, *in-vivo* and *in-vitro* many studies succeeded to control impulse activity by imprinting action potential sequences stimulating with sequences of light flashes (Boyden et al. 2005) or raising firing rates by study depolarization (Adesnik et al. 2010). Some of the latest advances in engineering Channelrhodopsins have specifically enhanced the usability of light gated ion channels for this type of applications (Cheta (Gunaydin et al. 2010) , CatCh (Kleinogel et al. 2011), bistable ChRs (Berndt et al. 2009)).

In contrast CoDyPs drives cells by a quantitatively controlled ongoing conductance fluctuations mimicking background synaptic activity. In this approach the neuron decides whether and when to generate action potentials in the way that reflects a realistic interplay of intrinsic dynamics and complex input patterns. It is worth to notice that CoDyPs is facilitated by slow and weak inactivation of and a low single channel conductance, molecular features that are not specifically helpful for precisely imprinting predetermined spiking patterns. ChIEF's strongly reduced inactivation supports the

generation of ongoing conductance fluctuations around the maintained mean level. The generally small single channel conductance of Channelrhodopsins is the basis of the small trial to trial fluctuations that make CoDyPs currents highly reproducible. The molecular property that appears as the most severe limitation of currently available optogenetic tools is the characteristic response time on the order of 7 to 8 ms of both ChIEF and ChR2. It would be desirable to develop Channelrhodopsin variants with faster off-kinetics to extend the use of CoDyPs even to the white noise limit. It will be interesting to test variants of channelrhodopsin 2 such as ChETA and the double mutant E123T/T159C to drive neurons at higher frequencies.

Perhaps the most surprising result of our study is the precision and ease with which CoDyPs induced conductance fluctuations can be predicted and designed. We found that a simple linear response theory approach is sufficient to computationally reconstruct dynamic conductance fluctuations with virtually perfect accuracy. In addition, filter parameters were only weakly dependent on stimulus conditions such that a small and easily parameterized library of response functions appears sufficient

Thus even in the cell with unknown ChIEF expression level, precise calibration of photon flux in the sample plane is sufficient to accurately predict a fluctuating conductance waveform. The absolute conductance scale can be adjusted using average and standard deviation of the firing rate measurements obtained from extracellular electrodes. In addition whole cell recordings at the end of the CoDyPs recording would provide the magnitude of the light induced conductances. Together with the long term stability of CoDyPs driven spiking patterns, our findings established that virtually all experimental paradigms previously realized by whole cell stimulation and recording can be performed using CoDyPs, including measurements of firing frequency – input current curves for different input statistics (Arsiero et al. 2007) and measurements of the functional input-bandwidth of neurons (Kondgen et al. 2008, Higgs et al. 2009, Tchumatchenko et al. 2011) With patterned illumination, each neuron can receive a particular stimulus extending the use of CoDyPs to the simulation of shared inputs. In this way correlations in the spike trains of the illuminated neurons due to partially correlated inputs can be measured, a task that is notoriously complicated using invasive methods. One can also make use of neuronal cultures patterning technique to build up isolated islands of neurons that can be addressed both individually and simultaneously thus increasing the precision

and the versatility of our continuous dynamic photostimulation paradigm. One should note that for many of those measurements, such as correlation gain or dynamic gain measurements, only the conductance waveform and not the absolute scale of conductance fluctuations needs to be known.

CoDyPs may also turn out effective for controlling the activity of intact networks *in-vivo*. Modeling studies of cortical networks raise the possibility that driving only a subset of neurons with naturalistic inputs can effectively control the state of the entire network if the inputs are shaped to match network generated inputs (Marre et al. 2009). While more theoretical work is needed to clarify the dynamic properties of cortical networks (Monteforte et al. 2010, Jahnke et al. 2008, Zillmer et al. 2009) one expects in general that complex and time dependent inputs can control the network dynamics while preserving its intrinsic complexity (Molgedey et al. 1992). CoDyPs can be used to examine whether such naturalistic perturbation approaches can be used to control cortical networks *in-vivo*.

The possibility to detect action potentials over long periods of time and from many individual neurons in parallel will enable us to address new questions. Screening for the effect of mutations or short term protein knockdown will allow the dissection of the protein network underlying the dynamical properties of neurons. Comparisons of individual neurons might reveal individual differences with respect to dynamical properties. Combined with patch clamp measurements in previously identified cells it will be possible to reveal the biophysical basis of encoding diversity.

4. References:

- Adesnik, H. & Scanziani, M. (2010) Lateral competition for cortical space by layer-specific horizontal circuits. *Nature* 464, 1155-1160
- Alijani A, Richardson M (2011) Rate response of neurons subject to fast or frozen noise: From stochastic and homogeneous to deterministic and heterogeneous populations. *Phys Rev E* 84: 1–9.
- Arsiero, M., Luscher, H.-R., Lundstrom, B.N. & Giugliano, M. (2007) The Impact of Input Fluctuations on the Frequency-Current Relationships of Layer 5 Pyramidal Neurons in the Rat Medial Prefrontal Cortex. *Journal of Neuroscience* 27, 3274-3284
- Bamann, C., Kirsch, T., Nagel, G. & Bamberg, E. (2008) Spectral Characteristics of the Photocycle of Channelrhodopsin-2 and Its Implication for Channel Function. *Journal of Molecular Biology* 375, 686-694.
- Berndt, A., Yizhar, O., Gunaydin, L.A., Hegemann, P. & Deisseroth, K. (2009) Bi-stable neural state switches. *Nat. Neurosci* 12, 229-234.
- Bialek, W., Rieke, F., Steveninck, R.R. de R. van & Warland, D. (1991) Reading a Neural Code. *Science* 252, 1854-1857 .
- Boucsein C, Tetzlaff T, Meier R, Aertsen A, Naundorf B (2009) Dynamical response properties of neocortical neuron ensembles: Multiplicative versus additive noise. *J Neurosci* 29: 1006–1010
- Borst, A. & Theunissen, F.E. (1999) Information theory and neural coding. *Nat Neurosci* 2, 947-957.
- Boyden, E.S., Zhang, F., Bamberg, E., Nagel, G. & Deisseroth, K. (2005) Millisecond-timescale, genetically targeted optical control of neural activity. *Nat Neurosci* 8, 1263-1268.
- Brunel N, Latham P (2003) Firing rate of the noisy quadratic integrate-and-fire neuron. *Neural Comput* 15: 2281–2306.
- Brunel N, (2000) Dynamics of sparsely connected networks of excitatory and inhibitory spiking neurons. *J. Comput. Neurosci.* 8, 183 .
- Brunel N, Chance F, Fourcaud N, Abbott LF (2001) Effects of synaptic noise and filtering on the frequency response of spiking neurons. *Phys Rev Lett* 86: 2186–2189.

- Carandini M, Heeger DJ. (1994) Summation and division by neurons in primate visual cortex. *Science*. May 27;264(5163):1333-6.
- Carandini M, Mechler F, Leonard CS, Movshon JA. (1996) Spike train encoding by regular-spiking cells of the visual cortex. *J Neurophysiol*. Nov;76(5):3425-41.
- Chance FS, Abbott LF, Reyes AD (2002) Gain modulation from background synaptic input. *Neuron* 35: 773–782.
- De la Rocha J. , Marchetti C. , Schiff M., Reyes A.D. , (2008) Linking the response properties of cells in auditory cortex with network architecture: Cotuning versus lateral inhibition. *J. Neurosci*. 28, 9151.
- De la Rocha, J., Doiron, B., Shea-Brown, E., Josic, K. & Reyes, A. (2007) Correlation between neural spike trains increases with firing rate. *Nature* 448, 802-806 .
- Ditlevsen, S., Lansky, P. (2005) Estimation of the input parameters in the Ornstein-Uhlenbeck neuronal model. *Phys. Rev. E* 71, Art. No. 011,907.
- DeAngelis, G.C., Ohzawa, I. & Freeman, R. D. (1993). Spatiotemporal organization of simple cell receptive fields in the cat's striate cortex:II. Linearity of temporal and spatial summation. *Journal of neurophysiology* 69, 1118 – 1135.
- Eggermont, J. J, Johannesma, P.M. & Aertsen, A.M. (1983). Reverse correlation methods in auditory research. *Quarterly reviews of Biophysics*, 16, 341 – 414.
- Fourcaud-Trocme, N., Hansel, D., van Vreeswijk, C. & Brunel, N. (2003) How Spike Generation Mechanisms Determine the Neuronal Response to Fluctuating Inputs. *J. Neurosci*. 23, 11628-11640.
- Froemke R.C. , Merzenich M.M. , Schreiner C.E. (2007) A synaptic memory trace for cortical receptive field plasticity. *Nature* 450, 425.
- Gluss, B. (1967) A model for neuron firing with exponential decay of potential resulting in diffusion equations for probability density. *Bull Math Biophysics* 29, 233–243.
- Goldberg JM, Brown PB (1969) Response of binaural neurons of dog superior olivary complex to dichotic tonal stimuli: some physiological mechanisms of sound localization. *J Neurophysiol* 22: 613–636.
- Greenberg DS, Houweling AR, Kerr JND (2008) Population imaging of ongoing neuronal activity in the visual cortex of awake rats. *Nat Neurosci* 11: 749–751.
- Gunaydin, L.A. et al. (2010) Ultrafast optogenetic control. *Nat Neurosci* 13, 387-392.
- Hestrin S. (1993) Different glutamate receptor channels mediate fast excitatory synaptic currents in inhibitory and excitatory cortical neurons. *Neuron*. Dec;11(6):1083-91.

- Higgs, M.H. & Spain, W.J. (2009) Conditional Bursting Enhances Resonant Firing in Neocortical Layer 2-3 Pyramidal Neurons. *Journal of Neuroscience* 29, 1285-1299.
- Jahnke, S., Memmesheimer, R.-M. & Timme, M. (2008) Stable irregular dynamics in complex neural networks. *Phys. Rev. Lett* 100, 048102
- Kleinlogel, S. et al. (2011) Ultra light-sensitive and fast neuronal activation with the Ca²⁺-permeable channelrhodopsin CatCh. *Nat Neurosci* 14, 513-518 .
- Knight B (1972) Dynamics of encoding in a population of neurons. *J Gen Physiol* 59: 734–766.
- Koendgen H, Geisler C, Fusi S, Wang XJ, Luescher HR, et al. (2008) The dynamical response properties of neocortical neurons to temporally modulated noisy inputs in vitro. *Cereb Cortex* 18: 2086–2097.
- Lindner B, Schimansky-Geier L (2001) Transmission of noise coded versus additive signals through a neuronal ensemble. *Phys Rev Lett* 86: 2934–2937
- Margrie TW, Brecht M, Sakmann B (2002) In vivo, low-resistance, whole-cell recordings from neurons in the anaesthetized and awake mammalian brain. *Pflugers Arch* 444: 491–498.
- Marre, O., Yger, P., Davison, A.P. & Frégnac, Y. (2009) Reliable recall of spontaneous activity patterns in cortical networks. *J. Neurosci* 29, 14596-14606.
- Mainen, Z.F. & Sejnowski, T.J. (1995) Reliability of spike timing in neocortical neurons. *Science* 268, 1503-1506 .
- Meister, M. Pine, J., & Baylor, D.A. (1994) Multi-neuronal signals from the retina: acquisition and analysis. *Journal of neuroscience methods*, 51, 95 – 106.
- Mokeichev A, Okun M, Barak O, Katz Y, Ben-Shahar O, Lampl I. (2007) Stochastic emergence of repeating cortical motifs in spontaneous membrane potential fluctuations in vivo. *Neuron*. Feb 1;53(3):413-25.
- Molgedey, Schuchhardt & Schuster (1992) Suppressing chaos in neural networks by noise. *Phys. Rev. Lett* 69, 3717-3719 .
- Monteforte, M. & Wolf, F. (2010) Dynamical Entropy Production in Spiking Neuron Networks in the Balanced State. *Phys. Rev. Lett.* 105, 268104 .
- Murphy B.K. , Miller K.D. (2009), Balanced amplification: A new mechanism of selective amplification of neural activity patterns. *Neuron* 61, 635.
- Naundorf B, Geisel T, Wolf F (2005) Action potential onset dynamics and the response speed of neuronal populations. *J Comput Neurosci* 18: 297–309.
- Okun M, Lampl I. (2008) Instantaneous correlation of excitation and inhibition during ongoing and sensory-evoked activities. *Nat Neurosci*. May;11(5):535-7.

- Ostojic S, Brunel N (2011) From spiking neuron models to linear-nonlinear models. *PLoS Comput Biol* 7: e1001056.
- Reid, R. C. & Alonso, J.M. (1995) Specificity of monosynaptic connections from thalamus to visual cortex. *Nature*, 378, 281 – 284.
- Renart A. et al (2010) The asynchronous state in cortical circuits. *Science* 327, 587.
- Rieke, F., Bodnar, D.A. & Bialek, W. (1995) Naturalistic Stimuli Increase the Rate and Efficiency of Information Transmission by Primary Auditory Afferents. *Proceedings: Biological Sciences* 262, 259-265.
- Schwartz O, Pillow JW., Rust NC., Simoncelli EP (2006) Spike triggered neural characterization. *Journal of vision* 6, 484 – 507.
- Silberberg G, Bethge M, Markram H, Pawelzik K, Tsodyks M (2004) Dynamics of population rate codes in ensembles of neocortical neurons. *J Neurophysiol* 91: 704–709.
- Shu Y. , Hasenstaub A., McCormick, D.A. (2003) Turning on and off recurrent balanced cortical activity. *Nature* 423, 288.
- Stern P, Béhé P, Schoepfer R, Colquhoun D. (1992) Single-channel conductances of NMDA receptors expressed from cloned cDNAs: comparison with native receptors. *Proc Biol Sci. Dec* 22;250(1329):271-7
- Tchumatchenko T, Malyshev A, Wolf F, Volgushev M (2011) Ultra-fast population encoding by cortical neurons. *J Neurosci* 31: 12171–12179
- Tchumatchenko, T., Malyshev, A., Geisel, T., Volgushev, M. & Wolf, F. (2010) Correlations and synchrony in threshold neuron models. *Phys. Rev. Lett* 104, 058102.
- Tsodyks M, Sejnowski T. (1995) Rapid state switching in balanced cortical network models. *Network Comput. Neural Syst.* 6, 111 .
- Tuckwell, H.(1988) Introduction to theoretical neurobiology, Vol.2: Nonlinear and stochastic theories. Cambridge Univ. Press, Cambridge .
- Tuckwell, H. (1989) Stochastic Processes in the Neurosciences. SIAM, Philadelphia.
- Tuckwell, H.(2006): Spatial neuron model with two-parameter Ornstein-Uhlenbeck input current. *Physica A* 368, 495–510 .
- Wei W, Wolf F (2011) Spike Onset Dynamics and Response Speed in Neuronal Populations. *Phys Rev Lett* 106: 1–4.
- Wehr M. , Zador A.M., (2003) Balanced inhibition underlies tuning and sharpens spike timing in auditory cortex. *Nature* 426, 442.

Van Vreeswijk C., Sompolinsky H., (1996) Chaos in neuronal networks with balanced excitatory and inhibitory activity. *Science* 274, 1724 .

Vogels T.P., Abbott L.F., (2009) Gating multiple signals through detailed balance of excitation and inhibition in spiking networks. *Nat. Neurosci.* 12, 483.

Zillmer, R., Brunel, N. & Hansel, D. Very long transients, irregular firing, and chaotic dynamics in networks of randomly connected inhibitory integrate-and-fire neurons.(2009) *Phys. Rev. E* 79, 031909.

CHAPTER 4

Materials and Methods

1. Cell culture:

1.1. Cell preparation:

Cell cultures were prepared according to Brewer et al. 1993. Hippocampal neurons were obtained from Wistar-Kyoto (WU) rat embryos at 18 days of gestation (E18). The pregnant rat was anaesthetized with CO₂. The embryos were then removed by a caesarean section, decapitated and transferred to petri dishes cooled on ice. The skull cavity was opened and the brain removed. Hippocampi were surgically isolated under the microscope and transferred to a mixture of 9 ml Neurobasal and 1 ml HEPES buffer. The supernatant was removed and the isolated hippocampi were trypsinized in Trypsin/EDTA buffer for 15 minutes at 37 °C. Trypsinized hippocampal neurons were then transferred to a 10% FCS solution. Then the cells were homogenized 15 times with a syringe and a needle of 1 mm diameter. The cell suspension was then centrifuged at 1200 rpm for 2 minutes. The pellet was re-suspended in 2 ml of serum free B27/Neurobasal medium supplemented with 0.5 mM glutamine and bFGF. Cells were counted in a Neubauer chamber. Cells were then cultured on multielectrode arrays (Standard MEA; type TiN-200-30iR from Multichannel Systems, Fig 4.1) coated with a mixture of poly-D-lysine and laminin at a density of 1000 cells per mm². A droplet of approximately 100 µl cell suspension was added in the middle of the multielectrode array to cover the recording area. The arrays were then filled with 1 ml of the aforementioned serum free B27/Neurobasal medium. The cells were kept in an incubator at 37°C and a mixture of 5% CO₂+ 95% O₂. Half of the medium was changed every two days. The cultures were kept till 40 DIV. MEAs were sealed with gas permeable membrane dishes which allowed the long term culture. The culture dishes are sealed with a Teflon membrane, fluorinated ethylene-propylene. Although the membrane has no pores (thus

preventing infection), it is quite permeable to some small molecules notably oxygen and carbon dioxide. It is hydrophobic and thus relatively impermeable to water and water vapor. The membrane slows the shift in pH of carbonate buffered media caused by removal from an incubator with 5% CO₂ atmosphere, by about a factor of two compared to a standard culture dish with an air gap (Hales 2010).

All animals were kept and bred in the animal house of the Max Planck Institute for Experimental Medicine according to the German guidelines for experimental animals. Animal experiments were carried out with authorization of the responsible federal state authority.

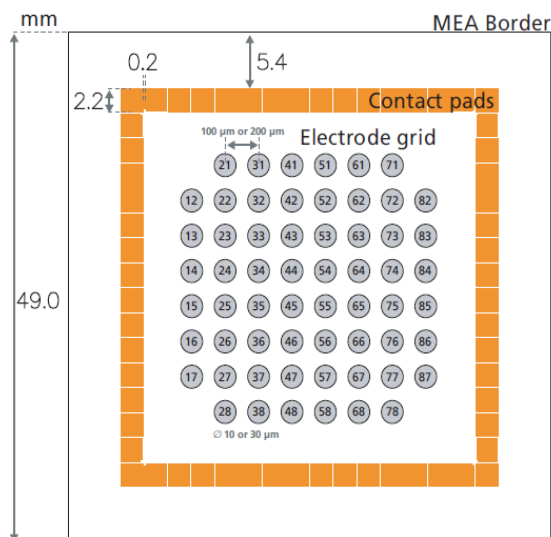


Figure 4.1.: Layout of Multielectrode Array TiN-200-30iR. showing the layout of electrodes (electrode diameter 30 μm and inter-electrode distance of 200 μm). The ground electrode is electrode number 15.

1.2. Cleaning procedure of the multielectrode arrays:

Multielectrode arrays are treated with 1ml Korda for 30 minutes to remove cells plated on the surface and clean the surface of the multielectrode array. Then the arrays are rinsed with 1ml double distilled water to remove cellular debris. Subsequently, the arrays are autoclaved at 120°C for two hours. Then in order to increase the hydrophilicity of the surface, 1 ml 10% FCS solution was added for 30 minutes. The surface was subsequently rinsed with water and becomes ready for coating.

1.3. Coating procedure of multielectrode arrays:

After cleaning the multielectrode arrays, 1ml of coating solution is added. The coating solution consists of 200 μ l poly-D-lysine and 160 μ l Laminin dissolved in 15 ml double distilled water. The multielectrode arrays are then put in the incubator at 37°C and a mixture of 5% CO₂+ 95% O₂. Before plating the cells, the coating solution is removed and the arrays are rinsed two times with double distilled water and left to dry.

1.4. Neuronal cultures quality control:

Hippocampal cultures were checked 2 days after plating. In case they did not grow processes, they were discarded. The following figure (Fig.4.2) exemplifies the morphology and structure of an E18 hippocampal culture grown on multielectrode arrays (in this case 21 DIV):

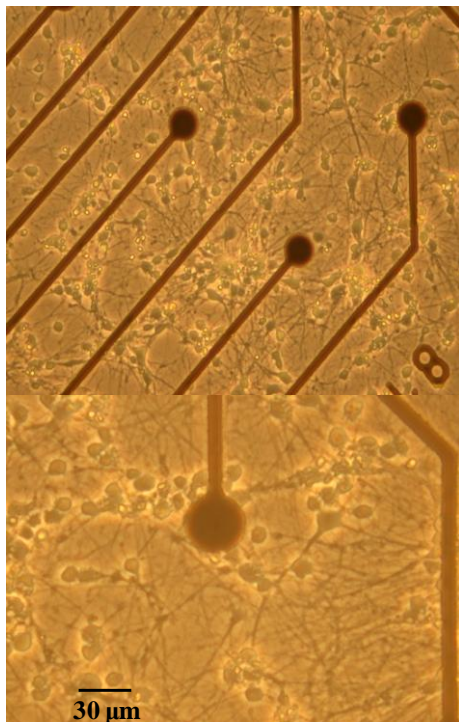


Fig 4.2: E18 hippocampal neurons grown on Multielectrode arrays (21 DIV) The black dots correspond to the electrodes. The upper picture is a 20X magnification and the lower picture is a 40X magnification

Cell culture materials:

Chemical / reagent /medium	Company	Catalog number
HEPES buffer (1M)	Gibco	15630
Neurobasal medium	Gibco	12348
B27	Gibco	17504- 044
Trypsin buffer: Trypsin 0.05 % (w/v) EDTA 0.02 % (w/v) In PBS without calcium and without magnesium.	Biochrome	L2143
Phosphate- buffered saline solution (PBS) prepared by mixing: 10 mM Potassium phosphate buffer (pH 7.4) 150 mM Sodium chloride	Gibco	18912- 014
Fetal Calf Serum	Biochrome	50215
L-Glutamine solution liquid (200 mM)	Sigma	G7513
Human recombinant basic fibroblast growth factor (bFGF) (5 ng/ml)	Gibco	13256029
Poly-D-Lysine	Sigma- Aldrich	P7886
Laminin (1 mg/ml)	Sigma - Aldrich	L2020
Korda	Ecolab	GU40

2. Electrophysiology:

2.1. Multielectrode arrays measurements:

Recordings were done on 21 DIV hippocampal neuronal cultures (transfected at 14 DIV with AAV-CAG-CHOP2 virus). Data from MEAs were captured at 25kHz using a 64-channel A/D converter and MC_Rack software (Multichannel Systems, Reutlingen). The MCS measurement card has 64 analogue input channels, with a resolution of 16 bit, a programmable gain and an input voltage range of ± 400 mV to ± 4 V, depending on the gain level specified. Sixty of these serve as input channels for the multi electrode array (MEA), three serve as analogue inputs, and one of which serves as a combined channel for 16 digital inputs, which each set a single bit. Amplifier gain was set to 1100. After high pass filtering (Butterworth 2nd order, 100 Hz) action potentials are detected in a cutout recorded 1ms before and 2ms after crossing a threshold of -20 μ V, which was > 3 times standard deviations of the baseline activity. Routinely, it was made sure that the amplifier noise does not exceed ± 10 μ V which was indicated by manufacturer to be the acceptable noise level. Standard recording were performed for a maximum of 30 minutes. Longer recordings were performed under continuous perfusion.

2.2. Perfusion system:

For long term experiments, a continuous perfusion system was employed where the culture was continuously perfused with sterile serum free B27/Neurobasal medium. A slow and steady supply of Carbogen gas was performed using a water sealed gasometer . The flow rate that was found to be optimal is 1ml/hour where the medium with the multielectrode array chamber is totally exchanged each one hour.

2.3. Synaptic blockade experiments:

30 μM Bicucilline or 100 μM Picrotoxin were used to completely block GABA_A receptors. 100 μM D-AP5 were used to completely block NMDA type receptors. 50 μM NBQX were used to block AMPA type receptors is used. In case complete synaptic blockade is needed, a mixture of the three aforementioned synaptic blockers is used.

Materials for synaptic blockade experiments:

Chemical	Company	Catalog number
Bicucilline	Sigma - Aldrich	14340
Picrotoxin	Sigma - Aldrich	P1675
D-AP5	Sigma - Aldrich	A5282
NBQX disodium salt	Sigma - Aldrich	N183

3. Whole Field Photostimulation:

3.1. Illumination setup:

3.1.1. Light source used for illumination:

The key requirements for the light source were high light power at around 480 nm, fast and well controllable modulation of the light power and stable illumination over several hours. An additional requirement for the illumination of the spatially extended MEAs is homogeneous light power density over an area of 1×1 mm. All these requirements were met by a blue light emitting diode (LED, Luxeon rebel color with Lambertian dome, Philips Lumileds) with 5 W maximal power consumption, placed 25 mm below the illuminated hippocampal neuronal cultures grown on multielectrode arrays. The absorption spectra of the LEDs have a large overlap with the absorption spectra of channelrhodopsin 2 (Fig 4.3). The light output was controlled via the voltage of STG 2008 stimulus generator, converted to current in a custom made analog driver circuit, resulting in a input of 1 W at the LED for each Volt at the D/A-board. Rise-time to maximum Light power was $< 20 \mu\text{s}$.

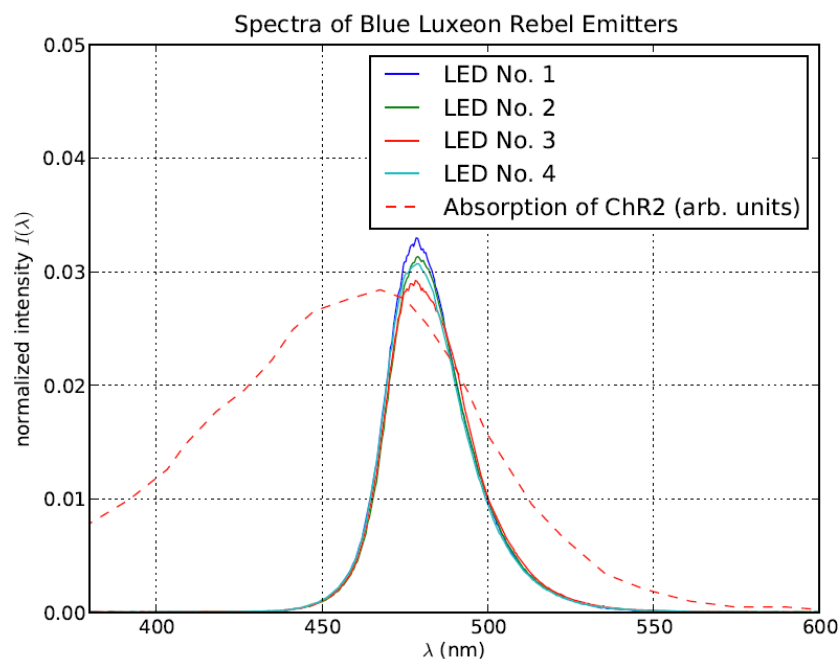


Fig 4.3: Blue Luxeon Rebel LED and Channelrhodopsin 2 absorption spectra overlapped. The spectra of 4 blue luxeon rebel LEDs overlapped reflecting the reproducibility of their spectra. The absorption spectra of Channelrhodopsin 2 have a large overlap with the spectra of the LEDs.

3.1.2. Irradiance measurement:

The irradiance arriving to the cell culture is measured with a custom-made device which is placed on the microscope instead of the culture. It consists of a piece of soda lime glass with the same dimensions as a MEA, onto the middle of which a photodiode combined with a trans impedance amplifier (OPT101 from TI/Burr-Brown) is glued with epoxy resin. For the rather high irradiance deriving from the LED to the culture, a suitably calibrated neutral density filter must be put in front of the photodiode to lower the incident power to a measurable range. For this task, a small piece of ND 5 Baader foil is placed between the light source and the OPT101. For precision measurements, this piece of filter also must be calibrated for the wavelength employed. By adapting the feedback resistor of the OPT101, its output can either be adjusted to yield 1 V per 1 mW/mm²; otherwise, a short computation is necessary to derive the correct value of the irradiance incident on the culture. The spatial structure of the irradiance above the LED is measured with a pinhole in front of the photodiode, which is moved on a micrometric cross table. As we are looking for a relative measurement of irradiance covering several square millimeters in the plane of the culture, no calibration of the photodiode is required. The light power distribution is shown in Fig 4.4. On the other hand, the relationship between command voltage and irradiance is shown in Fig 4.5.

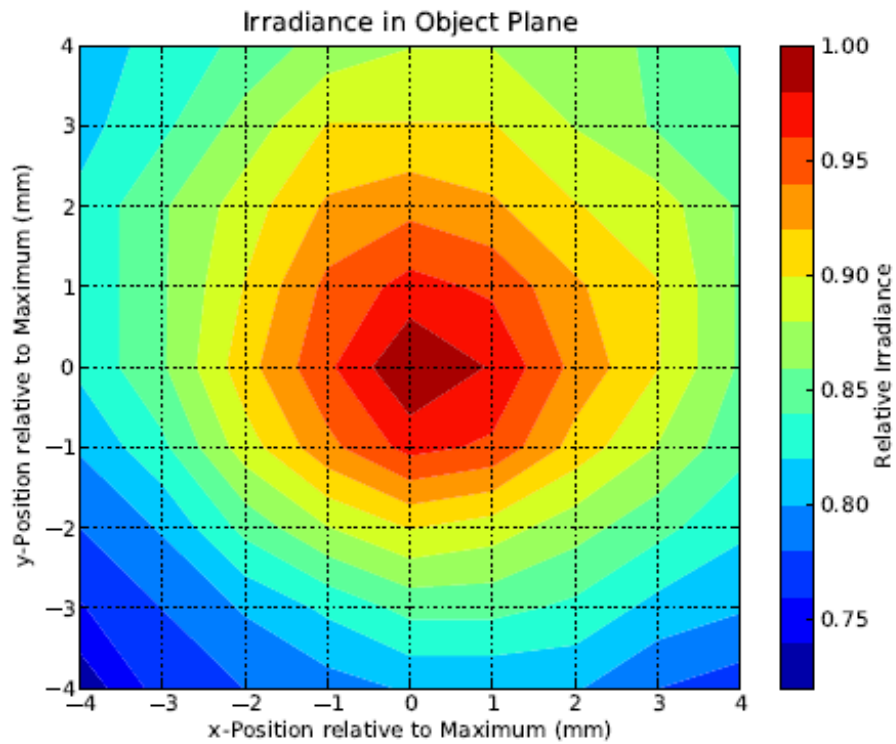


Fig 4.4: Relative irradiance measured by a photodiode The multielectrode array active area where the electrodes are placed is the middle $1 \times 1 \text{ mm}^2$. The above figure shows that the relative irradiance does not nearly fall off over the inner most $1 \times 1 \text{ mm}^2$.

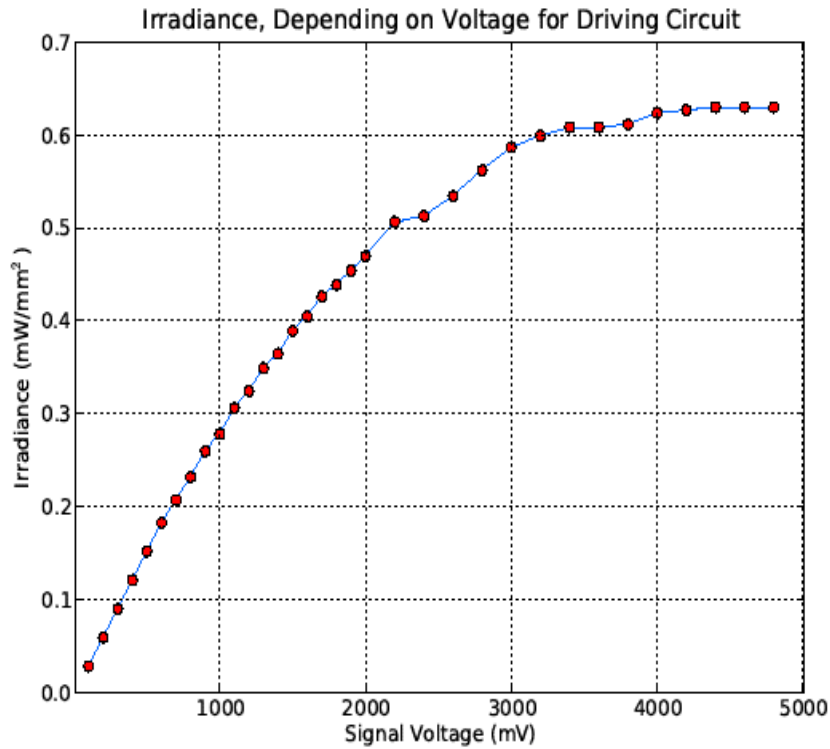


Fig 4.5.: Relationship between the command voltage from STG 2008 (Multichannel systems, Reutlingen) and the irradiance (mW/mm²) as measured by photodiode

3.2. Photostimulation paradigms:

For *the optogenetic induction of network level plasticity* (Chapter 2), two paradigms of whole field blue light stimulation were designed: 40x1 second (1) rectangular (constant) and (2) ramp pulses with frequency of 0.5Hz. The stimulation pulses were designed on MC_stimulus software (Multichannel systems, Reutlingen) and used to drive the STG2008. The stimulus generator STG2008 is driven; one of its analogue output lines is attached to a power amplifier which drives the photo-stimulation LED, a blue Luxeon Rebel Color, which stimulates the culture in whole field illumination. The signals picked up by the MEA amplifier are fed into the MC Card installed in the measurement PC. To be able to time the stimulus with the measurement, a ttl-signal is switched from low to high on one of the STGs SYNC outputs and fed into a digital input on the MC Card.

Twenty two experiments with constant stimulation on nineteen cultures and nineteen experiments with ramp stimulation, on sixteen cultures, were performed. In each experiment, before the onset of the stimulation, the spontaneous activity of the culture was recorded for 5 minutes. Then the culture was stimulated with one of the aforementioned stimulation paradigms. After offset of the stimulation the spontaneous activity was recorded for 12 minutes.

As for *continuous dynamic photostimulation experiments* (Chapter 3), the intensity over time of the stimulus is recorded with a photodiode as described earlier and stimulus was generated by a Matlab script that feed the Ornstein Uhlenbeck stimuli into the STG 2008. For the design of the parameter and the procedure by which each specific OU process is generated, please check part 5.1 stimulus generation.

4. Molecular Biology:

4.1. Cloning:

4.1.1. Cloning Channelrhodopsin 2 construct under an α MHC promoter for cardiac specific expression:

4.1.1.1. Transformation procedure of pcDNA3.1-CHOP2-YFP :

pcDNA3.1-CHOP2-YFP was obtained from Prof. Ernest Bamberg at the Max Planck Institute for Biophysics (Frankfurt). 100 μ l pre-prepared chemocompetent DH5 α cells were thawed on ice. pcDNA (2.2 μ g/ μ l) was diluted to 220 ng/ μ l. 1 μ l of pcDNA solution is added to the cell solution and mixed gently. The mixture is left on ice for 20 minutes. Then it is heated at 42 °C for 2 minutes in the thermomixer. After that, the mixture is added briefly on ice. Near the flame in sterile condition, 1 ml of fresh LB medium is added to the cell solution (it is important to note that the transfer of LB medium from bottle to the tube should also be done near the flame).

4.1.1.2. Culturing transformed cells:

The cell solution is put at 37 °C for one hour with shaking. Near the flame, the cells are plates in two LB-Ampicillin agar plates. Agar plates are then incubated overnight at 37 °C. Subsequently, one colony was taken from the agar plate and added to a sterile flask containing 100 ml LB medium + 100 μ l ampicillin then the flask is shacked overnight at 37 °C.

4.1.1.3. Maxi Preparation of pcDNA3.1-CHOP2-YFP:

For the DNA extraction from the aforementioned cultured cells the QIAGEN EndoFree Plasmid Purification Kit (Qiagen, Germany) was used and carried out the procedure

according to the enclosed protocol after the cell solution had been transferred into Falcon tubes and centrifuged at 5000 rpm for 15 min at room temperature. The DNA concentration was determined using UV spectrophotometer at 260 nm (dilution factor 1:100). As a quality control, the DNA was considered pure if the A260/A280 ratio is larger than 1.8 and the A260/A230 is larger than 2.0 – 2.2.

4.1.1.4. Transformation of the reverse α MHC plasmid:

The reverse α MHC plasmids (Fig 4.6.) was obtained from Prof. Wolfram Zimmermann at the department of pharmacology at the University of Goettingen hospital. The transformation, culturing and maxi preparation were performed according to the procedure in 4.1.1.1, 4.1.1.2, 4.1.1.3..

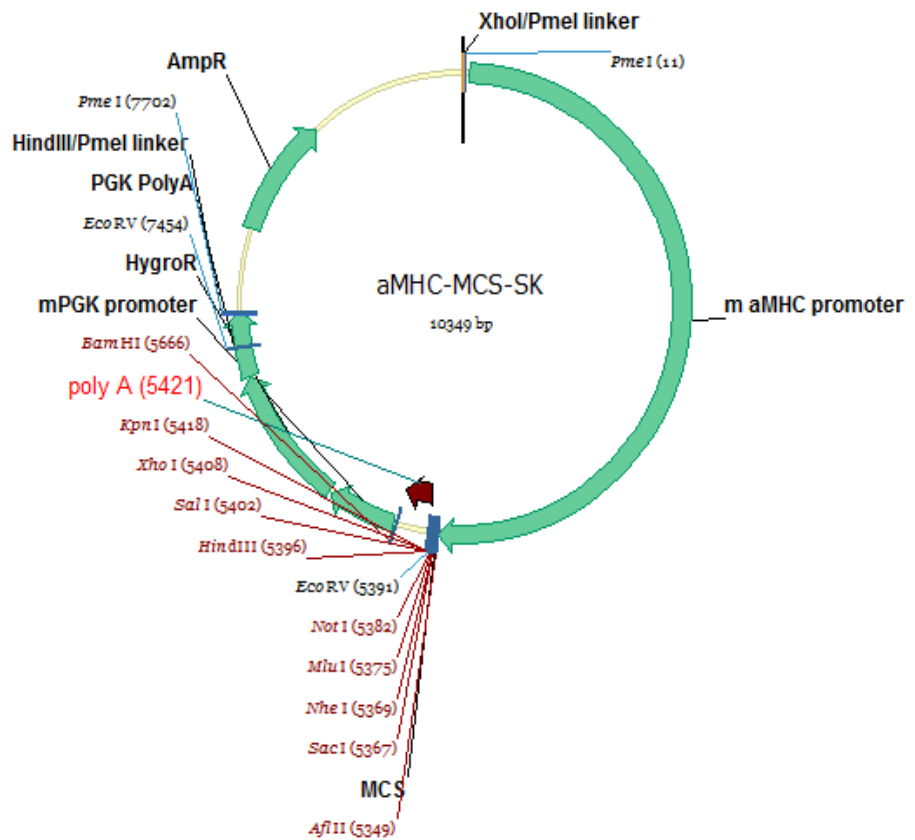


Fig 4.6: Plasmid map of the reverse α MHC plasmid

4.1.1.5. PCR cloning:

For the PCR experiment, two probes were prepared with different quantities of the template according to the following recipes:

Material	PCR probe 1	PCR probe 2
Forward primer (oligoname: COP2-fw-NheI, concentration: 50 pmole/l)	1 μ l	1 μ l
Reverse Primer (oligoname: YFP-rv-Sall, concentration: 50 pmole/l)	1 μ l	1 μ l
Template (pcDNA3.1-CHOP2-YFP)	1 μ l of 100 ng solution	0.5 μ l of 100 ng solution
TX10 Buffer	5 μ l	5 μ l
dNTPs mixture (200 μ M)	1 μ l	1 μ l
High fidelity polymerase (mixture of Taq polymerase + proof reading)	1 μ l	1 μ l
Double distilled water	40 μ l	40.5 μ l
Total volume	50 μ l	50 μ l

Sequences of the primers were as follows:

COP2-fw-NheI: 5'-CTA GGC TAG CAT GGA TTA TGG
AGG CGC CCT GAG-3'

YFP-rv-SalI: 5'-ACG CGT CGA CTT ACT TGT ACA GCT
CGT CCA TG-3'

The two probes are put in the thermocycler and the following
cycling program is applied:

Segment	Cycles	Temperature	Time
1	1	95 °C	5 minutes
2	30	95 °C	30 seconds
		60 °C	1 minute
		72 °C	10 minutes
4	1	72 °C	10 minutes
5		4 °C	hold

4.1.1.6. Gel electrophoresis:

1 % agarose gel is prepared by dissolving 0.5 g Agarose (electrophoresis grade) in 50 ml TBE buffer by cooking it in the microwave at 600 Watt for 1.5 minutes then one drop of

Ethidium Bromide is added. After cooling a bit, the 1% agarose solution is poured into the gel holder. Meanwhile, the probes are prepared as follows: first 10 μ l DNA ladder, 5 μ l α MHC reverse plasmid mixed with 1 μ l loading buffer, 5 μ l PCR probe 1 mixed with 1 μ l loading buffer, 5 μ l PCR probe 2 mixed with 1 μ l loading buffer. As soon as the gel solidifies, the gel is transferred to the electrophoresis chamber, soaked in TBE buffer and then the probes are loaded into the gel. The voltage across the gel is set to 90V for 30 minutes. Concerning the PCR probes, the band of interest corresponding to CHOP2-YFP is around 1.6 kb. The band was observed clearly in the case of PCR probe 1 with a higher template volume (1 μ l) that was run on the gel. After that a preparative gel was run with a higher volume of PCR probe 1 according to the aforementioned procedure. The band of interest (1.6 kb) was excised and the DNA was extracted from the gel fragment using the NucleoSpin Extract kit (Macherey Nagel) according to the enclosed protocol. After DNA extraction, ligation was performed as follows:

pGem-T-Easy plasmid	1 μ l
PCR product	3 μ l
X2 T4 Ligase Buffer	5 μ l
T4 Ligase enzyme	1 μ l
Total volume	10 μ l

A control is prepared in the same way but instead of the PCR product, sterile bidistilled water is used. The ligated PCR products were transformed and cultured according to the

aforementioned procedure and plated on Ampicillin Agar Plates supplemented with 40 μ l X-Gal and 40 μ l IPTG overnight. The ligand control had nearly no white colonies and was full of blue colonies. Concerning the plates of the ligated PCR products there was a large number of white colonies and blue colonies. Whitish colonies were picked and cultured in test tubes then spotted on ampicillin agar plates. A Mini preparation was then performed using NucleoSpin plasmid kit (Macherey Nagel) following the enclosed protocol. The best clone of pGem-T-Easy-CHOP2-YFP was chosen according to results of digestion with EcoR1 that gave the expected band of the insert (1.6 kb) and the sequencing results.

4.1.1.7. Digestion:

Digestion at 37 °C using the restriction enzyme NheI was performed according to the following recipe:

	Probe 1	Probe 2
pGem-T-easy-CHOP2-YFP	50 μ l (3 μ g)	--
Reverse α MHC plasmid	--	5 μ l (1 μ g)
X10 Buffer(2)	10 μ l	10 μ l
BSA 100X	1 μ l	1 μ l
Nhe I	3 μ l	3 μ l
Double distilled water	37 μ l	83 μ l
Total volume	100 μ l	100 μ l

The digestion products were then purified using NucleoSpin extract kit following the enclosed protocol. Then digestion, using the restriction enzyme Sall, was performed according to the same aforementioned digestion recipe. The digestion probe 1 (pGEM-T-easy-CHOP2-YFP) was run on a 1% agarose preparative gel and the band of interest (1,6 kb) is isolated from the gel. The digestion probe 2 (containing the reverse α MHC plasmid) was dephosphorylated for one hour at 37 °C by adding 1 μ l shrimp alkaline phosphatase and 5 μ l T X10 SAP enzyme buffer to 44 μ l of purified digestion probe 2. After dephosphorylation, the reaction is inactivated by adding 50 μ l distilled water and putting the reaction mixture at 65 °C for 20 minutes.

4.1.1.8. Ligation:

The ligation probe is prepared by mixing 1 μ l of ligase buffer, 1 μ l ligase enzyme, 1.5 μ l reverse alpha MHC plasmid and 6.5 μ l insert. The ligation control was prepared as aforementioned but the insert was replaced with double distilled water. The probes were then put at 37°C overnight. The ligation and the ligation control probes were plated on LB-ampicillin agar plates. The cloning product the α MHC-CHOP2-YFP plasmid (Fig 4.7) was produced after preparing DNA from colonies of ligation product grown on LB-Ampicillin agar plates and further confirmations were done by sequencing

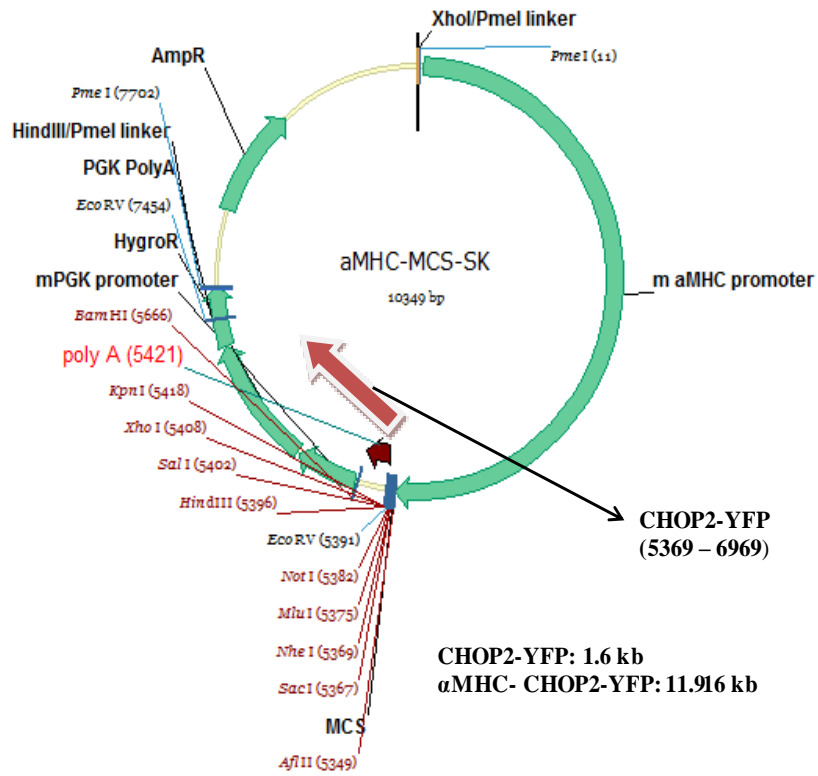


Fig 4.7: Plasmid map of the cloned α MHC-CHOP2-YFP

4.1.2. Cloning tandem construct pcDNA3.1-hChR2-hBR under an α MHC promoter for cardiac specific expression:

The transformation and culturing of DH5 α chemically competent cells was performed according to the aforementioned procedure (please put the procedure here). Then digestion of plasmid containing tandem construct and the reverse α MHC plasmid was performed according to the following recipe:

Reverse α MHC	5 μ l	-
pcDNA3.1-hChR2-hBR	-	3.1 μ l
10 X Buffer 2	10 μ l	10 μ l
100 X BSA	1 μ l	1 μ l
Not I	3 μ l	3 μ l
Hind III	3 μ l	3 μ l
H ₂ O bid.	78 μ l	79.9 μ l
Total volume	100 μ l	100 μ l

Enzymatic activities of both restriction enzymes were indicated with 20,000 U/ml. The probes were incubated for 5 h at 37°C. For the purification of the digested pcDNA and the α MHC vector the NucleoSpin® Extract II Kit (Macherey-Nagel, country) was used and carried out according to the enclosed protocol. A 0.7% agarose gel was prepared. The probes (5 μ l each) were mixed with 1 μ l loading buffer and poured into the gel slots. 12 μ l of DNA marker were used. The gel was run for 1.5 h at 70 V. The mixture for the dephosphorylation of the digested pcDNA and the α MHC vector was prepared according to the following recipe:

Sample	34 μ l
H ₂ O	10 μ l
SAP buffer	5 μ l
SAP	1 μ l
total volume	50 μ l

The sample was incubated for 1h at 37°C. The reaction was inactivated by adding 50 μ l H₂O to it and incubating again for 20 min at 65°C. Afterwards the samples were purified again with the NucleoSpin Extract II Kit according to the enclosed procedure. 10 μ l of the aforementioned digested and purified pcDNA mixed with 2 μ l loading buffer were run on a 0.7% agarose gel for 2 h in order to separate the insert of interest ('the tandem construct') from the rest of the plasmid. Afterwards, the band of interest was excised from the gel under UV light and extracted from the gel using the QIAquick Gel Extraction Kit Protocol (Qiagen, Germany). The ligation of the insert and the α MHC vector was set up according to the following scheme:

Buffer	1 μ l
T4 ligase	1 μ l
α MHC vector	1.5 μ l
Insert	6.5 μ l
Total volume	10 μ l

In addition, a control ligation was set up containing 6.5 µl H₂O instead of the insert. The ligation was incubated at 37°C. The transformation and culturing was performed according to the aforementioned procedure (The best clone was chosen and verified by sequencing).

4.1.3. Cloning ChIEF into an AAV viral backbone:

pCAGGS_oChIEF_tdtomato plasmid that was obtained from the lab of Roger Tsien (University of California, San Diego) was cloned into an AAV plasmid (pACAGEGCr_AAV). The cloning procedure can be briefly summarized as follows: the pCAGGS_oChIEF plasmid was cut with EcoRI and XhoI and the 2.6kb fragment containing the oChIEF with tdTomato was isolated.

On the other hand, the pACAGWGCr_AAV plasmid was cut with EcoRI and XhoI and the 5.2kb fragment, which is the AAV backbone was isolated .

Both fragments are ligated and transformed into E.coli with ampicillin selection according to the aforementioned procedures.

4.2. Site directed mutagenesis:

The site directed mutagenesis was performed in order to generate the mutant C128S by transforming the Cysteine residue (coded by TGC) in the wild type Channelrhodopsin 2-YFP to Serine (coded by TCC).

4.2.1. The primers design:

The primers we used were:

GTGGCTTCTCACCTCCCCGGTCATTCTCATT for the forward direction (forward primer named COP2-C128S-fw) and

AATGAGAATGACCGGGGAGGTGAGAAGCCAC (reverse primer named COP2-C128S-rv). The primers are prepared as 12 pmole solutions by diluting 1 µl of 100 pmole solution in 8,33 µl double distilled water.

4.2.2. Mutant strand synthesis reaction:

The template DNA used is the pGem-Teasy-CHOP2 plasmid. The site directed mutagenesis kit (Stratagene, Germany) was used to perform the procedure. To briefly outline the procedure: 4 sample reactions are prepared. Two reactions are prepared according to the following recipe: 5 μ l 10% reaction buffer was mixed with 2 μ l of (1 μ l of template DNA in 100 μ l double distilled water corresponding to 8 ng DNA), 1 μ l of forward primer (12 pmole), 1 μ l of reverse primer (12 pmole), 1 μ l of dNTPs, 1 μ l of *PfuUltra* HF DNA polymerase (2.5 U/ μ l) and 39 μ l double distilled water. The other two reactions were the same as the aforementioned reaction with the exception that 1 μ l of (1 μ l of template DNA in 10 μ l double distilled water solution was used corresponding to 40 ng DNA). The cycling parameters for the QuickChange II-E Site directed mutagenesis method (Stratagene, Germany) are as follow.

Segment	Cycles	Temperature	Time
1	1	95 °C	30 seconds
2	16	95 °C	30 seconds
		55 °C	1 minute
		68 °C	5 minutes

4.2.3. Dpn I digestion of the amplification products:

One reaction from each of the two reaction groups was digested with 1 μ l of *Dpn* I restriction enzyme (10 U/ μ l). Then all reactions were cleaned up with StrataClean Resin.

4.2.4. Electroporation of XL-1 Blue Competent Cells:

Before beginning the procedure, one has to make sure that the electroporation cuvettes (0.1-cm gap), and 1.5-ml microcentrifuge tubes have been thoroughly chilled on ice. Sterile SOC medium is preheated to 37 °C. The electroporator has the following settings: 1700 V applied, field strength of 17 kV/cm, resistance of 200 Ω and capacitance of 25 μ F. The electroporation competent cells are then thawed on ice. 40 μ l of cells was added to the chilled 1.5 ml microcentrifuge tube. 2 μ l of the resin purified mutagenesis reaction is added to 40 μ l of cells. The DNA and cells are mixed then transferred to a chilled electroporation cuvette (0.1-cm gap). Each sample is pulsed once and immediately 960 μ l sterile SOC medium (held at 37 °C) is added to resuspend the cells.

4.2.5. Transformation of the reaction products:

After electroporation, 50 μ l of each reaction is plated on an LB-ampicillin agar plate then the solution is centrifuged and the supernatant is plated on another LB-ampicillin plate. It is important to note that the plate of 8 ng template reactions (50 μ l plated volume) was better than the other plates evidenced by the higher number of colonies grown, The number of colonies in the untreated reaction (without Dpn I) was higher than the number of colonies in the case of treated reaction (with Dpn I) as Dpn I removes the parent methylated and hemimethylated plasmid leaving the mutated plasmid intact. 10 colonies were picked up from the plate on which the 8 ng template reaction was plated and left overnight at 37 °C on the shaker with a speed around 220- 225 rpm. The DNA was purified according to the aforementioned procedure. The 10 clones were subsequently sequenced and one clone (clone 2) was chosen to be the best as it has the desired mutation and the whole channel sequence was preserved.

4.2.6. Cloning Mutated channelrhodopsin 2 (C128S) into the reverse cardiac plasmid (α MHC):

Clone 2 was cultured according to the aforementioned procedures. Then subsequently digested along with the reverse α MHC plasmid using the restriction enzymes NheI-HF and SalI-HF. The digestion probes were left at 37°C for one and half hours. After digestion the probes were purified using the NucleoSpin Extract II kit according to the enclosed protocol. The digestion probe of the reverse α MHC plasmid is dephosphorylated for one hour at 37 °C according to the aforementioned procedure. The digestion probe of the mutated channel was run on gel and the band corresponding to the insert (the band at 1.6 kb) was extracted using the NucleoSpin Extract II according to the enclosed protocol. The purified DNA probes are then ligated according to the aforementioned procedure. The ligation products were then transformed and mini prepped according to the aforementioned procedures. The mini prepared ligation products were digested with NheI/SalI. Two bands one at 10.6 kb and 1.6 kb corresponding to the α MHC plasmid and the insert (C128S channel) accordingly.

Media used:

SOC medium: SOC medium is prepared by first preparing the SOB medium(per one liter): 20 g tryptone, 5 g yeast extract, 0.5 g NaCl, double distilled water to one liter then the SOB medium is autoclaved and 10 ml filter sterilized 1 M MgCl₂ and 10 ml filter sterilized 1 M MgSO₄. Then SOC medium (per 100 ml) is prepared by adding 98 ml autoclaved SOB medium to 2 ml of filter sterilized 20% (w/v) glucose solution.

LB medium: prepared by mixing 10 g tryptone, 5 g yeast, 5 g NaCl in 1 L bidistilled water. The pH is adjusted with NaOH to 7.2 and the medium is subsequently autoclaved.

LB-Ampicillin agar plate: prepared by mixing 10 g Bactotrypton, 5 g yeast extract, 5 g NaCl and 14 g Agarose in 1 L bidistilled water. The pH is

adjusted to 7,2 using NaOH and then 4 ml Ampicillin (20 mg/ml) are added to the solution.

Materials for cloning:

Material	Company	Catalog number
Tx10 Buffer 2	New England Biolabs	B 700025
dNTPs mixture	New England Biolabs	N0447L
High fidelity polymerase	Roche	11732641001
Agarose (electrophoresis grade)	Sigma Aldrich	A2929
Ethidium bromide stock solution (10 mg/ml)	Life technologies	15585 - 011
pGEM-T-Easy vector system	Promega	A1360
T4 ligase enzyme system	New England Biolabs	M00202S
X-Gal	Sigma Aldrich	B4252
IPTG	Sigma Aldrich	I6758
EcoR1 restriction enzyme	New England Biolabs	R01015
BSA 100X	New England Biolabs	B90015
NheI restriction enzyme	New England Biolabs	R01315
TX10 SAP Buffer	Promega	M821A
SAP enzyme	Promega	M820A
Sall restriction enzyme	New England Biolabs	R01382
1 Kb DNA Ladder (1 µg / 1 µl)	Invitrogen	15615 - 016

4.3. Establishment of HEK-CHOP2 stable cell line:

HEK-293 cells were transfected either in suspension or plated on a 6 well plate using the following recipe: 2 µg pcDNA 3.1-CHOP2 construct mixed with 3.2 µl enhancer, 100 µl EC buffer and 10 µl effectene for a single transfection reaction. The cells were then selected using G418. After two weeks of selective pressure using Geneticin, the remaining cells were cryopreserved. The cryopreserved cells were polyclonal stable cell lines. In order to establish the monoclonal stable cell line, one of the cryotubes of the polyclonal HEK-CHOP2 and HEK-63 cell line was trypsinized and transferred to a 96 well plate where a serial dilution was performed in order to obtain 1 cell per well. After three days of culture along with the selection pressure using Geneticin, the clusters produced from single cells were transferred and diluted in a 6 well plate with DMEM/F12 + GlutaMax™ medium supplied with G418. Then the cells were cryopreserved and these cells represent the monoclonal HEK-CHOP2 cell line.

Materials for the establishment of the stable HEK cell line

Material/Media/Buffer	Company	Catalog number
Effectene (1 mg/1 ml)	Qiagen	133197784
EC buffer	Qiagen	1018740
Enhancer (1mg/ 1ml)	Qiagen	133197789
Geneticin (G418) (50 mg/ml solution)	Gibco	10131-027

4.4. Microarray analysis using RT²PCR arrays:

4.4.1. Experimental design:

A set of experiment consists of a test culture and a control culture. A test culture is a hippocampal neuronal culture on multielectrode array transfected with channelrhodopsin2 – YFP adeno- associated virus. The spontaneous activity of the test culture was recorded for 5 min then stimulated with 40 1s pulses of constant blue light at 0.5 Hz frequency than the recording was stopped 15 minutes after stimulation. As for the control cultures, we used two types of controls. The first control is hippocampal neuronal cultures plated on multielectrode arrays that are not transfected with channelrhodopsin 2. This control was stimulated in the same fashion as the test culture. The second control is hippocampal neuronal cultures plated on multielectrode arrays that are transfected with channelrhodopsin 2virus and that were recorded without stimulation with blue light. In each set of experiment, the fold change in synaptic plasticity genes (for the set of the synaptic plasticity genes in the microarray, please check fig 4.8) was calculated by comparing a test culture with its corresponding control culture (our fold change cutoff was ± 2). Then all set of experiments were averaged to determine which synaptic plasticity genes are up-regulated or down-regulated. We have two sets big sets of experiments corresponding to each of the control we are using.

Adam10	A01	Adcy1	A02	Adcy8	A03	Akt1	A04	Arc	A05	Bdnf	A06	Camk2a	A07	Camk2g	A08	Cdk2	Cebpb	Cebpδ	Ctrl
Creb1	B01	Crem	B02	Dig4	B03	Egr1	B04	Egr2	B05	Egr3	B06	Egr4	B07	Ephb2	B08	Fos	Gabra5	Gnai1	Gria1
Gria2	C01	Gria3	C02	Gria4	C03	Gria1	C04	Gria2a	C05	Gria2b	C06	Gria2c	C07	Gria2d	C08	Grip1	Gria1	Gria2	Gria3
Gria4	D01	Gria5	D02	Gria7	D03	Gria8	D04	Homer1	D05	Igf1	D06	Inhba	D07	Jun	D08	Junb	Killo	Mapk1	Mmp9
Ncam1	F01	Nkx1	F02	Nkx1b	F03	Ngf	F04	Ngf	F05	Nos1	F06	Npx2	F07	Nrcal	F08	Nr1h3	Nr1h2	Nr1h2	Pcdh8
Pick1	F01	Pim1	F02	Plat	F03	Piegl	F04	Ppp1ca	F05	Ppp1cc	F06	Ppp1r14a	F07	Ppp2ca	F08	Ppp3ca	Ppica	Pp1cg	Pp1gl
Rab3a	G01	Rela	G02	Reh	G03	RGD1562511	G04	Rgs2	G05	Rheb	G06	Sirt1	G07	Srf	G08	Syrpo	Timp1	Tnf	Ywhaq
Rplp1	H01	Hprt1	H02	Rpl13a	H03	Ldha	H04	Acb	H05	RGDC	H06	RTC	H07	RTC	H08	RTC	PPC	PPC	PPC
	F01	H02	H03	H04	H05	H06	H07	H08	H09	H10	H11	H12	H13	H14	H15	H16	H17	H18	H19

Fig.4.8: The RT²PCR synaptic plasticity gene microarray layout. It depicts the 84 synaptic plasticity related genes that are measured simultaneously, 5 house keeping genes, genomic DNA control, reverse transcriptase control and positive PCR control.

4.4.2. RNA isolation:

Immediately after the experiment, the reaction was stopped by aspirating the culture medium and washing the culture with 1ml of PBS and mRNA was extracted using the RNeasy Micro Kit (QIAGEN, Germany). To briefly outline the procedure, after aspiration of culture medium, the cells were washed three times in 1 ml of PBS (pH 7.4). Cells were lysed by adding 350µl of buffer RLT to the cell-culture dish. The cells were detached with a cell scraper. The lysate was collected in a 1.5 ml RNase-free collection tube and vortexed for at least 2 minutes. Cell lysate was further homogenized by pipetting it up and down at least 15 times. 350µl of 70% ethanol (prepared with RNase-free water) was added to the lysate and mixed by pipetting. The sample was transferred to an RNeasy MinElute Spin column and centrifuged for 15 seconds at 10,000 rpm. The flow through was discarded and 350µl of Buffer RW1 was added to the column and centrifuged again for 15 seconds at 10,000 rpm to wash the spin column. The flow through was discarded and 10µl of DNase (27 units mixed with 70µl of buffer RDD) was added to the spin column, and incubated for 15 minutes at 30°C. After the incubation, 350µl of Buffer RW1 was added and the column centrifuged for 15s at 10,000 rpm to wash the column again. Flow through was discarded and 500µl of Buffer RPE was added. The column was centrifuged for 15s at 10,000 rpm. The flow through was discarded and 500µl of 80% ethanol (prepared with RNase-free water) was added to the column and centrifuged for 2 minutes at 10,000 rpm. The column was placed in a new collection tube (2 ml) and centrifuged with the lid open for 5 minutes at 12,000 rpm to evaporate the remaining ethanol from the column. After centrifugation, the spin column was placed in a 1.5 ml collection tube and 14µl of RNase-free water was added to the centre of the spin column. The spin column was incubated for 1.5 minutes at room temperature and then centrifuged for 1 minute at 12,000 rpm to elute the RNA. After this, the RNA can be stored at -20°C until it is used for synthesizing cDNA.

4.4.3. cDNA synthesis:

Before synthesizing the cDNA the concentration and quality of mRNA was measured using a Nanophotometer. A260/A280 ratio of 1.9-2.1 was considered acceptable to guarantee the purity of RNA. The most important consideration for cDNA synthesis was that the starting concentration of mRNA was the same for both test and control cultures in an experiment. The cDNA synthesis was carried out using RT2 First Strand Kit (QIAGEN, Germany). First the genomic DNA elimination mix was prepared by mixing RNA, Buffer GE 5X and RNase-free water in a ratio of 4:1:5, in a 1.5 ml RNase-free tube. The mix was then incubated for 15 minutes at 42°C. Then the samples were placed in ice for 2 minutes. To each sample, 4µl of Buffer BC3, 1µl of Control P2, and 2µl of Reverse Transcriptase mix were added. The mix was incubated for 15 minutes at 42°C. Immediately after, the samples were transferred to 95°C for 5 minutes to stop the reaction. Finally the volume of each sample was adjusted to 110µl with RNase-free water.

4.4.3.1. Pre-amplification:

In experiments where the amount of RNA isolated is small (<50 ng/ µl), a preamplification step was performed using RT2 PreAMP cDNA Synthesis kit. First of all, a genomic DNA elimination mix for each RNA sample is prepared in a sterile PCR tube. The mix is prepared as follow: 30ng RNA, 2 µl buffer GE and the volume is completed to 10 µl using RNase-free water. The genomic DNA elimination mix is then incubated at 42°C for 5 minutes then placed immediately on ice for at least 1 min. Subsequently, the reverse transcription mix is prepared accordingly (volume for 1 reaction): 4 µl 5x Buffer BC3, 1 µl Control P2, 1 µl cDNA Synthesis Enzyme Mix, 1 µl RNase inhibitor and 3 µl RNase-free water. The 10 µl reverse transcription mix is added to each tube containing 10 µl genomic DNA elimination mix. The mixture is mixed

gently by pipetting up and down. The mixture is then incubated at 42°C for exactly 30 minutes. The reaction is then immediately stopped by incubating at 95°C for 5 min. The reaction is placed on ice then proceed with the preamplification protocol. First, the RT2 PreAMP PCR Mastermix and RT2 PreAMP Pathway primer mix (Rat synaptic plasticity pathway primer mix) at room temperature. The preamplification mix is then prepared according to the following recipe (volume for one reaction): 12.5 µl RT2 PreAMP PCR Mastermix and 7.5 µl RT2 PreAMP Pathway Primer Mix. 5 µl cDNA synthesis reaction (prepared previously) is pipetted into a 0.2 ml PCR tube. Then 20 µl preamplification mix is added. Both mixtures are mixed gently by pipetting up and down. The following real time cycler protocol is used for preamplification of cDNA:

Cycles	Duration	Temperature
1	10 min	95 °C
12	15 s	95 °C
	2 min	60 °C
Hold		4 °C

When cycling is finished, the tubes are taken out of the real time cycler and placed on ice. 2 µl Side Reaction Reducer is added to each preamplified reaction and mixed gently by pipetting up and down. The tubes are then incubated at 37°C for 15 minutes followed by heat inactivation at 95°C for 5 min. This is followed by an immediate addition of 84 µl of RNase free water. The preamplified samples are then used for the quantitative PCR

4.4.4. Quantitative PCR :

The gene expression of synaptic plasticity genes was measured using a RT2 Profiler PCR Array Rat Synaptic Plasticity (PARN-126F, QIAGEN, Germany) which measures 84 synaptic plasticity related genes and 5 House-keeping genes (HKG) in a 96-well array. The assay also includes genomic DNA control (GDC), reverse-transcriptase control (RTC) and Positive PCR control (PPC). The PCR mix was prepared according to the manufacturer's instructions. For each array: 1350µl of 2X RT2SYBR Green Mastermix, 102µl of cDNA synthesis reaction and 1248µl of RNase-free water. 25µl of PCR component mix was added to each well of the array. The reaction was carried out in Roche LightCycler 480. The PCR cycle was set as follows: 1 cycle at 95°C for 10 minutes (denaturation and activation of DNA Taq Polymerase) and 45 cycles of 15s at 95°C followed by 1 minute at 60°C (amplification and data collection).

4.4.5. Microarray data analysis:

The data analysis was performed online using the web-based software RT2 Profiler PCR Array Data Analysis version 3.5 (SABiosciences, Germany). First, melting curves were obtained from the qPCR to verify the specificity of PCR products. To analyze gene expressions, the Livak or the $2^{-\Delta\Delta Ct}$ method was used. The expression ratio was calculated as the normalized gene expression of the test sample divided by the normalized gene expression of the control. The result was obtained as the expression ratio of the target gene in the test sample relative to the target gene expression in the control, and is normalized to the expression of the geometric mean of reference genes (housekeeping genes, HKG). The fold-change was represented in the form of scatter plots with a boundary of ± 2 fold-change to account for up or down regulation. To test the statistical significance of the data Student's t-test was performed and the results represented in the form of a volcano plot. In the

volcano plot the data was expressed as the mean of fold-change across the experiments conducted and the fold-change with a $p < 0.05$ was considered significant.

4.4.6. Quality control:

4.4.6.1. Specificity of the PCR products:

The specificity of the PCR products was monitored with the help of melting curves obtained from the qPCR. Ideally, a single PCR product should appear as a single peak in the melting curve. However, sometimes there are multiple peaks indicating amplification of non-specific products. The gene products that showed multiple peaks in their melting curve were exempted from the analysis.

4.4.6.2. PCR array reproducibility:

PCR array reproducibility is assessed with the help of PPC (Positive PCR Control) in the microarray. If the Average PPC Ct is 20 ± 2 and no two arrays have Average PPC Ct are > 2 away from one another then, the experimental group passes the check.

4.4.6.3. Reverse transcriptional control (RTC):

If the difference in average RTC Ct value and average PPC Ct value ≤ 5 , then the experimental group passes the check.

4.4.6.4. Genomic DNA contamination (GDC):

The threshold for this control was set at Ct = 33. So, if the Ct value of GDC is ≥ 33 , then the experimental group passes the check.

4.4.6.5. Stability of the House Keeping Genes (HKG):

The result is obtained in terms of fold change of the target gene in the test sample relative to the control sample normalized to the expression of a reference gene. In our experiments, the target gene fold change was normalized to geometric mean of the Ct value of the 5 HKG. To check the robustness of the HKG, we also normalized the data to a single value of randomly picked HKG, instead of the geometric mean, and the result was not very distinct. Hence, proving the stability of our reference genes.

4.5. Western Blotting:

4.5.1. Cells used for western blotting:

For HEK-CHOP2 and HEK wild type, two six well plates were used on which 60000 cells were plated per well.

4.5.2. Protein extraction from cells:

The cells were washed with ice cold 5 ml PBS. An additional 1 ml PBS is added to the cells then discarded. The cells are scratched from the surface of the well plates using a scraper. The cells are then transferred into epis. The cells are then centrifuged at 2000 rpm for 2 minutes and the supernatant is discarded. The pellet is suspended in 400 μ l lysis buffer (composed of 4.5 ml

PBS, 500 μ l 10% SDS and half tablet of mini complete). The cell suspension is then sucked through a 23-G needle to be homogenized. Subsequently, the cell suspension is centrifuged at 14000 rpm for 15 minutes at 4°C. The supernatant containing protein is then stored at -80°C.

4.5.3. Samples preparation:

18,5 μ l of sample (protein extract) was mixed with 7.5 μ l loading buffer and 3 μ l reducing agent. The samples are then heated for 10 minutes at 70 °C. The samples are kept on ice until they are loaded into the SDS gel. A 1X dilution of running buffer is prepared. The inner chamber of the SDS gel electrophoresis apparatus is filled with 200 ml running buffer mixed with 500 μ l antioxidants. The outer chamber is filled the remaining volume of the running buffer. The samples are loaded against the marker in NuPAGE Novex Bis-Tris Mini Gels (Invitrogen) and run for 35 minutes in the running buffer at 200 V.

4.5.4. Blotting:

The nitrocellulose membrane is dipped in water. A sponge is dipped in water then in 1% transfer buffer. Transfer buffer is prepared by mixing 10 ml 50X Transfer buffer, 1ml 10% SDS and 200 ml methanol then volume is completed to 1 L by distilled water. The SDS gel is then dipped in distilled water. The Whatman paper is dipped in 1% transfer buffer. The blot is built up by putting a sponge followed by one Whatman filter paper then the gel then the nitrocellulose membrane then one Whatman filter paper followed by a sponge. The running settings of the blot were as follows: 10 V, 20 V and 30 V for 10 minutes each, followed by 40 V for 20 minutes and 50 V for one hour. The blot was then taken off. The nitrocellulose membrane is dipped in water.

4.5.5. Blocking:

The membrane is blocked and shaken at room temperature for one hour at room temperature. The block solution is prepared as follows: for each 10 ml of blocking solution, 0.5 g milk is mixed with 0.5 ml goat serum and 10 ml TBST. The blocking solution is then discarded and the membrane is incubated overnight at 4 °C with shaking in 10 ml blocking solution with the primary antibody mouse anti – GFP (abcam, Germany; 10^{-3} dilution). The blot is then washed 4 times in 10 ml blocking solution for 5 minutes. The membrane is then incubated in 10 ml blocking solution with 1 µl of secondary anti-rabbit antibody (10^{-5} dilution) for one hour at room temperature. The blot is then washed four times in 10 ml blocking solutions for 5 minutes. Then washing one time in 10 ml 1X TBST for 5 minutes then one time in 10 ml 1X TBS for 5 minutes.

4.5.6. Developing the blot.

The band of interest is around 60 kDa. It is important to note that no attempt for protein quantification was done as the aim of the experiment was to qualitatively detect whether the HEK stable cell lines expressed the construct CHOP2-YFP.

Solutions used in Western Blotting:

10X TBE: prepared by mixing 890 mM Tris (108 g), 890 mM Boric acid (55 g) and 20 mM EDTA and the volume is completed to 1 L.

10X TBS: prepared by mixing 200 mM Tris-HCl (pH 7,5), 1,4 M NaCl and the volume is completed to 1 L.

TBST is prepared by adding Tween 20 to TBS.

Materials for western blotting:

Material	Company	Catalog number
SDS	Fluka	71725
Mini complete tablet	Roche applied science	11836153001
NuPAGE Novex 4 – 12% BisTris Mini gels	Novex	NP0335
Goat serum	Gibco	16210-072
Mouse monoclonal to GFP	abcam	Ab1218
NuPAGE MES SDS Runining Buffer	Life technologies	NP0002
NuPAGE Sample Reducing agent	Life technologies	NP0009
NuPAGE Antioxidant	Life technologies	NP0005

4.6. Transfections:

4.6.1. HEK cell transfection with ChIEF:

The construct ChIEF-tdTomato was kindly provided by Dr. Roger Y. Tsien (UCSD). The transfection of the HEK 293 cells with ChIEF-tdTomato was performed with Amaxa Nucleofector (Amaxa), using 10^6 cells, 4 μg of DNA and program A-23. Cells were cultured in DMEM/F12 + GlutaMaxTM medium supplemented with 10% Fetal Calf Serum.

4.6.2. Viral transfection:

At 14 DIV, 2 μl of AAV-CHOP2-YFP viral solution is added to the culture.

Materials for transfection:

Material / Medium	Company	Catalog number
DMEM/F12 + Glutamax 1	GIBCO	31331-028
Nucleofection kit V	Lonza	VCA - 1003

5. Network dynamics data analysis:

5.1. Active electrodes:

Active electrode (AE) is defined as an electrode which has spontaneous firing rate of more than 0.1 Hz.

5.2. Average Firing rate:

The firing rate of active electrodes was computed as the total number of action potentials recorded by active electrodes divided by the duration of the recording and the number of AE:

$$v = \frac{\# \text{ Action potentials}}{\# \text{ AE } \times \text{ time interval}}$$

5.3. Peri-stimulus time histogram:

Peri-stimulus time histograms (PSTHs) were calculated using a 20 msec time bin. The level of activity of individual cultures was characterized by the corresponding spontaneous average firing rate, which varies from culture to culture. The average PSTH was obtained from the PSTHs of each experiment normalized with the spontaneous average firing rate of the corresponding culture

5.4. Burst detection:

The modified method suggested by S. Potter et al. 2002 in MEA-Bench is used. Bursts were defined as sequences of at least two spikes with all inter-spike intervals lower than a given threshold on individual active electrodes. The threshold was defined as $\frac{1}{4}$ of the inverse average firing rate of all active electrodes. After detecting bursts on all active electrodes, they were sorted in temporal order. Synchronized burst was defined as a group of bursts across several electrodes that

overlapped in time. After detecting all synchronized bursts, the synchronized bursts that were separated with less than $5/4$ of threshold merged into one synchronized burst (Fig 4.9).

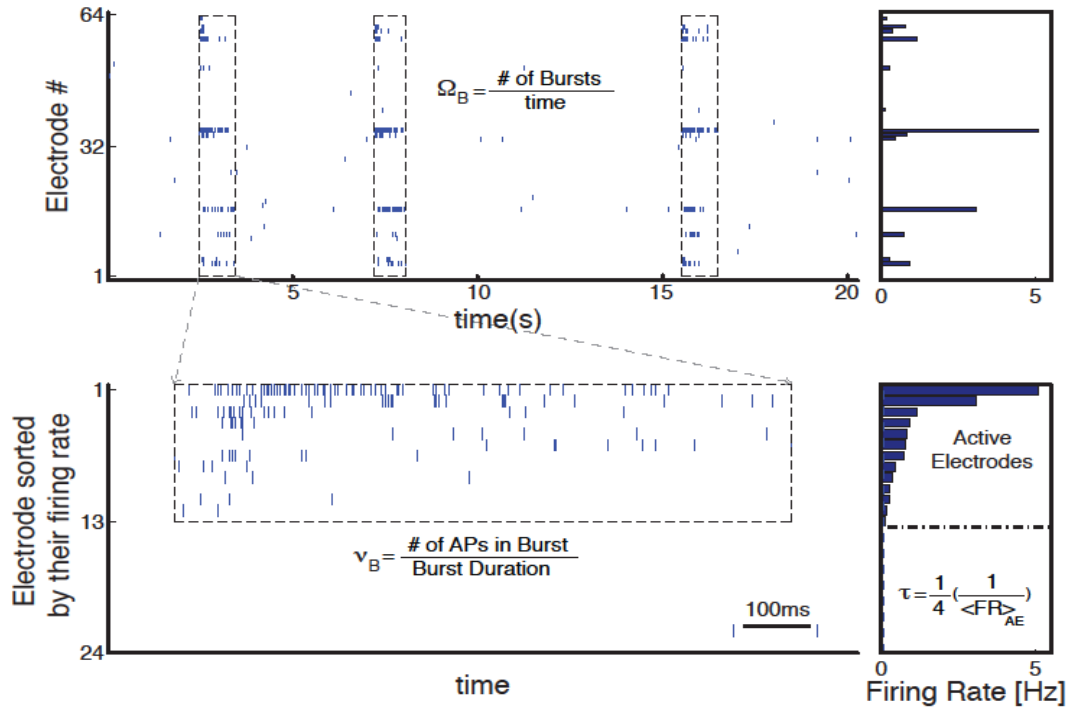


Fig 4.9: Burst detection methodology (please check section 5.4. for detailed description).

5.5. Burst structure:

Time-dependent firing rate (FR) is obtained by binning time and counting spikes with $\Delta t=10s$.

Burst rate (BR) was defined as the rate of the detected synchronized bursts in a time window of 10 seconds,

$$\Omega_B = \frac{\# \text{ Bursts}}{\text{Time}}$$

The average firing rate and burst rate over different experiments is simply the mean value at each time bin over all experiments.

Intra burst firing rate (IBFR) was computed as the total number of action potentials within the synchronized burst (burst size) divided by the burst duration defined as the time interval between the onset and offset of the corresponding synchronized burst,

$$v_B = \frac{\text{\# of APs in burst}}{\text{Burst duration}}$$

In order to compute the average IBFR over all experiments, first the average IBFR of the detected bursts in windows of 10 seconds were computed for each experiment and then the average over all experiments was taken.

As mentioned before, there is variation in the level of activity of individual cultures, therefore, we have computed the aforementioned quantities normalized to the spontaneous activity before stimulus. Then we have taken average over all experiments with the same experimental paradigm. The mean of these quantities after stimulation, 5minutes before ending of recording is compared to the mean of the unperturbed spontaneous activity before stimulation. The significant change of the FR, IBFR and BR for average over all experiments are quantified by using the Wilcoxon rank sum test which is a non parametric statistical hypothesis test. This test has the null hypothesis that the two vectors are independent samples from identical continuous distribution with equal medians. The bootstrap 95% confidence intervals were computed by taking shuffled 10000 random samples from individual experiments.

Silent period is a period of almost no activity after offset of the stimulation. It is defined as the duration between offset of the stimulation and onset of the first synchronize burst after stimulation. As the silent period varies between experiments and also the duration of resuming the ongoing burst activity varies between experiments, in order to compare the change in the activity on average, we took last five minutes to compare to spontaneous activity which is the period that all experiments are in the stationary active state again.

5.6. Cross correlation analysis:

In order to assess changes in the network synchronization, we computed the cross correlation functions before and after stimulation.

The spike trains of active electrodes were first converted to a binary sequence where one corresponded to a spike that occurred at a specific time step. The binary sequence is then converted to a spike density function by convolving the binarized spike train with a Gaussian kernel of standard deviation of 5 ms. The convolved spike train are then used in the computation of the cross correlation functions. For each data set, the cross correlations between all possible combination of active electrodes pairs was computed.

The cross correlation function was either normalized by the product of the standard deviation of the signals or by the product of the mean firing rate of both signals. In the first case, we obtained the cross correlation coefficient and in the second case, we obtained the fold change of the conditional firing rate. Then the cross correlations between all possible pairs of active electrodes were averaged for each data set to produce what we call petit average. The petit averages of all data sets are then averaged in order to compute the overall average across all data sets. The computation of the average cross correlation was done for before stimulation (the 5 minutes just before the stimulation) and for after stimulation (the last 5 minutes of the recording).

The Jackknife confidence intervals were computed by computing the average cross correlation function or the average conditional firing rate over all experiments removing one electrode at a time then the jackknife samples are sorted to give the 95% and 99% confidence interval. We had a total number of 236 Jackknife samples in the constant photostimulation condition and 352 Jackknife samples for the ramp photostimulation condition.

6. Continuous dynamic photostimulation experiments:

6.1. Stimuli generation:

Synthesis of a time series $\{V_i\}$ of command voltages with a time step Δt followed the iterative rule:

$$V_i = -(V_{i-1} - \bar{V}) \cdot \kappa + \sigma \sqrt{1 - \kappa^2} \xi_i, \quad \text{with } \kappa = \exp(-\Delta t / \tau_{corr}) \quad (1)$$

where the ξ_i are provided by a generator of $N(0,1)$ normally distributed random numbers. Equation 1 generates an Ornstein-Uhlenbeck process with the time average \bar{V} , the variance σ and the correlation time τ_{corr} . To protect the LED the voltage sequence was restricted to lie between 0 and 5 V. An alternative way to construct the sequence $\{V_i\}$ is to pass the white noise $\{\bar{V} + \sigma \cdot (1 + \kappa)^{0.5} \cdot (1 - \kappa)^{-0.5} \cdot \xi_i\}$ through an RC-type low pass filter with the time constant τ_{corr} . The light stimuli used here were all synthesized with the same random number sequence $\{\xi_i\}$ and represent therefore just differently filtered versions of the same white noise sequence. Three different correlation times were used: 1 ms, 5 ms and 50 ms. For each τ_{corr} four different combinations of average and standard deviation (SD) were generated, referred to as condition c1 to c4. Considering the slightly non-linear current-light relationship of the photo-diode, the respective values of average and standard deviation of the light-power were (in mW/mm²): (c1) 0.134 and 0.057; (c2) 0.161 and 0.052; (c3) 0.185 and 0.046 and (c4) 0.177 and 0.068. Each of the twelve different stimuli was presented ten times. In a subset of experiments (n=8) this was done in random order. In other cells the stimuli were presented in an interleaved order.

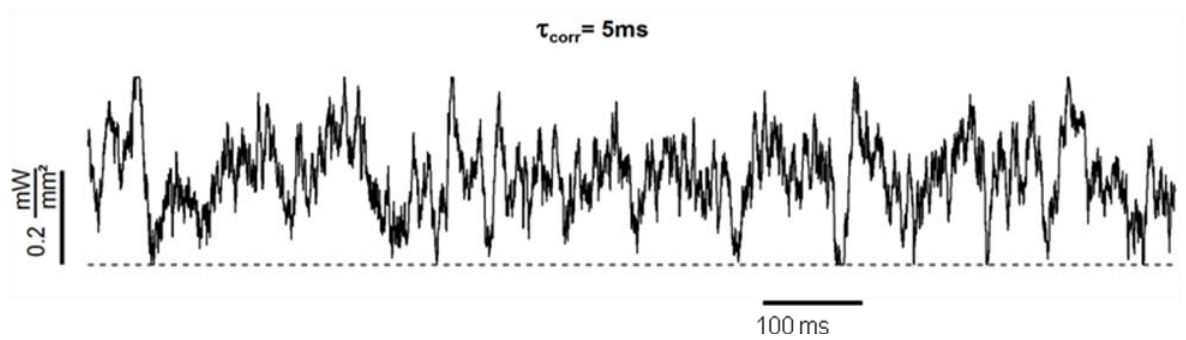


Fig 4.10: An exemplary trace of an Ornstein Uhlenbeck light waveform.

6.2. Data analysis:

Current responses to light steps were described by single exponential functions. As the currents deviate from a single exponential time course by a slight delay at the onset (< 1 ms) and, especially for channelrhodopsin 2, by the inactivation, the choice of the range to be fitted does influence the results of the exponential fit. This influence is minimized by starting the fit only 1 ms after the onset of the light step and by choosing the fit range's duration according to the estimated time constant. To this end the fit was iterated and after each round the fit range was set to three times the estimated time constant, until the change in this estimate was smaller than 3 %.

Each of the twelve different fluctuating light stimuli (four conditions c1 to c4 and three correlation times) was presented ten times to a given cell. The sequence of presentation was interleaved and in a subset of experiments ($n=8$) it was random. The ten current responses of a given cell, which were elicited by the individual trials with a given stimulus, were averaged to give the average response of this cell to this stimulus. When stimuli were applied in random order, the time between the first and last trial of a given stimulus was as long as 10 minutes. During this time small changes in the recording conditions or in the leak current could occur, causing a small offset between the respective currents. To demonstrate the reproducibility of the light-induced component of the measured currents, the offsets were accounted for by shifting the individual responses to achieve the same trial average for all trials. This was done only for the display in Fig. 3 but not for any quantification. Power spectral density was calculated over 50 % overlapping

intervals of 409.6 ms duration (4096 points), windowed with a Welch function. Before averaging, power spectral density of different recordings was normalized to 1 at 7.3 Hz, the frequency bin with the maximum power. This normalization assured that the shape of the average power spectral density faithfully reflects the average shape of all individual examples.

Pearson correlation coefficients r_p were calculated for successive trials of a given stimulus in a given cell. Those nine individual r_p values were averaged to give the average r_p for this cell and stimulus. The average autocorrelation function for a given cell and stimulus was calculated from the average response of this cell and stimulus. Autocorrelation functions were normalized to 1 at $t=0$. The average impulse response function (IRF) for a given cell and stimulus was calculated as the inverse Fourier-transformation F^{-1} of the transfer function, which is the ratio of the Fourier-transform of the average response $I(t)$ of this cell to this current $F(I(t))$ and the Fourier -transform of the respective stimulus $F(S(t))$:

$$IRF(t) = F^{-1}\left(\frac{F(I(t))}{F(S(t))}\right). \quad (2)$$

The overall averages of the autocorrelation function and IRF for a given stimulus were calculated as average over the respective cell averages. As the amplitudes of the IRFs varied considerably between cells and because the important aspect is the shape of the IRF more than its amplitude, IRF were normalized by their integral before averaging. The resulting average was then multiplied by the average integral of the individual IRFs to reveal a representative average IRF shape and amplitude. The 95% confidence intervals of the average autocorrelation functions and IRFs were computed by balanced bootstrap: the averages from N cells were each cloned 1000 times to yield $N \times 1000$ traces. Those were randomly grouped in 1000 samples of N traces each. Each sample was averaged resulting in 1000 bootstrap averages. For each time point the lowest 25 and largest 25 values of all the bootstrap averages are identified. The range covered by the remaining 950 values represents the bootstrap confidence interval at this time point.

The auto-correlation functions were fit with

$$C(\tau) = \frac{\tau_{corr} + \tau_{cut-off}}{2} \left(\frac{\exp\left(-\frac{|\tau|}{\tau_{corr}}\right) + \exp\left(-\frac{|\tau|}{\tau_{cut-off}}\right)}{\tau_{corr} + \tau_{cut-off}} + \frac{\exp\left(-\frac{|\tau|}{\tau_{corr}}\right) - \exp\left(-\frac{|\tau|}{\tau_{cut-off}}\right)}{\tau_{corr} - \tau_{cut-off}} \right). \quad (3)$$

This equation describes normalized the auto-correlation of an Ornstein-Uhlenbeck process with correlation time τ_{corr} passed through a RC-type low-pass filter with the time constant $\tau_{cut-off}$. The IRFs were described with a function comprising an initial delay t_d , followed by an exponentially growing term multiplied with an exponentially decaying term:

$$IRF(t) = \begin{cases} 0 & \forall t < t_d \\ A \cdot \left(1 - \exp\left(-\frac{t-t_d}{\tau_{act}}\right)\right) \cdot \exp\left(-\frac{t-t_d}{\tau_{inact}}\right) & \forall t \geq t_d \end{cases}. \quad (4)$$

As the light activated at current -60 mV has a negative sign, the amplitude A is negative.

References:

Brewer GJ, Torricelli JR, Evege EK, Price PJ. (1993) Optimized survival of hippocampal neurons in B27-supplemented Neurobasal, a new serum-free medium combination. *J Neurosci Res.* Aug 1;35(5):567-76.

Hales CM, Rolston JD, Potter SM. (2010) How to culture, record and stimulate neuronal networks on micro-electrode arrays (MEAs). *J Vis Exp.* May 30;(39).

Wagenaar DA, Pine J, Potter SM. (2006) An extremely rich repertoire of bursting patterns during the development of cortical cultures. *BMC Neurosci.* Feb 7;7:11.

CHAPTER 5

General discussion

In the presented thesis work, an “Optical Network Electrophysiology “ system that combines optical stimulation using optogenetic tools and multisite neuronal recording using microelectrode arrays was presented and its applicability to address questions related to neuronal network dynamics was demonstrated.

In the first part of the work, feedforward whole field blue light illumination was used to induce network level plasticity. Our study is the first report of network level potentiation using optical stimulation as previous studies have relied on electrical or chemical induction methods (Ivenschitz et al. 2006, Maeda et al. 1998). We studied the duration and internal structure of 4972 synchronized network bursts in 35 cultures and we observed that the process terminating network bursts is virtually unaffected by photostimulation while the coordination among distant neurons is selectively strengthened. The most remarkable result is that slowly rising ramps of blue light were more effective in potentiating network dynamics although the number of optically elicited spikes were much smaller than for pulsed light stimulation. It led us to conclude that a small number of events that are matched to the synaptic organization of a culture can more effectively induce a change of the collective dynamics of the network.

We were able to increase the average firing rate, average intraburst firing rate, average burst rate and spike synchronization after offset of the stimulation. The firing rate after offset of the stimulation increased compared to the spontaneous activity of the culture as a result of network level potentiation. The increased intraburst firing rate was largely due to the increased firing rate after stimulation and to a minimal extent due to decrease in burst duration. Furthermore, the interburst interval decreased after stimulation which is mainly responsible for the increase in burst rate. Our results are consistent with the findings from previous studies using electrical stimulation e.g. Maeda et al. 1998 were able to induce an increase of the burst rate and intraburst firing rate using high frequency tetanic stimulation. In comparison, our stimulation paradigm is able to induce potentiation without the need to use high frequency stimulation that might exhaust the network. Some of the changes

reported previously in bursting dynamics using electrical stimulation in relatively small data sets appeared more pronounced than our findings. The large size of the data set collected by us nevertheless makes it quite easy to identify and characterize the change in network dynamics with good precision and significance. On the other hand, the increase in spike synchronization that we observed after offset of stimulation reflect that there is a tighter coupling between neurons rather than a change in the overall organization of the bursts. The width of the cross correlation functions was generally much smaller than the mean burst duration either before or after stimulation for both ramp and constant photostimulation demonstrating that the change in correlation structure results from modifications in the fine structure within the burst. The half width at half maximum of the cross correlation function is on the order of 50 ms. This time is close to the decay time constant of NMDA receptor mediated synaptic currents indicating that the strong enhancement of correlations under all conditions can be explained by an enhancement of common input that has substantial NMDA synaptic inputs. Our results are consistent with the increased spike correlations that have been observed in the case of hippocampal neurons where chemical induction method was used (Ivenshitz et al. 2006). Though the observed changes appeared somewhat more pronounced in this study but it was based on relatively small number of cross correlation pairs (23 pairs) compared to our data set (2710 pairs for ramp photostimulation and 4451 pairs for constant photostimulation). Our correlation results again highlight the sensitivity gained by harnessing the potential of high yield network electrophysiology combining optogenetic stimulation and multielectrode recordings that allow efficient gathering of large data sets for a precise and reliable characterization of network dynamics

Using pharmacological blockers and microarray analysis, the network level changes were found to be mediated via conventional NMDA dependent synaptic plasticity mechanisms and calcium dependent signaling pathways as has been previously reported for network level potentiating using chemical induction methods (Ivenshitz et al. 2006).

Concluding our first study, we presented a simple photostimulation paradigm able to modify the intrinsic collective dynamics of a cultured neuronal network potentially maximizing spike synchronization. It offers an attractive alternative to stimulation paradigms that externally control neuronal networks. As important target applications of optogenetics include optical deep brain stimulation (Gradinaru et al. 2009) and the optical control of epileptic activity (Tonnesen et al. 2009), the need for mild effective stimulation

paradigms that minimize side effects and tissue damage is of great importance. Modifying neuronal network synchronization may have profound therapeutic implications for Schizophrenia, Parkinson's disease and Epilepsy in which aberrant synchronization is a hallmark symptom and causal element. It will complement or eventually replace electrical stimulation modalities that have been recently developed to provide mild and effective stimulation that does not hyperexcite the neuronal network (Popovych, Tass 2012). Modifying network synchronization can also be expected to be relevant in studying activity dependent developmental processes where the correlation structure of neural activity as in the visual pathway (e.g. Weliky 1999) or in the hippocampus (Quilichini et al. 2012) is relevant. For all such applications modifying the intrinsic ability of a network to generate correlated activity patterns might often be preferable to permanently impose desired activity patterns from the outside. We are confident that the approach that we presented in our study will substantially aid in the search for photostimulation paradigms that strengthen, reduce or abolish network synchronization building a toolbox for modifying collective neuronal network dynamics.

In the second part of the thesis work, our "Optical Network Electrophysiology" system was used to design a new photostimulation paradigm that aims to drive neurons in a more naturalistic *in vivo* like fashion. First, we were able to establish that channelrhodopsin 2 and its weakly inactivating variant ChIEF can be used to induce reproducible fluctuating conductances. Moreover, we were able to show that optical stimulation, using blue light pulses designed as a stochastic process with a defined statistical structure, can induce fluctuating conductances in *in-vitro* cultured neurons for long time generating reproducible spike sequences for the same noise realization.

It is important to mention that naturalistic stimulation of neurons and sensory systems have proven to be a powerful experimental strategy that has revealed fundamental aspects of neuronal processing including high rates of encoded sensory information (Bialek et al. 1999, Rieke et al. 1995, Borst et al. 1999) and the surprisingly high bandwidth of cortical population dynamics (Boucsein et al. 2009, Kondgen et al. 2008, Higgs et al. 2009, Tchumatchenko et al. 2011). It aims to characterize neuronal dynamical properties under *in vivo* like conditions.

The aforementioned studies have used conventional whole cell patch clamp that has the following disadvantages: measuring one cell at a time, limited time of recording and the difficulty of changing experimental conditions during the course of the experiment. A relatively small number of spikes is gathered as a result of the aforementioned shortcomings. Combining non invasive optical stimulation with microelectrode array recordings will help us to measure multiple cells at the same time for long time and the experimental conditions can be dynamically changed. We developed a non invasive optogenetic approach that meets the key requirements of stimulation applicable to studies aiming to use naturalistic stimulation: the stimuli are reliable, offer the necessary bandwidth and the stimulus waveform can be designed. Combined with high throughput electrophysiology using multielectrode arrays, this controlled non invasive method (continuous dynamic photostimulation “CoDyPs”) has the potential to enable large scale screening of neurons under in vivo like conditions, yet again highlighting the advantages of our established system to gather large amount of data. CoDyPs will set itself as an alternative for photostimulation paradigms that aim at imprinting spike sequences (Boyden et al. 2005) or raising firing rates (Adesnik et al. 2010). The advances in channelrhodopsin 2 engineering will also allow development of optimized tools to induce fast fluctuating conductances as we found that both ChR2 and ChIEF act as a low pass filter of 20 Hz cut off frequency and have characteristic response time on the order of 7 to 8 ms. Fast channelrhodopsin 3 variants such as ChETA and E123T/T159C double mutant hold the promise to drive neurons at high frequencies up to 200 Hz and would ultimately allow fast fluctuating conductances to be reliably induced.

The most interesting result of our study is the precision and ease with which CoDyPs induced conductance fluctuations can be predicted and designed. We found that a simple linear response theory approach is sufficient to computationally reconstruct dynamic conductance fluctuations with virtually perfect accuracy. In addition, filter parameters were only weakly dependent on stimulus conditions such that a small and easily parameterized library of response functions appears sufficient.

Together with the long term stability of CoDyPs driven spiking patterns, our findings established that virtually all experimental paradigms previously realized by whole cell stimulation and recording can be performed using CoDyPs, including measurements of firing frequency – input current curves for different input statistics (Arsiero et al. 2007) and

measurements of the functional input – bandwidth of neurons (Kondgen et al. 2008, Higgs et al. 2009, Tchumatchenko et al. 2011). One should note that for many of those measurements such as correlation gain or dynamic gain measurements only the conductance waveform and not the absolute scale of conductance fluctuations needs to be known.

With patterned stimulation, each neuron can receive a particular stimulus extending the use of CoDyPs to the stimulation of shared inputs. In this way, correlations in the spike trains of the illuminated neurons due to partially correlated inputs can be addressed, a task that is complicated using invasive methods. One can also make use of the state of the art neuronal cultures patterning techniques to build up isolated islands of neurons that can be addressed both individually and simultaneously thus increasing the precision and versatility of CoDyPs.

CoDyPs may also turn out effective for controlling the activity of intact networks in-vivo and to put them in a more naturalistic regime that mimic the synaptic drum-fire they are receiving. Modeling studies of cortical networks raise the possibility that driving only a subset of neurons with naturalistic inputs can effectively control the state of the entire network if the inputs are shaped to match network generated inputs (Marre et al. 2009). While more theoretical work is needed to clarify the dynamics properties of cortical networks (Monteforte et al. 2010, Jahnke et al. 2008, Zillmer et al. 2009) one expects in general that complex and time dependent inputs can control the network dynamics while preserving its intrinsic complexity (Molgedey et al. 1992). CoDyPs can be used to examine whether such naturalistic perturbation approaches can be used to control cortical networks in vivo.

As evident from both of our studies, that the possibility to detect action potentials over long periods of time and from many individual neurons in parallel combined with a non invasive photostimulation will enable us to address new questions e.g. screening for the effect of mutations or protein knockdown on the dynamical properties of neurons and also on their ability to be potentiated. It can also help us compare among individual neurons with respect to their encoding diversity thus contributing to understand the biophysical basis of such diversity.

Feedback closed loop stimulation will further increase our system versatility by providing a mean to photostimulate neurons depending on their current state. Using closed loop stimulation, it is possible to program an artificial feedback with defined rules and constraints. Closed loop electrical stimulation has been successfully used beforehand to clamp network activity (Wallach et al. 2011), to control bursting activity (Wagenaar et al. 2005) and realize embodiment by using the network represented on the network to control a robotic arm (Bakkum et al. 2007)

Closing the loop using our optical stimulation system would allow us to further extend the questions to be addressed as the photostimulation can be adjusted depending on the response of neurons thus offering a better control over neuronal dynamics. In the context of learning and memory, closing the loop would help to stabilize a learned sequence over long time and most interestingly, one can address the cellular & molecular mechanisms underlying such long term network level memory.

References:

- Adesnik, H. & Scanziani, M. (2010) Lateral competition for cortical space by layer-specific horizontal circuits. *Nature* 464, 1155-1160.
- Arsiero, M., Luscher, H.-R., Lundstrom, B.N. & Giugliano, M. (2007) The Impact of Input Fluctuations on the Frequency-Current Relationships of Layer 5 Pyramidal Neurons in the Rat Medial Prefrontal Cortex. *Journal of Neuroscience* 27, 3274-3284
- Bakkum DJ, Gamblen PM, Ben-Ary G, Chao ZC, Potter SM. (2007) MEART: The Semi-Living Artist. *Front Neurobot.* ;1:5.
- Boyden, E.S., Zhang, F., Bamberg, E., Nagel, G. & Deisseroth, K. (2005) Millisecond-timescale, genetically targeted optical control of neural activity. *Nat Neurosci* 8, 1263-1268
- Bialek, W., Rieke, F., Steveninck, R.R. de R. van & Warland, D. (1991) Reading a Neural Code. *Science* 252, 1854-1857
- Borst, A. & Theunissen, F.E. (1999) Information theory and neural coding. *Nat Neurosci* 2, 947-957.
- Boucsein C, Tetzlaff T, Meier R, Aertsen A, Naundorf B (2009) Dynamical response properties of neocortical neuron ensembles: Multiplicative versus additive noise. *J Neurosci* 29: 1006–1010
- Gradinaru V, Mogri M, Thompson KR, Henderson JM, Deisseroth K. (2009) Optical deconstruction of parkinsonian neural circuitry. *Science*. Apr 17;324(5925):354-9.
- Higgs, M.H. & Spain, W.J. (2009) Conditional Bursting Enhances Resonant Firing in Neocortical Layer 2-3 Pyramidal Neurons. *Journal of Neuroscience* 29, 1285-1299.
- Ivenshitz M, Segal M. (2006) Simultaneous NMDA-dependent long-term potentiation of EPSCs and long-term depression of IPSCs in cultured rat hippocampal neurons. *J Neurosci*. Jan 25;26(4):1199-210.
- Jahnke, S., Memmesheimer, R.-M., Timme, M. (2008) Stable irregular dynamics in complex neural networks. *Phys. Rev. Lett* 100, 048102
- Koendgen H, Geisler C, Fusi S, Wang XJ, Luescher HR, et al. (2008) The dynamical response properties of neocortical neurons to temporally modulated noisy inputs in vitro. *Cereb Cortex* 18: 2086–2097
- Maeda E, Kuroda Y, Robinson HP, Kawana A. (1998) Modification of parallel activity elicited by propagating bursts in developing networks of rat cortical neurones. *Eur J Neurosci*. Feb;10(2):488-96.

- Marre, O., Yger, P., Davison, A.P. & Frégnac, Y. (2009) Reliable recall of spontaneous activity patterns in cortical networks. *J. Neurosci* 29, 14596-14606.
- Monteforte, M. & Wolf, F. (2010) Dynamical Entropy Production in Spiking Neuron Networks in the Balanced State. *Phys. Rev. Lett.* 105, 268104 .
- Molgedey, Schuchhardt, Schuster (1992) Suppressing chaos in neural networks by noise. *Phys. Rev. Lett* 69, 3717-3719.
- Popovych OV, Tass PA. (2012) Desynchronizing electrical and sensory coordinated reset neuromodulation. *Front Hum Neurosci.*;6:58.
- Quilichini PP, Le Van Quyen M, Ivanov A, Turner DA, Carabalona A, Gozlan H, Esclapez M, Bernard C. (2012) Hub GABA neurons mediate gamma-frequency oscillations at ictal-like event onset in the immature hippocampus. *Neuron.* Apr 12;74(1):57-64.
- Rieke, F., Bodnar, D.A. & Bialek, W. (1995) Naturalistic Stimuli Increase the Rate and Efficiency of Information Transmission by Primary Auditory Afferents. *Proceedings: Biological Sciences* 262, 259-265.
- Tønnesen J, Sørensen AT, Deisseroth K, Lundberg C, Kokaia M. (2009) Optogenetic control of epileptiform activity. *Proc Natl Acad Sci U S A.* Jul 21;106(29):12162-7.
- Tchumatchenko T, Malyshev A, Wolf F, Volgushev M (2011) Ultra-fast population encoding by cortical neurons. *J Neurosci* 31: 12171–12179
- Wagenaar DA, Madhavan R, Pine J, Potter SM. (2005) Controlling bursting in cortical cultures with closed-loop multi-electrode stimulation. *J Neurosci.* Jan 19;25(3):680-8.
- Wallach A, Eytan D, Gal A, Zrenner C, Marom S. (2011) Neuronal response clamp. *Front Neuroeng.* Apr 6;4:3.
- Weliky M. (1999) Recording and manipulating the in vivo correlational structure of neuronal activity during visual cortical development. *J Neurobiol.* Oct;41(1):25-32.
- Zillmer, R., Brunel, N. & Hansel, D.(2009) Very long transients, irregular firing, and chaotic dynamics in networks of randomly connected inhibitory integrate-and-fire neurons. *Phys. Rev. E* 79, 031909 .

List of figures

Fig 1.1: Cartoon sketch of the mechanistic model of ChR2

Fig 1.2: Typical photocycle of channelrhodopsin 2

Fig. 1.3: Six state model

Fig 2.1.: Optical Network Electrophysiology

Fig 2.2: The network collective dynamic changes:

Fig 2.3: Control cultures collective network dynamics

Fig 2.4.: Network synchronization changes:

Fig 2.5.: Conditional firing rate fold change after constant photostimulation.

Fig 2.6. :Conditional firing rate fold change after ramp photostimulation.

Fig 2.7.: Collective network dynamics in the presence of APV/Picrotoxin.

Fig 2.8.: Collective network dynamics in the presence of NBQX/Picrotoxin.

Fig 2.9.: Microarray analysis of synaptic plasticity proteins

Fig3.1: Encoding in the mean and variance channel

Figure 3.2: Two ways to study *in-vivo*-like fluctuation driven spiking activity under controlled conditions

Figure 3.3: ChIEF supports large steady-state currents with a low-pass filter characteristics similar to ChR2

Figure 3.4.: Trial to trial reproducibility of CoDyPs driven currents

Fig 3.5.: The statistics of CoDyPs driven fluctuating currents obeys linear response theory,

Figure 3. 6: ChR2 and ChIEF have similar response characteristics.

Figure 3.7: Computational prediction of CoDyPs-driven currents

Figure 3.8: CoDyPs elicits stable and highly correlated action potential sequences over many hours

Figure 4.1...: Layout of Multielectrode Array TiN-200-30iR.

Fig 4.2: E18 hippocampal neurons grown on Multielectrode arrays (21 DIV)

Fig 4.3: Blue Luxeon Rebel LED and Channelrhodopsin 2 absorption spectra overlapped.

Fig 4.4: Relative irradiance measured by a photodiode

Fig 4.5.: Relationship between the command voltage from STG 2008 (Multichannel systems, Reutlingen) and the irradiance (mW/mm^2) as measured by photodiode

Fig 4.6: Plasmid map of the reverse α MHC plasmid

Fig 4.7: Plasmid map of the cloned α MHC-CHOP2-YFP

Fig.4.8: The RT²PCR synaptic plasticity gene microarray layout.

Fig 4.9: Burst detection methodology.

Fig 4.10: An exemplary trace of an Ornstein Uhlenbeck light waveform.

List of tables:

Table 1.1: Optical methods to control neuronal activity

Table 2.1 Synaptic plasticity genes and their averaged fold change.

Acknowledgments

I am greatly indebted to my family. Without their unconditional support, love and encouragement, I would not have been here writing those lines. Thanks Dad for being my teacher all the way and an example of a great person devoted to his work. Thanks Mom for supporting me emotionally, for always giving me the hope that things would be better, I love you so much. Thanks my sister for being there all the time.

I would like to thank my mentor, my teacher and my supervisor Prof. Fred Wolf for taking me on a great journey on the interface of experimental and theoretical neuroscience. I am very grateful for all the support he gave me to make our project succeed. Our trips from Santa Barbara to Washington enriched my knowledge and introduced me to the experts in many fields across neuroscience. The scientific exchanges I had with him were for me ounce in a life time experiences. His enthusiasm about neuroscience and his commitment to make your students compete on the highest scientific level is unprecedented.

I would like to thank my supervisor Prof. Walter Stühmer for the opportunity he gave me to work independently. The freedom, support and independence I enjoyed in his lab are unique for a PhD student and I am indebted for him. I learned a lot from him and I am thankful for every advice he gave me either personal or professional.

I would like to thank my supervisor Prof. Theo Geisel for the great support, for his continuous enthusiasm about my project and for his eagerness to explore new scientific venues. I enjoyed a lot the winter seminars that he organized where I had memorable experiences with highly talented people from our non linear dynamics department.

I would like to thank Dr. Andreas Neef for being there all the time when help is needed. The continuous dynamic photostimulation project would not be there without his great input and enthusiasm. My knowledge of biophysics grew by continuously interacting with him.

I would like to thank my colleague and friend Kai Bröking for his crucial role in building up our optical network electrophysiology setup. I would like to thank him for supporting and motivating me in tough times. Our collaboration has ever since been fruitful and I am hopeful it will continue to be so.

I would like to acknowledge the support of Dr. Ragnar Fleischmann in all technical aspects of the project and being there when help is needed.

I would like to thank Dr. Annette Witt for her immense support both on personal and professional level, for the great support in the cross correlation analysis and for allowing me to share her office.

I would like to thank Dr. Demian Battaglia for his continuous enthusiasm about the closed loop project and for interesting discussions on network electrophysiology that enriched my knowledge.

I would like to acknowledge the help of Ghazaleh Afshar in the burst analysis the discussions on network reconstruction with Olav Stetter and the support in computing offered by Markus schwamberger and Denny Fleigner.

I would like to thank Ayse Bolik and Viktorya Novak and Regina Wunderlich for solving any administrative problem I faced during the course of my PhD. Moreover, I would like to thank Ute Rust for supporting me in problems that faced me.

I would like to thank Robert Samhaber for being such a great student and for taking on his shoulder the responsibility of the patterning project.

I would like to thank Milena Ninkovic for being a great friend and supervisor. The expression of channelrhodopsin 2 in a cardiac specific manner would not have been possible without her.

I would like to thank Uschi and Sabine Martin for their support in the microarray experiments and providing me with the necessary guidance.

I would like to thank Barbara Scheufler and Sabine Stopler for providing the support for cell cultures.

I would like to thank the workshops of Max Planck Institute for experimental medicine and the Max Planck Institute for Dynamics and self organization for being up for the challenging tasks that they were given.

I was luckily to work for the past four years with a group of talented students: Gorur Srinivas Shandilya., Jatin Nagpal, Ricardo Merino, Hugo Crucos, Tanvi Butola, Anna Trawicka, Oana Toader, Ananya Tawari , Poaja Roa, I-Wen Chen that helped me enrich my teaching experience and has advanced my project in many ways.

I would like to thank IMPRS neuroscience program coordinators Sandra Drube and Michael Hörner for their commitment to make the life of students as easy as possible. Since my arrival to Goettingen, their support has never stopped. The IMPRS program has been the platform to form a great group of colleagues. I would like to thank Alonso, Suenke, Mayur, Natalia, Derya , Andrea, Mathieu, Jonas, Ilaria, Iliana, Federico, Chaitali, Ramya, Diana, Elinor, George, Sebastian, Hedvika, Giovanni, Mirko , Markus and David for making my life in Goettingen an enjoyable experience.

I am happy to have known Christopher Battle, Martin Biehl and Niko Deutschle. With them ,I had great philosophical discussions in our philosophy roundtable.

I was happy to know Prof. Steve Potter. Since then, he has been very supportive. I would like to thank him for hosting me at his house in Atlanta whenever I visit and for fruitful scientific discussions with members of his neuroengineering group at Georgia Tech.

I would like to thank Prof. Ernst Bamberg, Dr. Christian Bammann, Dr Sonja Kleinogel and Dr. Phil Wood at the Max Planck Institute for Biophysics in Frankfurt for providing the optogenetic constructs and for answering our questions on the biophysics of Channelrhodopsin 2.

I would like to thank Dr. Anna Suska and Dr. Oliver Shlüter for their providing me with the Channelrhodopsin 2 virus and for discussions on the network plasticity data and for Sandra for preparing the large batches of AAV viruses

I would like to thank Prof. Sara Solla and Prof. Adrienne Fairhall for their great support for me during the Methods in computational neuroscience course in Woods Hole and during their visits to Goettingen. I would like to thank my classmates at the methods in computational neuroscience course specially Pepe Alcamí, Maurizio De Pita and Belen Sancristobal for the continuous great friendship that developed in Woods Hole.

I would like to thank Rober Gütig for interesting novel ideas and energetic discussions during our weekly theory coffee.

My friends in Egypt and elsewhere around the world are an integral part of my life. I would like to express my gratitude to my best friends in Egypt: Ehab Ahmed Youssef whom I have known for 20 years , the talented writer Mohammed Metwally with whom I shared the best moments in life, Ahmed Abdel Aziz who has always been the most wise friend I have

ever known and Mohamed Arafa who has been a brother and a friend , for the greatest times of my life I have lived with them in Egypt, for their continuous support for years after years and for their unconditional love and passion about me and what I do.

For my best friends in Germany who gave me the sense of a second home, Dario Arcos Diaz in Mannheim with whom I had memorable times , Yuri LaTorre in Berlin with whom I shared everything and had the most intellectual discussions ever and Freidrich Reick in Hamburg who has always been fun to hang out with. I am very glade to have you in my life. With every one of them, I shared memorable moments that will ever be remembered.

I am grateful to the Egyptian Women Union that has been established after the 25th January revolution in Egypt and that put me in the arena of political activism in Egypt although I am living abroad. I am specifically indebted for the infamous Egyptian Feminist and writer Nawal El Saadawi for supporting me and for showing me the meaning of dedication for a lifetime cause.

Curriculum Vitae

Ahmed El Hady

Address: Am Fassberg 17, 37077, Goettingen, Germany.

Phone: +49-170-1866-408

Email: ahmed@nld.ds.mpg.de

Education

Faculty of Pharmacy, Cairo university

2001-2006

B.Sc. (Honor), Pharmaceutical sciences

2006

Master courses,

October 2007 – August 2008

International Max Planck Research School of Neurosciences,

Göttingen, Germany. Grade: B (Very Good).

PhD student,

October 2008 – September 2012

Department of non linear dynamics,

Theoretical Neurophysics research group,

Max Planck Institute for dynamics and self organization,

Advisor: Prof. Dr. Fred Wolf.

“Methods in computational neuroscience” summer school,

August 2 – 30, 2009

Marine Biological Laboratory, Woods hole, Massachusetts

“Emerging techniques in neuroscience” program,

October 23 – November 7, 2010

Kavli Institute for Theoretical Physics,

Santa Barbara, California

“FutureMed 2011” executive program,
Singularity University, NASA Ames Research Center,
San Jose, California

May 10 – May 15, 2011

Awards, Honors & prizes

- Aspen Socrates Winter Seminar scholarship 2012
- Falling Walls Lab scholarship 2011
- Future Med 2011 scholarship 2011
- Georg Lichtenberg fellowship 2009 – 2011
- MBL tuition fees scholarship 2009
- International Max Planck Research School Scholarship 2007 - 2008
- Graduation honor degree, Cairo University 2006
- Ideal student award, Cairo University 2005
- Excellence award, Cairo University 2001-2005

Professional experience

- Medical trainer, Medical department, *T3A industrial* April 2007 – September 2007
Cairo, Egypt.
- Research and development specialist, August 2006 – April 2007
Pharmaceutical dosage form design unit, *T3A*
Industrial Complex, Assiut, Egypt.

Training courses:

- “Matlab for image analysis” workshop, Physical chemistry institute, Goettingen (October 10 – 14, 2011)
- “Introductory course in laboratory animals: Handling, Techniques and Theory”, Max Planck Institute for Experimental Medicine, Goettingen (April 20 – 23, 2009)
- “*Analysis and models in neurophysiology*” course, Bernstein Center for Computational neuroscience, Freiburg (October 13 – 17, 2008)

- “*Mathematical Neuroscience*” workshop, Royal Society of Edinburgh, Edinburgh
(March 17 – 19, 2008)

Teaching experience:

- Organizer, Bernstein focus for Neurotechnology course on September 5 – 7, 2011
“Patterning neuronal cell culture”, Goettingen, Germany
- Organizer, course on “Multielectrode array recordings”, January 17 – 20 , 2011
Goettingen, Germany
- Supervision of Master thesis of Jatin Nagpal (Thesis title: “*Characterization of channelrhodopsin 2 response to fluctuating and constant light stimulation*”)
- Supervision of Bachelor thesis of Robert Samhaber (Thesis title: “*Patterned neuronal cultures on multielectrode arrays*”)
- Tutor, *Theoretical Neuroscience Course* January 7 – 11, 2009
International Max Planck Research School of Neurosciences,
Goettingen, Germany
- Junior lecturer, *Translational neuroscience workshop* June 6 – 8, 2008
Max Planck Institute for Experimental Medicine,
Goettingen, Germany

Peer reviewed conference proceedings:

El Hady A. , Broking K., Afshar G., Geisel T., Stuehmer W, Wolf F., “In Vitro Closed loop Optical Electrophysiology of Networks I: Whole field illumination Paradigm” ,*Proceedings of substrate integrated multielectrode array meeting 2010*, Reutlingen, Germany

El Hady A... “Stochastic optical stimulation”, *Janelia farm conference on “genetic manipulation of neuronal activity II”* , Virginia, United States

Afshar G. *, **El Hady A.** *, Schlueter O., Geisel T., Stuehmer W., Wolf F. “Optogenetic modification of network burst structure”, *Society for Neuroscience conference 2011 abstract* , Washington DC, United States.

Neef A. *, **El Hady A.** *, Nagpal J. *, Bröking K., Afshar G., Geisel T., Bamberg E., Fleischmann R. Stühmer W., Wolf F. “Continuous Dynamic Photostimulation - delivering defined, in-vivo-like fluctuating stimuli with Channelrhodopsins”, *Society for Neuroscience conference 2011 abstract*, Washington DC, United States.

El Hady A., Afshar G., Schlueter O., Geisel T., Stuehmer W., Wolf F. „Optogenetic induction of network level plasticity“ *Bernstein Center for computational neuroscience 2011 conference*, Freiburg, Germany

Neef A.*, **El Hady A.***, Nagpal J.*, Bröking K., Afshar G., Geisel T., Bamberg E., Fleischmann R., Stühmer W., Wolf F. Continuous Dynamic Photostimulation - inducing defined, in-vivo-like fluctuating stimuli with Channelrhodopsins *Bernstein Center for computational neuroscience 2011 conference*, Freiburg, Germany

Bröking, K., **Elhady, A.**,Fleischmann, R.1, Geisel, T.,Wolf, F. Photoelectric effect in multielectrode arrays *Proceedings of substrate integrated multielectrode array meeting 2010*, Reutlingen, Germany

Neef A., Piper C., **El Hady A.** “Imaging of optogenetically induced pH changes”. Janelia farm conference on biological sensors 2012, Virginia, United States.

Other Conference Abstracts:

Afshar G.*, **El Hady A.*** ,Geisel T., Stuehmer W., Wolf F. “Optical manipulation of neuronal networks bursting dynamics“. German Physics Society annual meeting, Dresden, Germany (March 13 – 18, 2011)

Bröking K., **El Hady A.**, Fleischmann R., Geisel T, Stuehmer W, Wolf F. “Optically clamping neurons in vitro“. German Physics Society annual meeting, Dresden, Germany (March 13 – 18, 2011)

Afshar G.*, **El Hady A.*** ,Geisel T., Stuehmer W., Wolf F. “Bursting dynamics in optically stimulated neuronal networks “ German Neuroscience Society Meeting, Goettingen, Germany (March 25 – 29, 2011)

Afshar G.*, **El Hady A.***, Geisel T., Stuehmer W., Wolf F. “ Adaptation and state switching in optically stimulated neuronal networks”, Spike frequency adaptation workshop, Max Planck Institute for Physics of Complex system, Dresden, Germany (October 26 – 27, 2010)

*Equally contributing authors

Research Papers:

Neef A*, **El Hady A***, Nagpal J*, Bröking K, Afshar G, Geisel T, Bamberg E, Fleischmann R, Stühmer W, Wolf F. Non-invasive induction of *in-vivo* like fluctuating currents by continuous dynamic photo-stimulation of Channelrhodopsins, *manuscript in preparation*.

El Hady A*., Afshar G*, Geisel T, Bamberg E, Stühmer W, Wolf F. Mild optogenetic stimulation effectively enhances intrinsically generated network synchrony, *manuscript submitted*.

Bröking K*, **El Hady A***, Fleishmann R, Rapp G, Geisel T, Stühmer W, Wolf F. Artificial synaptic connections by closed loop optical neurostimulation, *manuscript in preparation*.

Witt A, Neef A, **El Hady A**, Wolf F, Battaglia D. Precisely-phased local stimulation could induce distributed reorganization of inter-areal functional interactions, *manuscript under review*.

*Equally contributing authors

INVITED SCIENTIFIC TALKS:

- *CNS seminar 2008*, MPI for dynamics and self organization, Goettingen, Germany
- *Dynamics symposium 2009*, Pitztal, Austria
- *2010 Workshop on "Targeting ion channels for therapeutic and diagnostic applications"*
Ringberg Castle, Munich, Germany
- *Dynamics symposium 2010*, Leogang, Austria
- *Bernstein Focus for Neurotechnology symposium 2010*, Goettingen, Germany
- *Donders discussions 2010*, Nijmegen, Netherlands.
- Janelia farm conference on "genetic manipulation of neuronal activity II" 2010, Virginia, Washington.
- Potter's lab, laboratory for neuroengineering, Georgia Institute of Technology, Atlanta, Georgia
- Neuroseminar, Department of biomedical engineering, Georgia Institute of Technology, Atlanta, Georgia.
- Neurosenses PhD retreat 2011, German Primate Center, Göttingen, Germany
- Max Planck Institute Florida Seminar Series, Jupiter, Florida
- 2012 Gordon Research Seminar on "Photosensory receptors", Galveston, Texas.

PROFESSIONAL SCIENTIFIC ACTIVITIES:

- Associate editor and host of the special topics issue "closing the loop around neural system" in *frontiers in neural circuits* published as an ebook by frontiers
- Organizing committee member, Neurizons 2009 and Neurizons 2011.

PROFESSIONAL ORGANIZATIONS:

- Member, Society for Neuroscience.
- Member, IEEE.
- Member, IEEE computational intelligence society.